AD-A193 320 STUDIES IN SUPPORT OF OXIDATION-RESISTANT COMPOSITE MATERIALS(U) GENERAL ATOMICS SAN DIEGO CA J L KAAE ET AL. 01 FEB 88 GA-A19195 AFOSR-TR-88-0204 1/2

UNCLASSIFIED FF9620-86-C-0011 F/G 11/4 NL

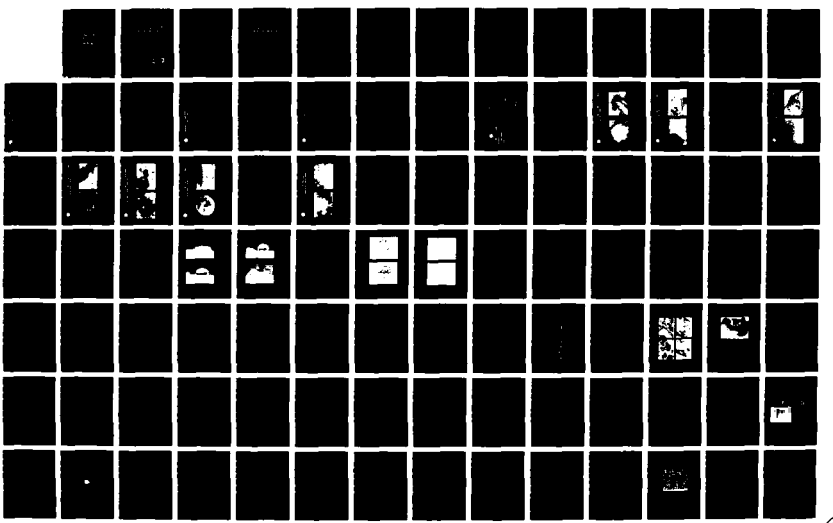

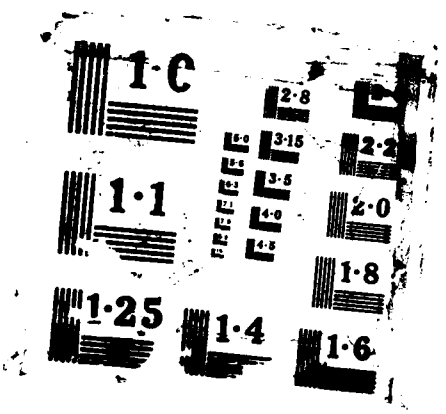
1·C
1·1
1·25
1·4
2·8
3·15
3·5
4·0
4·5
2·2
2·0
1·8
1·6

(2)

GA Technologies

GA-A19195

STUDIES IN SUPPORT OF OXIDATION-RESISTANT COMPOSITE MATERIALS

FINAL REPORT

by
J. KAAE, M. DRESSELHAUS, J. MacKENZIE, B. McQUILLAN,
R. PRICE, G. REYNOLDS, H. STRECKERT, and D. TILLEY

Prepared under
AFOSR Contract F49620-86-C-0011
for the Air Force Office of Scientific Research
Department of the Air Force

FEBRUARY 1988

SECURITY CLASSIFICATION OF THIS PAGE

AD-A193 340

REPORT DOCUMENTATION PAGE

Form Approved OMB No. 0704-0188

1a. REPORT SECURITY CLASSIFICATION: Unclassified	1b. RESTRICTIVE MARKINGS: None
2a. SECURITY CLASSIFICATION AUTHORITY: Not applicable	3. DISTRIBUTION/AVAILABILITY OF REPORT: Approved for public release; Distribution Unlimited
2b. DECLASSIFICATION/DOWNGRADING SCHEDULE: Not applicable	
4. PERFORMING ORGANIZATION REPORT NUMBER(S): GA-19195	5. MONITORING ORGANIZATION REPORT NUMBER(S): AFOSR-TR- 88-0284
6a. NAME OF PERFORMING ORGANIZATION: General Atomics; 6b. OFFICE SYMBOL (If applicable):	7a. NAME OF MONITORING ORGANIZATION: Air Force Office of Scientific Research
6c. ADDRESS (City, State, and ZIP Code): P. O. Box 85608, San Diego, CA 92138-5608	7b. ADDRESS (City, State, and ZIP Code): Bolling Air Force Base, Washington, D.C. 20332J6448
8a. NAME OF FUNDING/SPONSORING ORGANIZATION: Air Force Office of Scientific Research; 8b. OFFICE SYMBOL (If applicable): NC	9. PROCUREMENT INSTRUMENT IDENTIFICATION NUMBER: Contract F49620-86-C-0011
8c. ADDRESS (City, State, and ZIP Code): Bolling Air Force Base, DC 20332J6448	10. SOURCE OF FUNDING NUMBERS: PROGRAM ELEMENT NO. 61102F; PROJECT NO. 2303; TASK NO. A3; WORK UNIT ACCESSION NO.

11. TITLE (Include Security Classification)
Studies in Support of Oxidation Resistant Composite Materials Final Report

12. PERSONAL AUTHOR(S)
J. L. Kaae, M. Dresselhaus, J. MacKenzie, B. McQuillan, R. Price, G. Reynolds, H. Streckert, D. Tilley

13a. TYPE OF REPORT	13b. TIME COVERED	14. DATE OF REPORT (Year, Month, Day)	15. PAGE COUNT
Final	FROM Nov 1985 TO Dec 1987	February 1, 1988	128

16. SUPPLEMENTARY NOTATION

17. COSATI CODES			18. SUBJECT TERMS (Continue on reverse if necessary and identify by block number)
FIELD	GROUP	SUB-GROUP	Oxidation Resistant Composite Materials

19. ABSTRACT (Continue on reverse if necessary and identify by block number)

Studies on elements required for oxidation resistant composite materials have been carried out in four areas:

1. investigations of moisture resistant sealant glasses for carbon-carbon composite materials and their interactions with oxidation barrier coatings.
2. investigations of the effects of electrochemical modification of carbon surfaces on the wetability of these surfaces by sealant glasses.
3. investigations of alkoxides sol-gel precursors of ceramic materials.
4. investigations of the formation of ceramic fibers through the oxidation of inter-calculated carbon fibers.

20. DISTRIBUTION/AVAILABILITY OF ABSTRACT: ☒ UNCLASSIFIED/UNLIMITED ☐ SAME AS RPT. ☐ DTIC USERS	21. ABSTRACT SECURITY CLASSIFICATION: Unclassified
22a. NAME OF RESPONSIBLE INDIVIDUAL: Dr Donald Ulrich	22b. TELEPHONE (Include Area Code): (202) 767-4963; 22c. OFFICE SYMBOL: NC

DD Form 1473, JUN 86 — Previous editions are obsolete. — SECURITY CLASSIFICATION OF THIS PAGE

GA Technologies

GA-A19195

STUDIES IN SUPPORT OF OXIDATION-RESISTANT COMPOSITE MATERIALS

FINAL REPORT

by
J. KAAE, M. DRESSELHAUS,* J. MacKENZIE,** B. McQUILLAN,
R. PRICE, G. REYNOLDS, H. STRECKERT, and D. TILLEY†

Prepared under
AFOSR Contract F49620-86-C-0011
for the Air Force Office of Scientific Research
Department of the Air Force

*Massachusetts Institute of Technology.
**University of California at Los Angeles.
†University of California at San Diego.

GA PROJECT 3815
FEBRUARY 1988

TABLE OF CONTENTS

TABLE OF CONTENTS (Continued)

OBJECTIVES OF RESEARCH EFFORT

This is the final report on an AFOSR contract entitled "Studies in Support of Oxidation-Resistant Composite Materials." The program was divided into four tasks.

Task I was a study of the factors that control the critical interactions between the sealant glasses used in oxidation protection systems for carbon-carbon composites and the primary oxidation barrier coatings of silicon carbide or silicon nitride. This study encompassed: (1) study of the wetting characteristics of potential sealant glasses on silicon carbide and silicon nitride over the intended range of service conditions; (2) study of the surface and interface reactions between sealant glasses and silicon carbide or silicon nitride; (3) study of the time dependence of the wetting characteristics of sealant glasses on silicon carbide or silicon nitride.

Task 2 was an investigation of the effects of electrochemical modification of carbon surfaces on the wettability of these surfaces by sealant glasses. In particular, it was addressed to investigations of methods for improving the wetting of sealant glasses on the matrix carbon phase of carbon-carbon composites. The electrochemical carbon surface modification work also interacted with subcontract work at the University of California at San Diego where unique organometallic compounds that can serve as precursors for oxidation-resistant ceramic compounds are being synthesized. This interaction of the two programs involved study of the reaction of these organometallic compounds with the electrochemically modified carbon surfaces.

The potential for producing improved ceramic materials for matrices of composites that employ ceramic fibers was investigated in

Task 3. The program concentrated on alkoxide or sol-gel precursors of these ceramic materials, among which are silicon carbide, silicon nitride and silicon oxynitride. A similar formation of silicon carbide from sol-gel precursors was studied under subcontract at the University of California at Los Angeles, and a strong interaction occurred between the two program.

Task 4 started out to study the formation of oxidation resistant regions near the surfaces of graphite fibers through the decomposition of graphite intercalation compounds. However, it was found that under certain conditions this technique can be used to produce unique ceramic fibers, and effort was concentrated on developing an understanding of the nature and properties of these fibers, which may have great technical significance. The intercalated graphite fibers and the ceramic fibers were characterized, in part, at the Massachusetts Institute of Technology under a subcontract of this program.

TASK 1: SURFACE REACTIONS OF SEALANT MATERIALS FOR OXIDATION - RESISTANT CARBON - CARBON COMPOSITES

INTRODUCTION

Oxidation protection systems for carbon-carbon composites incoporate sealants (tpyically glasses) that can seal cracks in the primary oxidation barrier (typically a silicon carbide or silicon nitride coating). The effectiveness of the sealant depends on its ability to wet both the coating material and the carbon substrate. The objective of this task is to study the wetting characteristics of typical sealant materials on different forms of silicon carbide and silicon nitride, including the nature of the surface and interfacial reactions and the time-dependence of the wetting characteristics.

As discussed in the previous progress report, alkali borosilicate glasses were picked as representative sealant glasses. Although high borate glasses wet carbon substrates well and have viscosities in a suitable range (10^2 - 10^5 poise) over a wide temperature range (500 - 1200°C), they are very susceptible to moisture attack. Alkali borosilicate glasses with a molar ratio of alkali metal oxide to B_2O_3 of 1:1 offer the possiblity of greatly improved moisture resistance. (Ref. 1) Lithium oxide was selected as the alkali metal oxide because of its thermodynamic stability in contact with carbon. Three ternary glass compositions were selected where the Li_2O: B_2O_3 ratio was held equal to 1 and the silica content was varied. The compositions selected are shown in Table 1-1.

TABLE 1-1

COMPOSITION OF TERNARY ALKALI BOROSILICATE GLASSES SELECTED FOR SURFACE REACTION STUDIES

Glass Identification Number	Molar Composition (%)		
	Li_2O	B_2O_3	SiO_2
1	25	25	50
2	33	33	33
3	38	38	25

PREPARATION OF SEALANT GLASSES

The glasses were prepared by dry blending fine powders (<325 mesh) of lithium metasilicate, boric acid, silica, and lithium carbonate. Slurry mixing with methyl alcohol was used to ensure complete mixing of the constituents. After evaporating the alcohol, the frit was fused in a platinum crucible in air at 1000°C and was held at temperature for 8-16 h.

The glasses were quenched by pouring onto a graphite slab. The glass specimens were stored in a vacuum dessicator.

DETERMINATION OF LEACHING AND MOISTURE RESISTANCE

A series of tests was made to verify that alkali borosilicate glasses with a 1:1 ratio of Li_2O to B_2O_3 are relatively resistant to moisture attack. The resistance of the glasses to leaching in water and hydration in moist air was evaluated using powdered specimens in the particle size range 300-500 μm. Sample preparation followed the recommendations of ASTM Standard Test Method C-225, "Resistance of Glass Containers to Chemical Attack". The tests were run on 0.5-1 g samples contained in tight weave polymer cloth bags that were suspended from a microbalance with platinum wire. B_2O_3 glass was included in the tests for comparison.

For the leaching tests, weighed samples were immersed in deionized water at ambient temperature, and each container of water and a specimen was evacuated for 10 min to remove all the air from the cloth bag. The samples were suspended from the microbalance without removal from the water and the weight loss was recorded. After times ranging from 1 to 100 h, depending on the leaching rate, the specimens, were removed from the water, were dried, and were weighed.

The test results are shown in Table 1-2. The table shows, the initial leaching rate in % per h. The rate remained almost contant throughout the tests for all glasses. The leaching rate is plotted against the silica contents in Fig.1-1. Compared to the leaching rate of pure B_2O_3, the leaching rates of the $LiO_2 \cdot B_2O_3 \cdot SiO_2$ glasses fall, by more than three orders of magnitude as the silica content increases to 50%.

For testing the hydration rate in moist air, weighed samples were suspended from a microbalance in a loosely closed beaker containing water and a wet paper liner. The relative humidity within the beaker (measured with a thin film hygrometer) was 99%. The weight

TABLE 1-2

LEACHING OF POWDERED GLASSES IN DE-IONIZED WATER AT AMBIENT TEMPERATURE

Glass Type (Table 1)	Time of Leaching (h)	Maximum Weight Loss (%)	Initial Rate of Leaching (%/h)
1	88	5.4	0.056
2	101	11.8	0.17
3	70	52	1.0
B_2O_3	1.4	72.4	69.0

GA Technologies

POWDERED LITHIUM BOROSILICATE GLASS IN WATER AT 20°C

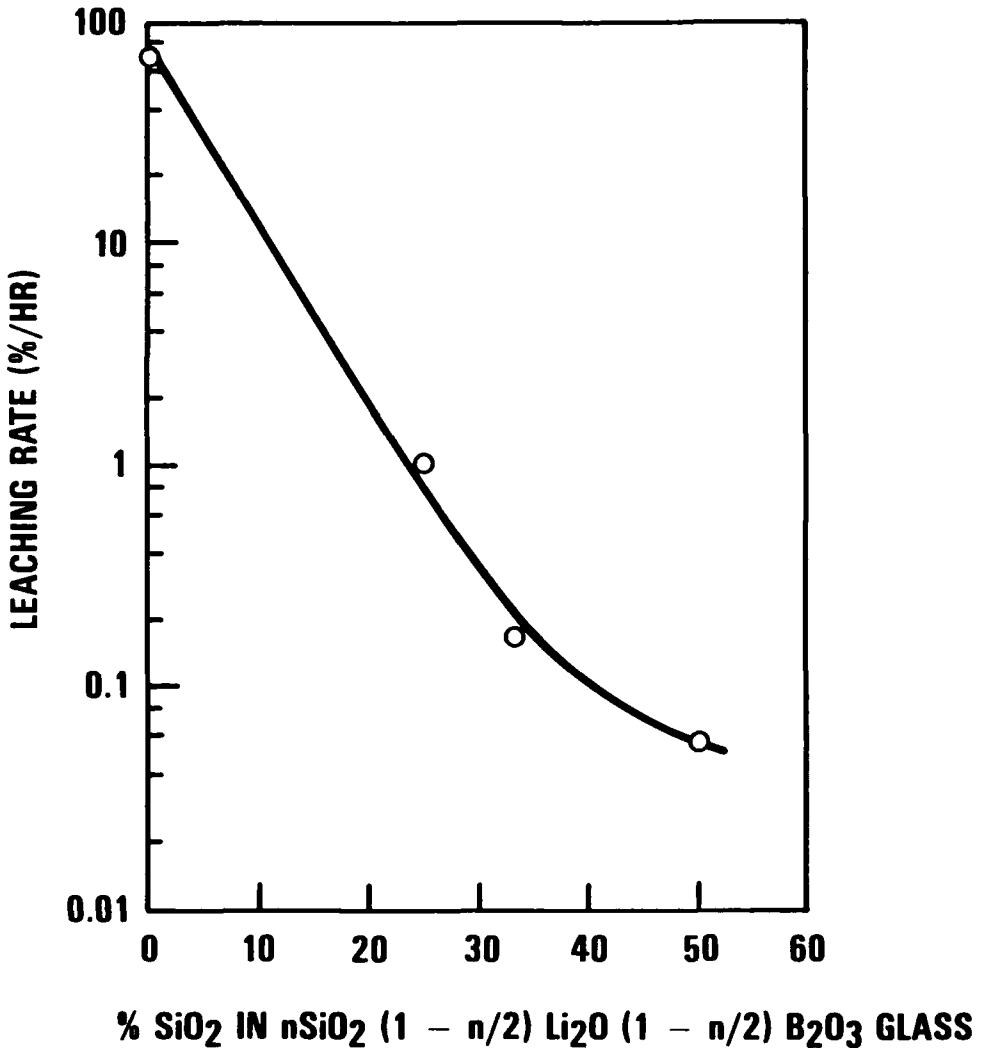

Fig 1-1 Leaching rate of powdered ternary lithium borosilicate glasses in water at ambient temperature as a function of silica content.

H-973(10)
2-5-87

increase was recorded for a period of 24-68 h. To distinguish between chemical hydration and physical adsorption, some specimens, were then suspended in dry air in a beaker with a layer of "Drierite" dessicant (relative humidity 2%) for 4 h at ambient temperature, and the sample weight change was recorded.

Table 1-3 shows the recorded maximum weight gains and the residual weight gains after a hydration - dehydration cycle. The table also shows the initial rate of weight increase. The rate remained fairly constant throughout each test except for the tests on the B_2O_3 glass, where the rate decreased as the test progressed.

Figure 1-2 shows the hydration rate (initial rate of weight gain) plotted against the SiO_2 content of the glasses. The hydration rate follows a similar trend to the leaching rate (Fig. 1-1), falling sharply with increasing silica content.

For the B_2O_3 glass, virtually all the weight increase remained after exposure to dry air, indicating that the weight increase was due to the chemical hydration of B_2O_3 to boric acid. In sharp contrast to B_2O_3 glass, the weight increases in the ternary glasses were immediately and almost completely reversed when the humidity in the air was reduced. Even at ambient temperature most of the weight gain was reversed within 30 min. This shows that the weight gain in these glasses was due to physical adsorption rather than chemical reaction.

The hydration and leaching rates reported here for powdered glass samples are much higher than are observed on monolithic samples. Monolithic samples of the same glasses (approximately 1 cm^3 pieces) were exposed to moist air (99% relative humidity) for 650 h. The weight gain in the B_2O_3 glass was 19.7%, while the weight changes in the ternary glasses ranged from -0.01 to +0.03%.

TABLE 1-3
HYDRATION OF POWDERED GLASS IN MOIST AIR AT AMBIENT TEMPERATURE

Glass Type (Table 1)	Time of Hydration (h)	Maximum Weight Gain (%)	Weight Gain Retained After Dehydration (%)	Initial Rate of Hydration (%/h)
1	24.3	2.9	0.1	0.12
2	23.3	5.1	--	0.21
3	27	8.5	--	0.32
B_2O_3	67.5	67.5	~65	2.9

POWDERED LITHIUM BOROSILICATE GLASS IN MOIST AIR AT 20°C

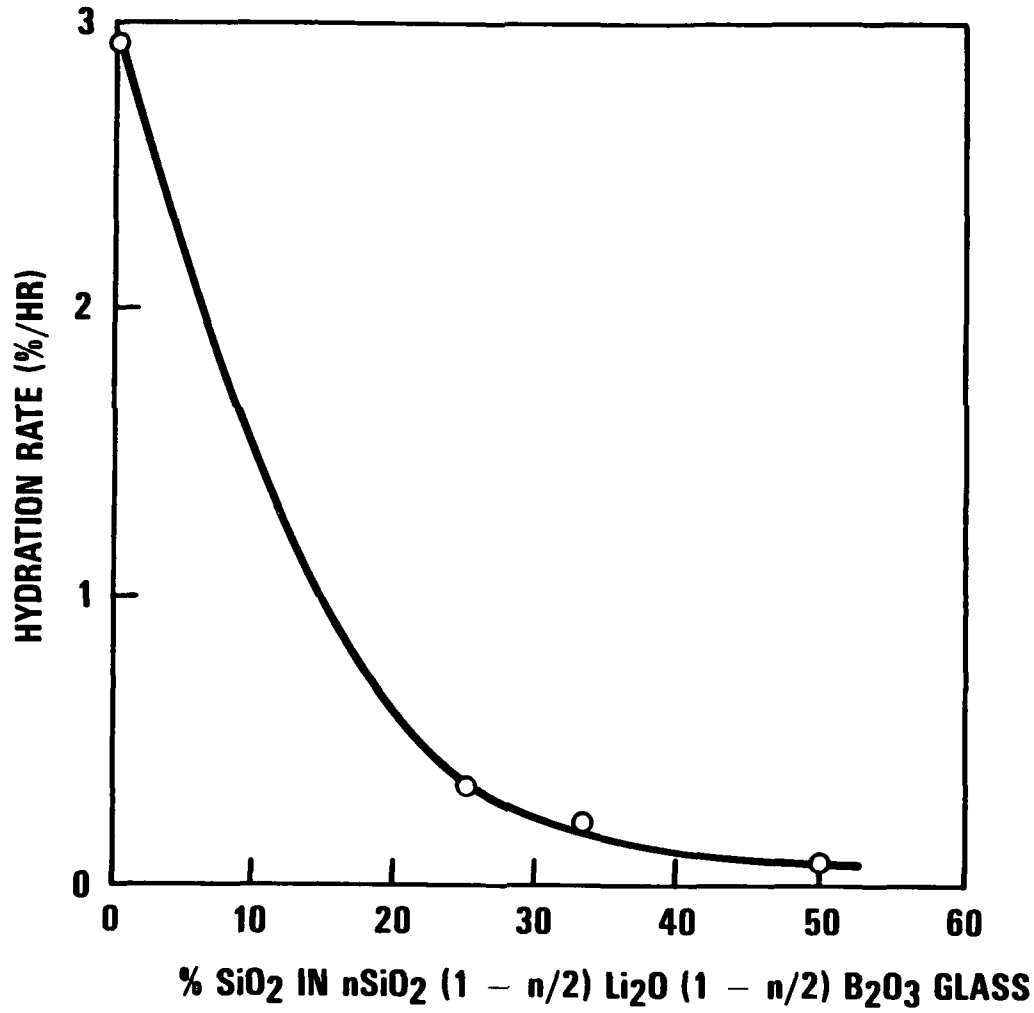

H-973(9)
2-5-87

Fig 1-2 Hydration rate of powdered ternary lithium borosilicate glasses in moist air at ambient temperature as a function of silica content.

INTERACTION OF SEALANT GLASSES WITH Si, SiC AND Si3N4

The interaction of the three sealant glasses with representative coating materials was studied by the sessile drop method. The following substrate materials were used:

1. Pure highly polished silicon single crystal wafers with a (111) orientation. Although pure silicon is not normally used as protective coating, chemically vapor deposited (CVD) silicon carbide frequently contains free silicon.

2. Chemically vapor deposited silicon carbide made at GA Technologies Inc. (Refs. 2,3) by decomposition of methyltrichlorosilane in hydrogen at 1600°C in a fluidized bed of inert particles. Deposits of this type have been throughly characterized and are chemically pure, fully dense stoichiometric β (cubic) SiC. They contain columnar grains about 4μm in diameter and exhibit a slight preferred orientation with (111) planes parallel to the surface. The as-deposited surface is quite smooth and no polishing was required.

3. Chemically vapor deposited silicon nitride made at GA by decomposition of silicon tetrachloride with ammonia at 1200°C in a fluidized bed of inert particles. The material consists of chemically pure (hexagonal) silicon nitride. The as-deposited surface is rough and most samples were diamond polished before use.

The principle of the sessile drop method is illustrated in Fig. 1-3. In the classical treatment of the sessile drop, the contact angle, θ, is set by the relative value of three surface tensions:

SESSILE DROP TEST

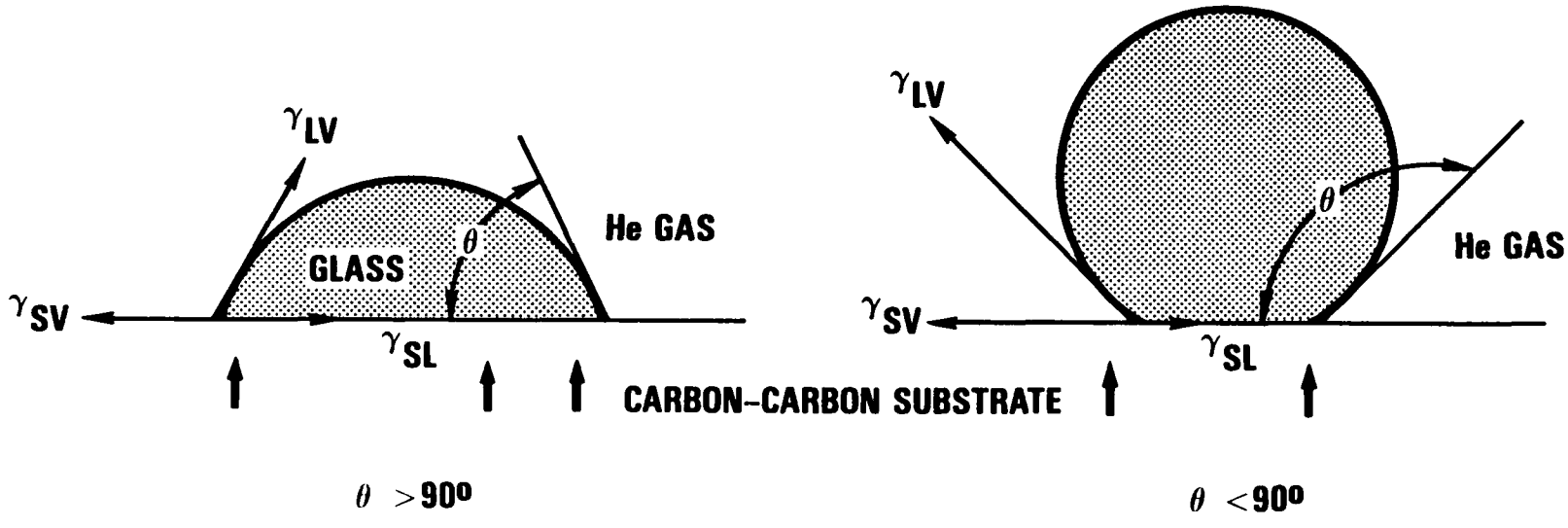

(A) - WETTING DROP ON SUBSTRATE

(B) - NON-WETTING DROP ON SUBSTRATE

Fig 1-3 Sessile drop test: relation between contact angle, θ, and surface tension.

H-973(8)
2-5-87

the solid-vapor interfacial tension (γ_{SV}), the liquid surface tension (γLV), and the solid-liquid interfacial tension (γ_{SL}), according to the equation:

$$\gamma_{SV} = \gamma_{SL} + \gamma_{LV} \cos\theta \quad .$$

where θ is the contact angle. Although this classical model is open to question and has never been fully verified, the sessile drop method for measuring the contact angle, θ, remains a useful empirical method for assessing the wetting of solids by liquids.

In the initial series of tests, pieces of each of the three glasses (Table 1-1) about 1 mm across were placed on Si, SiC and Si_3N_4 surfaces in a furnace in air and the temperature was raised to 600°C (the temperature where glass viscosity becomes low enough to allow the glass to assume the shape of a sessile drop). After holding at 600°C for 5 h, the specimens were removed, and the contact angles, θ, were measured with a machinists' microscope. Then the specimens were reinserted into the furnace, the temperature was raised to 700°C, and after 1 h the specimens were removed and the contact angle was measured. This sequence was repeated for temperatures of 800°C, 900°C and 1000°C. Contact angles were measured at four points on each sessile drop, rotating the specimen 90° between measurements. Drops that became detached in handling were replaced at the same point before replacing the specimens in the furnace.

The contact angles are listed in Table 1-4 and are plotted as functions of temperature in Fig. 1-4. The beads of glass remained adhered to the silicon substrates at all temperatures. The beads became detached from the SiC and Si_3N_4 substrates after heating at 600°C and in a few cases after heating to higher temperatures, as noted in Table 1-4. For the SiC substrate some beads became detached even though the low contact angle indicated that excellent wetting had occurred. For all temperatures and substrates, the contact angle for glass 1 (50% SiO_2)

TABLE 1-4
CONTACT ANGLES OF SESSILE DROPS OF GLASSES ON Si, SiC, AND Si_3N_4 SUBSTRATES IN AIR, 1 H AT TEMPERATURE

Temperature (°C)	Substrate	Contact Angle, (Mean of 4 Measurements) Glass 1 (50% SiO_2)	Glass 2 (33% SiO_2)	Glass 3 (25% SiO_2)
600	Si	127 ± 8	66 ± 3	67 ± 5
	SiC	154 ± 7[a]	55 ± 3[a]	42 ± 3[a]
	Si_3N_4	[a]	64 ± 7[a]	57 ± 7[a]
700	Si	117 ± 6	22 ± 4	36 ± 15
	SiC	85 ± 5	20 ± 4	43 ± 8[a]
	Si_3N_4	70 ± 8[a]	33 ± 4	26 ± 3
800	Si	88 ± 2	11 ± 3	9 ± 2
	SiC	70 ± 17	7 ± 1[a]	3 ± 1
	Si_3N_4	60 ± 6	15 ± 1	5 ± 1
900	Si	60 ± 6	9 ± 2	6 ± 3
	SiC	27 ± 5	6 ± 1[a]	<2
	Si_3N_4	25 ± 6[a]	10 ± 2	4 ± 2
1000	Si	18 ± 8	6 ± 2	6 ± 1
	SiC	<2	<2	<2
	Si_3N_4	<2	<2	<2

(a) Drop detached from substrate in handling

GA Technologies

WETTING OF LITHIUM BOROSILICATE GLASS ON VARIOUS SUBSTRATES IN AIR

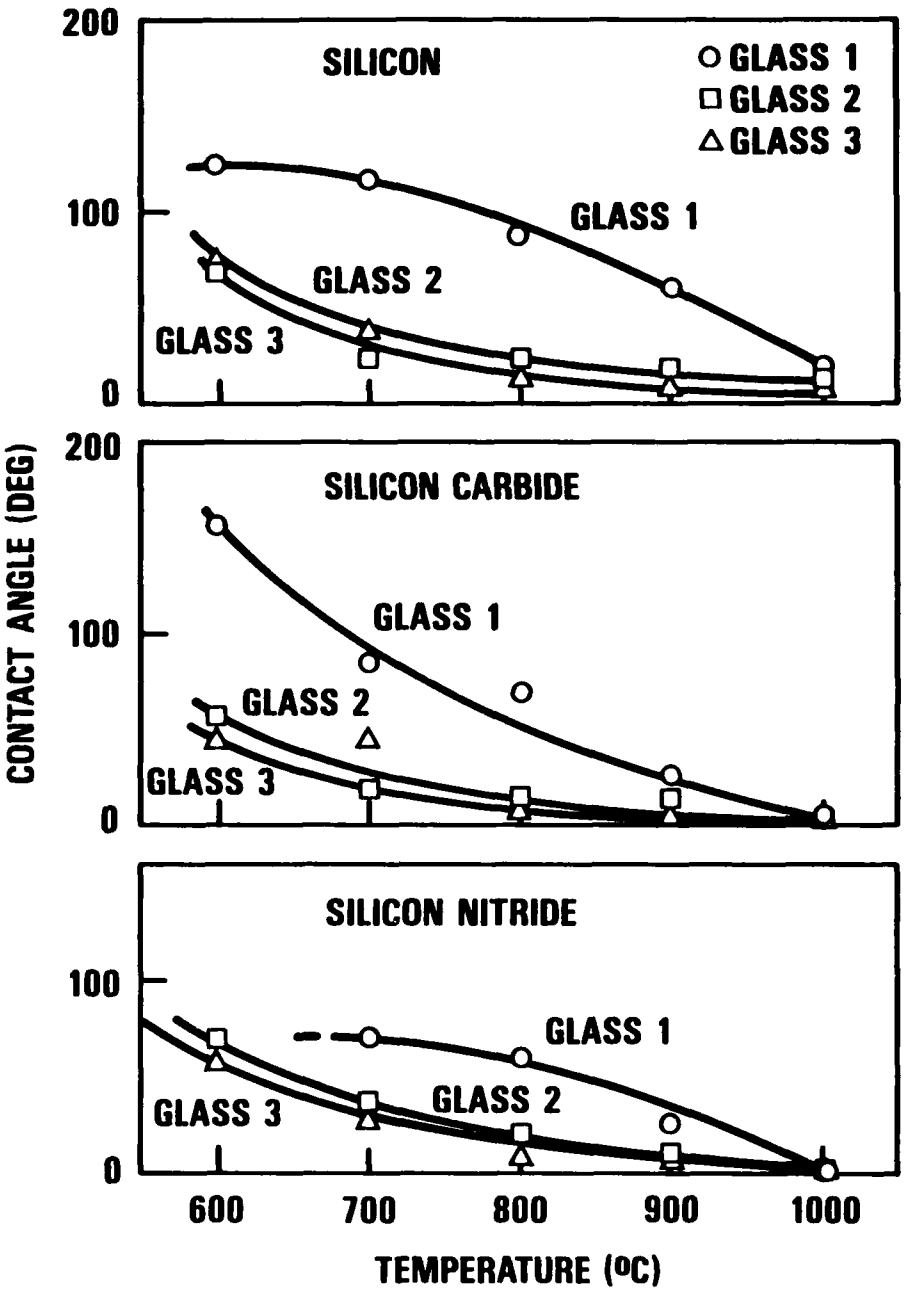

H-973(11)
2-5-87

Fig 1-4 Contact angle of lithium borosilicate glasses on Si, SiC, and Si_3N_4 substrates in air as a function of temperature.

was higher than those of glasses 2 and 3 (33% and 25% SiO_2). This probably reflects the higher liquid surface tension of high silicia glass, since the liquid surface tension of silica is known to be higher than that of boria. The contact angle decreased progressively with temperature for each glass-substrate combination. (Fig.1-4). Contact angles shown as less than 2° in Table 1-4 indicate specimens, where the beads of fused glass had spread over the substrate giving almost complete wetting.

The appearance of the substrate in contact with the glass was quite different for the three substrates. The silicon substrate showed clear evidence of chemical reaction with the glasses. For glass compositions 2 and 3, the glass beads developed some porosity at 700°C and above. The reflectivity of the silicon substrate was reduced in a zone several millimeters ahead of the periphery of the glass drop. Scanning electron micrographs of the interaction zone are shown in Fig.1-5 for a drop of Glass 2 melted on a silicon substrate at 800°C. The interaction zone at some points shows fingers of glass extending out away from the glass with a feathery film at the top (Fig 1-5b). The fact that the film appears white in the micrograph suggests that it is electrically insulating. After heating to 900°C and 1000°C optical interference colors could be seen for about 1 mm ahead of the edge of the interaction zone, indicating the build-up of a silica film on the silicon as expected.

The SiC substrates also showed interaction with the glasses. The beads of glasses 2 and 3 developed porosity at 700°C and above. A zone of decreased substrate reflectivity spread ahead of the drop periphery. Figure 1-6a shows an optical micrograph of the general appearance of a drop of Glass 2 on an SiC substrate after heating to 800°C, and Fig.1-6b shows the outer edge of the interaction zone. The interaction zone consisted of a thin film containing crystalline-appearing particles (Fig.1-6b) but without the feathery appearance seen on silicon

1 SiO_2:1 Li_2O:1 B_2O_3 ON SILICON AFTER 60 MIN IN AIR AT 800°C

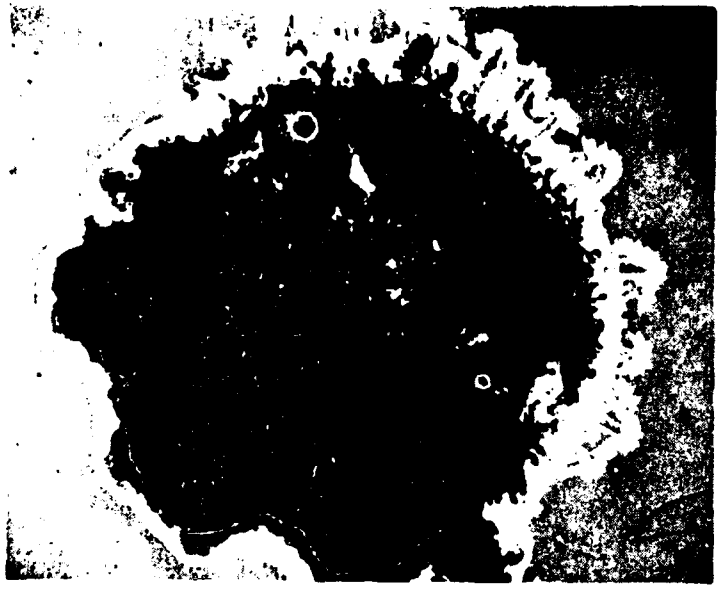

(a) 20 X

(b) 250 X

Fig 1-5 Scanning electron micrographs of silicon substrate with a drop of glass #2 (table 1) after heating at 800°C for 60 minutes in air. (a) Entire drop; (b) Interaction zone.

H-973(7)
2-5-87

1 SiO_2:1 Li_2O:1 B_2O_3 ON SiC AFTER 60 MIN IN AIR AT 800°C

(a) 10 X

(b) 500X

H-973(6)
2-5-87

Fig 1-6 Micrographs of SiC substrate with a drop of glass #2 (Table 1) after heating at 800°C for 60 minutes in air. (a) Entire drop (optical micrograph); (b) Edge of interaction zone (scanning electron micrograph).

substrates (Fig.1-5b). In contrast to silicon substrates, the glass beads were easily detached from the SiC substrates. The area under the center of the drop still appeared fairly shiney, without indications of etching as if there was no reaction at this position. As with the silicon substrates, after tests at 900°C and 1000°C a band of interference colors could seen on the SiC just ahead of the interaction zone indicating formation of a silica film on the SiC.

Of the three substrates tested, the silicon nitride showed least interaction with the glasses. Up to 800°C, no change in substrate appearance could be detected. Figure 1-7 shows micrographs of a drop of glass 2 on a Si_3N_4 substrate after heating to 800°C in air for 1 h. The edge of the spread-out glass drop is shown at 500x in Fig.1-7b. The substrate appearance is unchanged. After tests at 900°C and 1000°C, a narrow band (about 0.5 mm wide) of substrate around the glass drop showed interference colors.

Since the presence of interference colors on the substrates around the glass drops indicate thickening of the silica film on the substrates, the oxidizing character of the atmosphere is likely to influence the wetting charateristic of the glasses on the substrates. To investigate this influence, the tests at 800° were repeated in a helium atmosphere. The contact angles are shown in Table 1-5. For glass 1, the atmosphere has little effect, but for the other two glasses, the contact angles in helium were higher than in air. The effect is most marked for the silicon carbide substrates.

Consistent with the higher contact angles, silicon and silicon carbide specimens tested in a helium atmosphere showed less evidence of glass-substrate interactions than those tested in air. Figures 1-8 to 1-10 show scanning electron micrographs of drops of glass 2 heated at 800°C for 1 h in helium on silicon, silicon carbide, and silicon nitride, respectively.

GA Technologies

1 SiO_2:1 Li_2O:1 B_2O_3 ON Si_3N_4 AFTER 60 MIN IN AIR AT 800°C

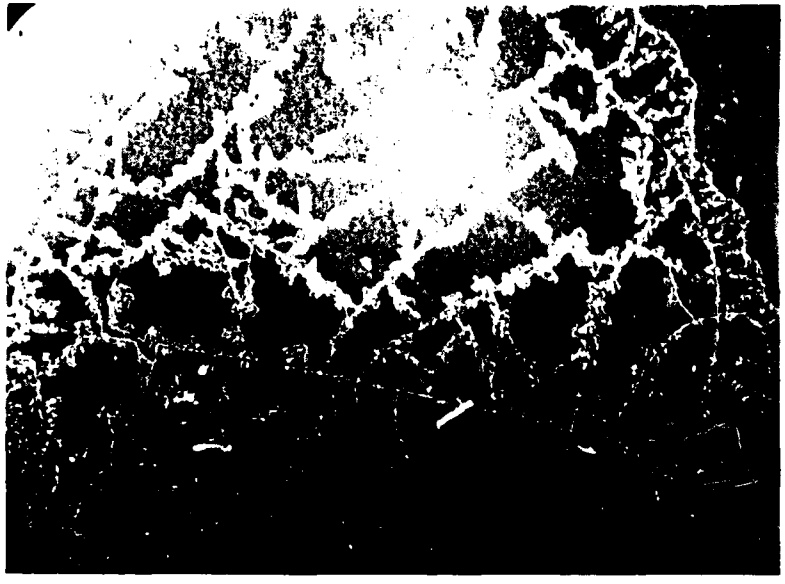

(a) 20 X

(b) 500 X

Fig 1-7 Scanning electron micrographs of Si_3N_4 substrate with a drop of glass #2 (Table 1) after heating at 800°C in air for 60 minutes. (a) Entire drop; (b) Outer edge of drop.

H-973(5)
2-5-87

TABLE 1-5

CONTACT ANGLES OF SESSILE DROPS OF GLASSES ON Si, SiC AND SI_3N_4 SUBSTRATES AT 800°C: EFFECT OF ATMOSPHERE

Substrate	Atmosphere	Contact Angle, (Mean of 4 Measurements)		
		Glass 1 (50% SiO_2)	Glass 2 (33% SiO_2)	Glass 3 (25% SiO_2)
Si	Air	88 ± 2	11 ± 3	9 ± 2
	Helium	79 ± 32	19 ± 10	16 ± 3
SiC	Air	70 ± 17	7 ± 1	3 ± 1
	Helium	55 ± 13	87 ± 6	90 ± 3
Si_3N_4	Air	60 ± 6	15 ± 1	5 ± 1
	Helium	55 ± 4	18 ± 4	30 ± 1

GA Technologies

1 SiO_2:1 LiO_2O:1 B_2O_3 ON SILICON AFTER 60 MIN IN HELIUM AT 800°C

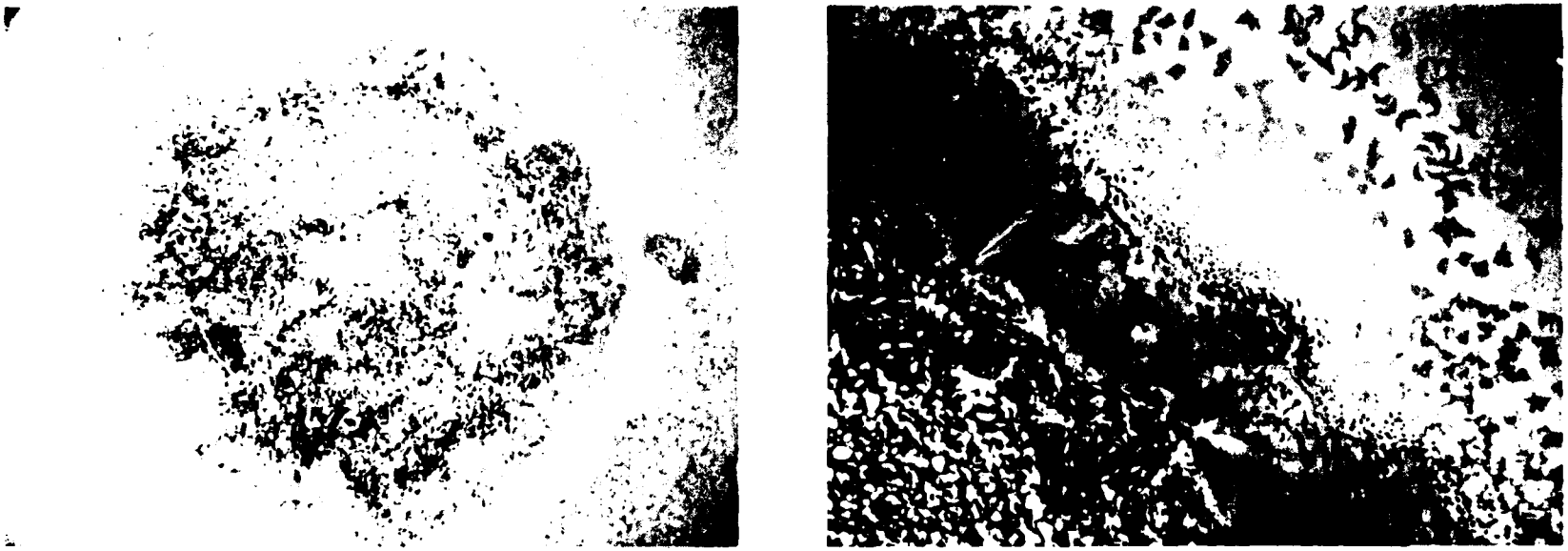

(a) 50 X

(b) 200 X

Fig 1-8 Scanning electron micrographs of silicon substrate with a drop of glass #2 (Table 1) after heating at 800°C in helium for 60 minutes. (a) Entire drop; (b) Interaction zone.

H-973(4)
2-5-87

1 SiO_2:1 Li_2O:1 B_2O_3 ON SiC AFTER 60 MIN IN HELIUM AT 800°C (DROP DETACHED)

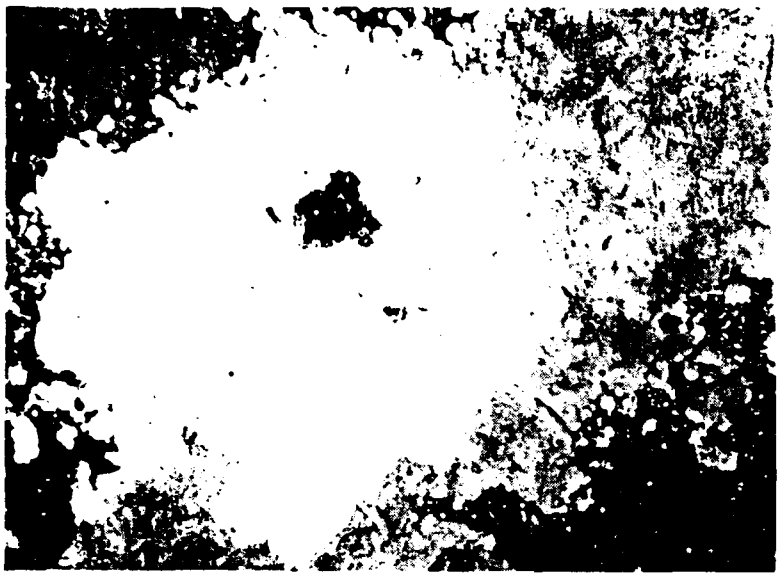

(a) 20 X

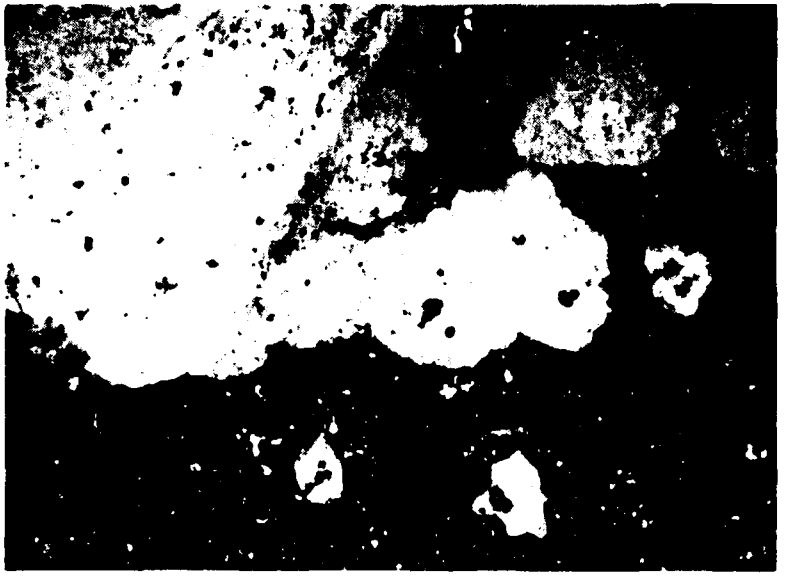

(b) 500 X

H-973(3)
2-5-87

Fig 1-9 Scanning electron micrographs of SiC substrate with a drop of glass #2 (Table 1) after heating at 800°C in helium for 60 minutes (drop detached) (a) entire contact area; (b) Outer edge of interaction zone.

GA Technologies

1 SiO_2:1 Li_2O:1 B_2O_3 ON Si_3N_4 AFTER 60 MIN IN HELIUM AT 800°C

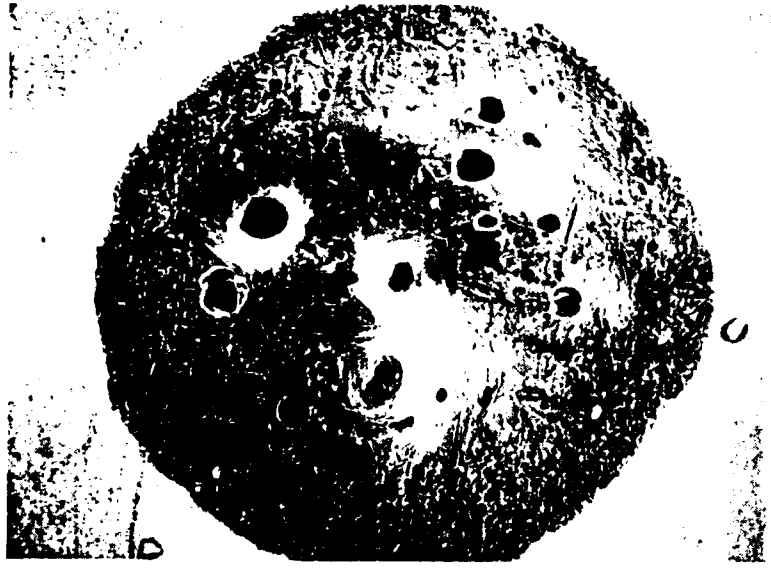

(a) 35 X

(b) 500 X

H-973(2)
2-5-87

Fig 1-10 Scanning electron micrographs of Si_3N_4 substrate with a drop of glass #2 (Table 1) after heating at 800°C in helium for 60 minutes (Unpolished substrate) (a) Entire drop; (b) Outer edge of drop.

For silicon, the difference may be seen by comparing Fig. 1-8 with Fig. 1-5. The interaction zone for the specimen heated in helium is smaller and does not show the feathery "fingers" characteristic of the specimens heated in air. Features that appear to be etch pits with an unusual crescent shape can be seen in the silicon ahead of the interaction zone (Fig.1-8b). Also, the interaction zone does not appear white in the micrographs, indicating that the composition is less electrically insulating than for specimens tested in air.

The glass drops on the SiC substrates heated in helium became detached in handling. Figure 1-9 shows the area of the substrate where the drop of glass 2 had been located. Unlike the samples heated in air, the area under the center of the drop was somewhat pitted. When examined by scanning electron microscopy the pits showed up dark while the general area that had been covered by the drop showed white. The area immediately surrounding the drop location appeared gray (Fig.1-9). Since non-conducting areas tend to appear white, the appearance is consistent with an area covered by a silica film which extends somewhat beyond the area originally covered by the drop but which is pitted through to the substrate in a few places.

Figure 1-10 shows a drop of glass 2 melted on a Si_3N_4 substrate at 800°C in helium. Unlike the substrate shown in Fig.1-7, this substrate had not been polished before the test and appears rough in Fig. 1-10b. No evidence for interactions between the substrate and the glass could be seen. The rough substrate probably accounts for the anomalously high contact angle for glass 3 in Table 1-5.

To investigate further the role of a silica film in the substrate-glass interactions, a further series of tests was run using substrates that had been pre-oxidized to build up a silica film about 1 μm thick. The oxidation conditions (derived from Ref. 4) are shown in Table 1-6, together with the measured contact angles for glass 2 at 800°C in helium. For silicon and SiC, the contact angles were significantly

1 SiO_2:1 Li_2O:1 B_2O_3 ON PRE-OXIDIZED SiC AFTER 60 MIN IN HELIUM AT 800°C

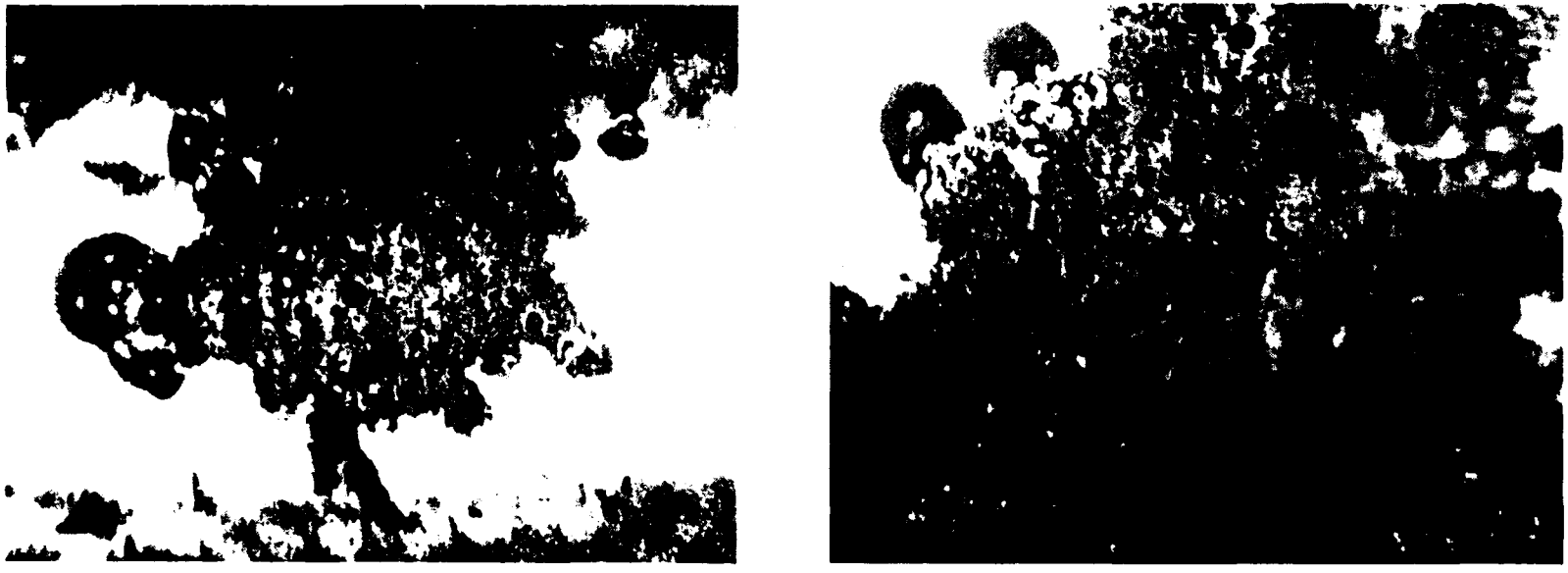

(a) 15 X

(b) 25 X

Fig 1-11: Optical micrographs of pre-oxidized SiC substrate after wetting with glass #2 at 800°C in helium for 60 minutes. Reflective outer regions are substrate with uniform SiO_2 film. Dark inner region is substrate free from SiO_2 film. Black spheres are non-wetting beads of glass.

H-973(1)
2-5-87

lower on the pre-oxidized substrate than on the as-deposited substrate. Aside from the lower contact angle, the appearance of the pre-oxidized silicon substrate was not much different from the as-deposited substrate. However, the pre-oxidized SiC substrate behaved differently from as-deposited substrate. The appearance is shown in optical micrographs in Fig.1-11. The glass wet and flowed readily on the SiC surface. The glass in the area left behind beaded up into non-wetting spheres (black in Fig.1-11), leaving a darkened area of substrate free from the interference color that covered the outer part of the substrate (light in Fig. 1-11). Some remaining drops of wetting glass can be seen at a few places around the edge of the darkened area. The contact angles listed in Table 1-6 were taken from the remnants of wetting glass. It appears that as the glass spread over the pre-oxidized SiC it dissolved the silica film. The increased SiO_2 content of the glass may have raised its surface tension enough to increase the contact angle above 90°, causing the glass film to break up into non-wetting beads. The same mechanism may explain the tendency for glass drops to detach easily from SiC even after complete wetting. The pre-oxidized Si_3N_4 subtrates behaved similarly to as-deposited substrates with no evidence for glass-substrate interactions.

The results obtained to date on glass-substrate interactions may be summarized as follows:

1. Ternary lithium borosilicate glasses wet silicon, SiC and Si_3N_4 substrates. The contact angle decreases with increasing temperature between 600°C and 1000°C and increases with the increasing silica content of the glass.

2. Micrographic examination showed evidence for chemical reaction between the glasses and silicon substrates with the reaction zone spreading by "fingers" ahead of the glass drop. The glass drops adhered firmly to the silicon at all temperatures.

TABLE 1-6

CONTACT ANGLES OF SESSILE DROPS OF GLASS 2 (SiO_2:Li_2O: B_2O_3) ON Si, SiC AND Si_3N_4 AT 800°C FOR 1 H IN HELIUM: EFFECT OF SUBSTRATE PRE-OXIDATION

	Pre-Treatment (In Air)		
Substrate	Temperature (°C)	Time (h)	Contact Angle (°)
Si	None	--	19 ± 10
	1300	16	2
SiC	None	--	87 ± 6
	1500	16	14
Si_3N_4	None	--	18 ± 4
	1500	16	25

3. Some chemical interaction was also evident between the glasses and silicon carbide substrates, but in this case the glass drops frequently become detached. For as-deposited SiC, tested in air, the area under the detached drop appeared relatively free from attack.

4. Minimal interaction occurred between the glass and silicon nitride except for a narrow band around the edge of the glass drop where the appearance of interference colors at temperatures above 900°C indicated some thickening of the oxide film. This was probably due to glass consituents diffusing into the silica film and increasing the permeation of oxygen.

5. In a helium atmosphere the contact angles between the glass drop and the substrate tended to be higher than in air, and the extent of interaction lower. For silicon carbide substrates the area covered by the bead appeared pitted in contrast to the smooth appearance after tests in air.

6. When the specimens were pre-oxidized to build up a silica film and then were tested in helium, the contact angles tended to be lower and the extent of the interactions with silicon and SiC tended to be higher, probably because the thicker silica film allows more opportunity for interdiffusion at the glass interface. For a pre-oxidized SiC substrate the glass tended to spread readily over the substrate, dissolving the silica film. The glass layer then broke up into non-wetting beads of high silica glass. The same mechanism may explain the tendency for glass drops to detach easily from SiC substrates, even after complete wetting.

REFERENCE

1. Adams, P.B. and D.L. Evans "Chemical Durability of Borate Glasses", Mater. Sci. Res., 12, 525 (1978).
2. Gulden, T.D. "Deposition and Microstructure of Vapor Deposited Silicon Carbide", J. Am. Ceram. Soc., 51. 424 (1968).
3. Price, R.J. "Structure and Properties of Pyrolytic Silicon Carbide", Am. Ceram. Soc. Bull., 48, 859 (1969)
4. Schirocky, G.H., R.J. Price and J.E. Sheehan, "Oxidation Characteristics of CVD Silicon Carbide and Silicon Nitride", GA Technologies Report No. GA-A18696 (1986).

TASK 2: SURFACE MODIFICATION OF MATRIX MATERIALS FOR OXIDATION-RESISTANT CARBON-CARBON COMPOSITES

INTRODUCTION

The objective of this task is to study the wetting behavior of sealant glasses or glass-like precursors on the matrix carbon phase of carbon-carbon composites. The wettability of any liquid on a solid is related to the relative interfacial energies at the solid/liquid/gas interfaces. For a particular glass in an air atmosphere, the wetting will depend on the surface chemistry of the carbon which we can control to a considerable degree because the nature of the functional groups bonded to the surface can be modified considerably by various chemical or electrochemical pretreatments.

One type of carbon substrate, glassy carbon, has been selected for study in this program. Glassy carbon is very similar structurally to the matrix carbon in carbon-carbon composites. Electrochemical modification of the surface of glassy carbon specimens has been carried out, and the variability of wetting of these modified surfaces by a glass precursor has been observed.

MATERIALS PREPARATION

The initial step in the fabrication of glassy carbon specimens involved the molding of several 0.625 in. diameter phenolic resin cylinders that were between one and two inches long. These cylinders were made from Monsanto's Resinox 755. They had initial densities in the cured state of 1.26 g/cm^3, which indicated that there was no significant porosity in the parts.

In the molding procedure, a metal die contained within a clam-shell heating element was filled with Resinox 755 powder. The powder was put under an initial pressure of about 1000 psi, and the temperature was raised until the powder began to melt at about 100°C and the pressure started to fall off. After a delay of about a minute, the pressure was increased to 10,000 psi; this was maintained for about 30 minutes as the temperature continued to increase to about 175°C. The heater was then turned off, and the cured phenolic rod was pressed out of the mold at a temperature of about 75°C.

These cured rods were then sliced into thin disks; the disks were packed in alumina powder and subsequently carbonized in flowing argon by heat treatment to 900°C over a five-day period (a heating rate of about 7.5°C/h). The density of the resulting glassy carbon disks increased to about 1.42 g/cm^3. The char yield on carbonization was in the range of 62 to 68%, and the volume shrinkage of the disks during carbonization was in the range of 40 to 45%.

SURFACE MODIFICATION

Electrochemical processing of the carbon surface can yield a wide variety of surface functional groups of interest. Mechanical properties of fibers or films in carbon/carbon composites are dependent on the functional groups on the surface.

The surface treatment prior to experimentation is a critical parameter in obtaining reproducible results. The following method was selected for the surface pretreatment: a smooth surface was prepared by polishing with 600 grit sandpaper, followed by 30, 9, 6, and 1 μm alumina slurry on wool polishing cloth. The carbon substrate was rinsed copiously with water between each medium. A final rinse to remove impurities was performed in 1M KOH.

For the elecrochemical surface treatment, a standard three-electrode cell was used in conjuntion with a PAR 173 potentiostat/galvanostat and a PAR 175 universal programmer which permitted the electrode potential to be swept between preset values. The current-voltage curves were displayed on a Houston Model 2000 x-y recorder. All experiments were performed in 1M H_2SO_4 aqueous electrolyte with a Pt coil counterelectrode and an Saturated Calomel Electrode (SCE).

Electrodes were prepared by attaching a copper wire with conducting silver epoxy to the carbon substrate. After inserting the wire into a 5 mm o.d. glass tube, epoxy resin was applied to protect the contract region from the electrolyte.

Figure 2-1 illustrates a typical voltammogram obtained in 1M H_2SO_4 with a freshly polished electrode. Curve 1 was obtained by first scanning anodically until oxygen was evolved, then reversing the scan until hydrogen was evolved, and then again scanning in the anodic direction (all scans at 100mV/sec). Various oxidation and reduction

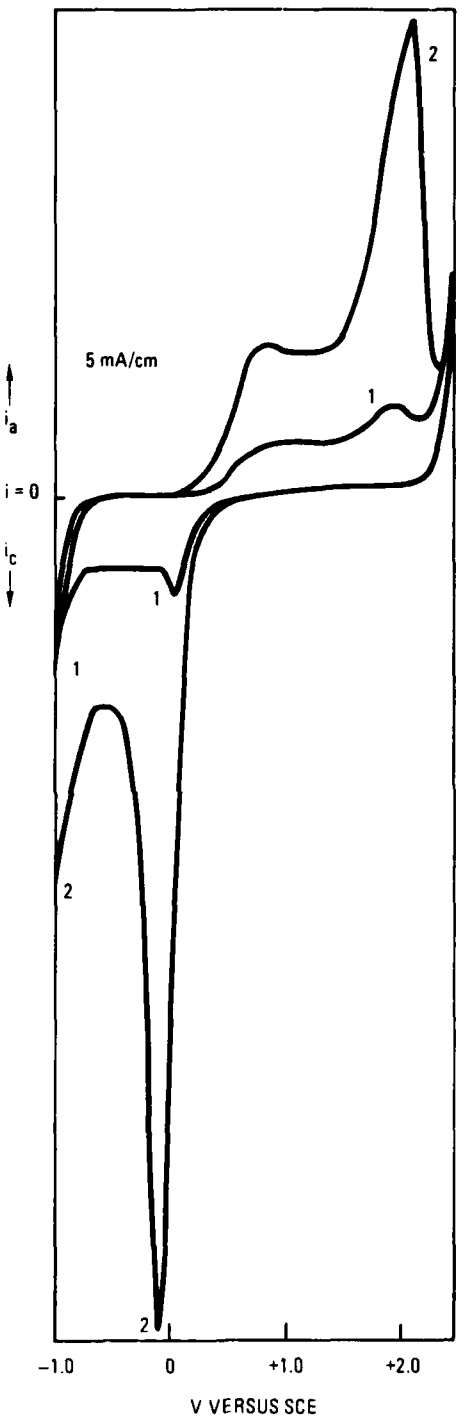

Fig. 2-1 Typical current voltage curve of a glassy-carbon electron in 1M H_2SO_4 electrolyte.

waves are apparent in the figure. It appears that most of these waves are due to the presence of surface functional groups. Their presence and magnitude were independent of stirring rate suggesting they remained fixed on the surface and did not diffuse into solution. No other electroactive species were added to the electrolyte to account for these waves.

Curve 2 in Fig. 2-1 was obtained by first maintaining the electrode at +2.0V for 2 min. Heavy oxygen evolution was apparent at the electrode surface under this condition. The voltammogram was then obtained by scanning in the same fashion used for Curve 1. This voltammogram differs considerably from Curve 1 indicating the surface groups were changed quantitatively and qualitatively by the constant potential treatment.

That the surface groups were not removable from the substrate was shown by the following test. An electrode was oxidized at +2.0V, and a voltammogram similar to curve 2 was obtained. The electrode was subsequently removed from the electrolyte, rinsed with water, dried, and put back in the cell. A second voltammogram was obtained which mimicked the first except for a slight reduction in the magnitude of the redox waves. This experiment was repeated for all electrochemical treatments with similar results. It has been suggested by others that this type of treatment leads to a surface that contains quinone groups (sample a). Another surface and set of voltammograms was obtained by a cathodic surface modification. The electrode was maintained at -2.0V where hydrogen evolution occurred (sample b). This treatment produces a surface with low oxygen coverage where any oxygen encountered would be alcohol-like.

A third surface condition (sample c) was obtained by repetitively cycling the electrode between the above two potentials. This cyclic scanning has been found to produce very uniform oxygen coverage. Stopping at the cathodic limit will result in a hydroquinone-like surface.

A freshly polished surface with no electrochemical treatment was used as a fourth sample (sample d).

WETTING STUDIES

Initial wetting experiments performed were of the sessile-drop type in an air atmosphere. A glass-like siloxane resin, GR908F from Owens-Illinois, was used because of its extremely low melting temperature. The experiments were performed at 110°C; the substrates were removed from the furnace, cooled and photographed. Contact angles were measured directly from the photographs with a protractor.

The wetting angles that occurred on the four different surface conditions are shown in Figs. 2-2 and 2-3. For the surface condition produced by holding at +2.0V for 10 min. (a heavily oxidized surface) the wetting angle was ~90° (Fig. 2-2a), indicating some wetting.

For the surface produced by treating at -2.0V for 10 min. which yielded a more reduced surface, the wetting angle was ~130° (Fig. 2-2b), indicating no appreciable wetting.

The wetting angle on the carbon electrode that was cycled between -2.0 and +2.0V for 20 min. is shown in Fig. 2-3c. The contact angle was ~130° on this surface.

The contact angle for an electrode which was freshly polished with no electrochemical treatment is shown in Fig. 2-3d. This air-oxidized surface resulted in a wetting angle of ~90°.

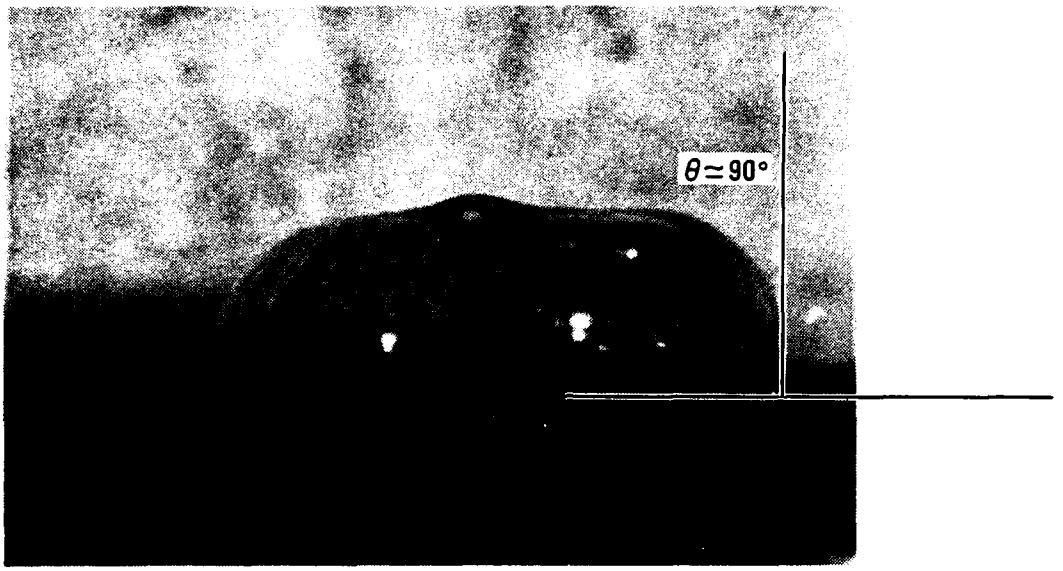

(a)

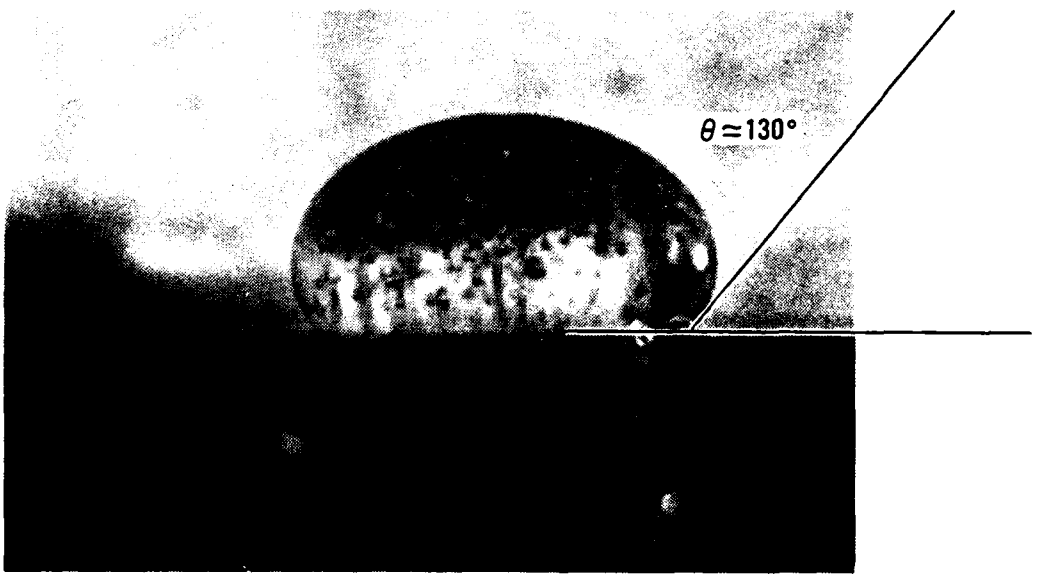

(b)

Fig. 2-2 Wetting angles for siloxane resin on glassy-carbon substrates. Sample (a) substrate treated at +2.0V for 10 min. Sample (b) substrate treated at -2.0V for 10 min.

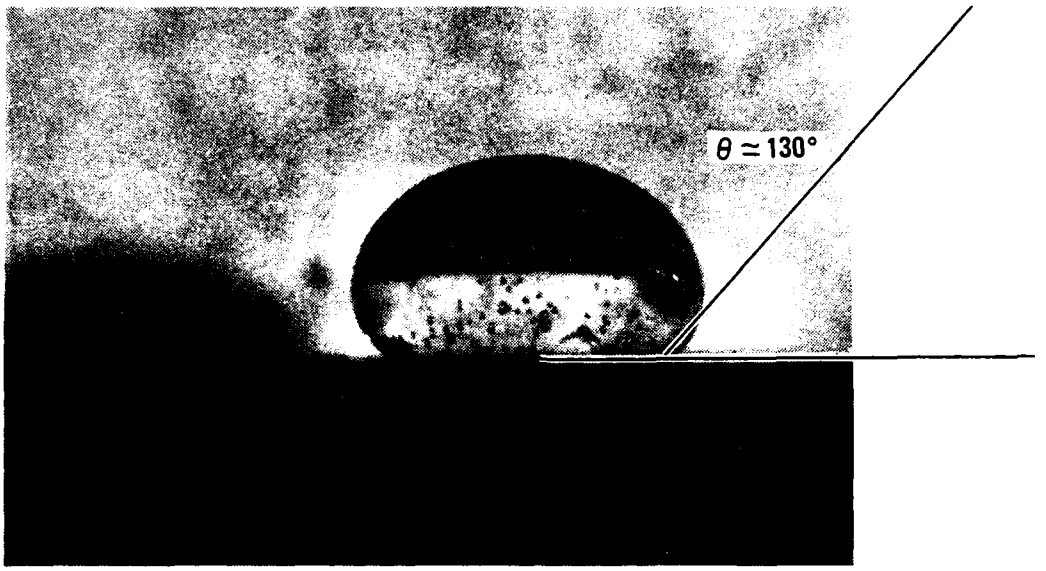

(c)

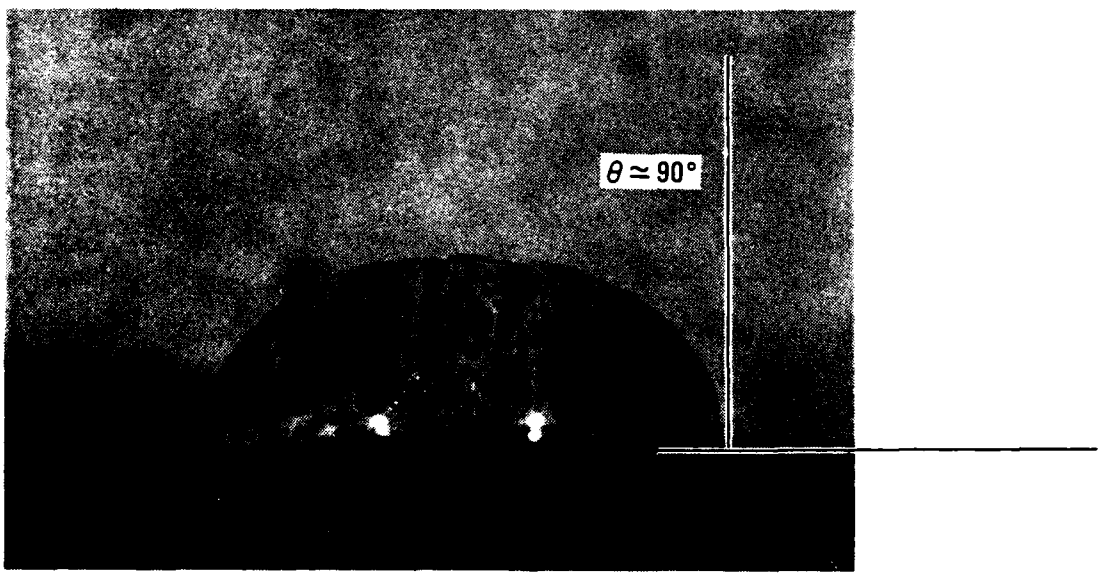

(d)

Fig.2-3 Wetting angles for siloxane resin on glass-carbon substrates. Sample (c) repetitively cycled between -2.0 and +2.0V for 20 min. Sample (d) freshly polished, no electrochemical treatment.

SURFACE ANALYSIS

The contact angle in sessile drop experiments is related to the surface energy of the liquid and the substrate. The surface energy of the substrate will depend on a variety of factors including the surface morphology and chemical composition and oxidation states of the surface functional groups.

Scanning electron microscopy was used to further characterize the surface. Pictures of the surfaces obtained in the SEM are displayed in Fig. 2-4 and 2-5. The surface treated at +2.0V for 10 min is shown in Fig. 2-4, sample a. The surface is covered with a network of cracks which result in a field of isolated, flat "islands".

The surface treated at -2.0V for 10 min is shown in Fig. 2-4, sample b. The surface differs radically from the previous one; it contains a large number of small craters. The craters are of a fairly narrow size distribution and are probably sites where hydrogen evolution occurred.

The surface of sample c repetitively cycled between +2.0 and -2.0V and is shown in Fig. 2-5. It has a similar appearance as the surface in Fig. 2-4a with a network of cracks. However, the "islands" formed are approximately one-half the size of the previous sample. Although both oxygen and hydrogen were evolved on this surface, no cratering is evident on the surface as in Fig. 2-4b.

Fig. 2-5d depicts the surface of a freshly polished sample. It is relatively featureless except for some "scratches" and a few raised particles. The scratches are most likely artifacts from the polishing

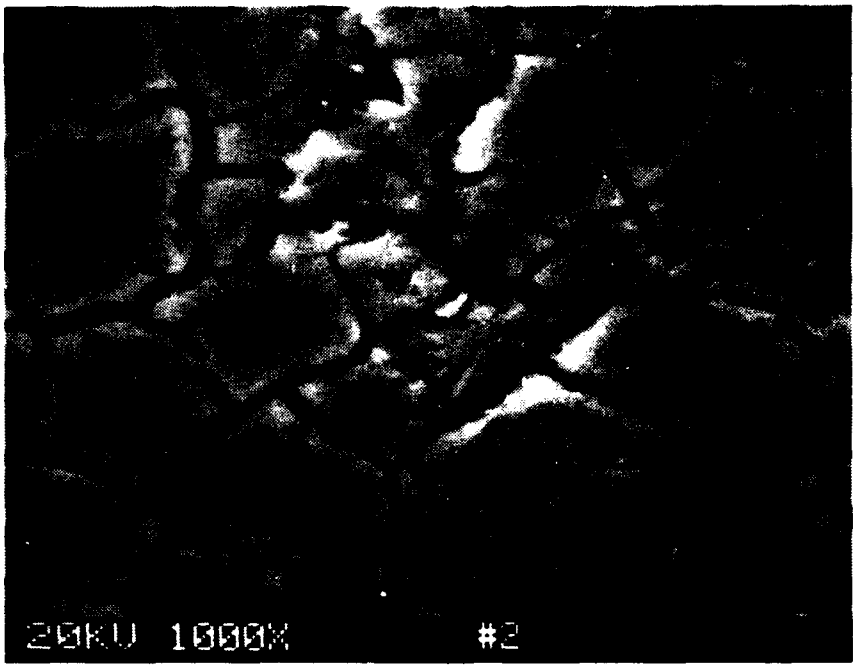

(a)

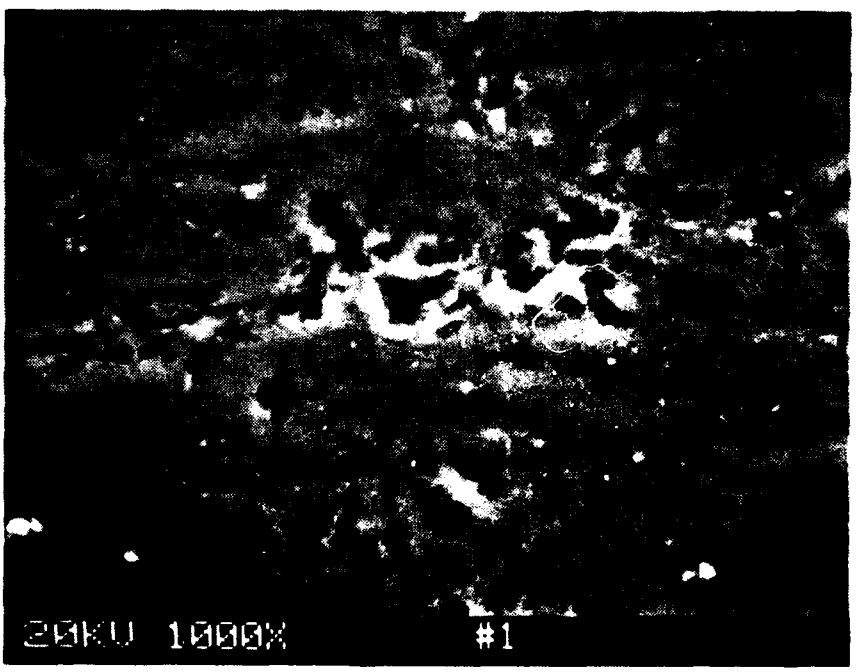

(b)

Fig.2-4 SEM pictures of glassy-carbon electrodes at 1000 x magnification. Sample (a) treated at +2.V for 10 min. Sample (b) treated at -2.0V for 10 min.

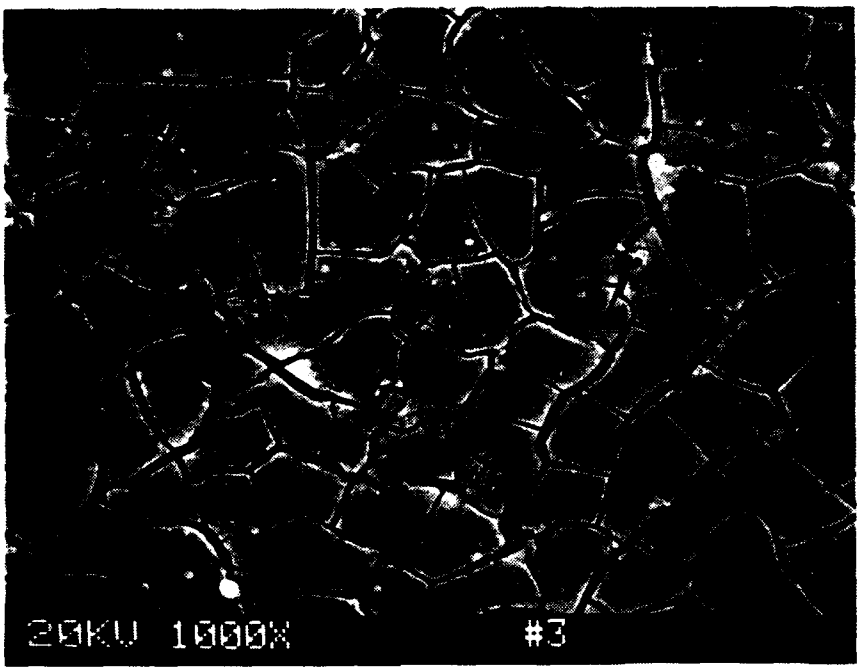

(c)

(d)

Fig.2-5 SEM pictures of glassy-carbon electrodes at 1000x magnification. Sample (c) repetitively cycled between -2.0 and +2.0V for 20 min. Sample (d) freshly polished with no electrochemical treatment.

step of the sample pretreatment. The particles could be either dust or contamination left behind from the alumina polish. It clearly has the lowest macroscopic surface area of the various surfaces.

Information concerning the chemical composition of the carbon surfaces is necessary for an understanding of the wetting behavior. X-ray Photoelectron Spectroscopy (XPS) can provide a semi quantitative estimation of the chemical group concentration on the surface. Four separate types of surface functionalities can be detected on these samples. They are summarized in Table 2-1 as: 1. carbon with no oxygen containing species (C/CH_x) 2. alcohol or ether-like groups (C-OH, C-O-C) 3. carbonyl or aldehydes ($C{=}O, C^{-H}_{=O}$) 4. carboxyl groups ($C^{-O}_{=O}$).

The oxidation treatment doubled the concentration of carbonyl groups and tripled the carboxyl groups. The reducing treatment lowered oxygen concentratiion and increased the proportion of carbon with no oxygen containing groups.

The untreated sample contained a higher proportion of oxygen containing groups than the reduced surfaces, but had less oxygen containing groups than the samples given the oxidation treatment.

Surface roughness and morphology can have a marked effect on wetting. For our set of conditions, the surface chemistry is the predominant factor affecting wettability. The surfaces shown in Fig. 2-4a and 2-5c are most similar in terms of surface morphology, but show the largest difference in wetting angle.

The surface shown in Fig. 2-4a is morphologically very different from that of Fig 2-5d, but the surface chemistry of sample d resembles that of sample a more than the other samples do as shown in Table 2-1. The wetting angles for both these surfaces are ~90° as illustrated in Fig.2-2 and 2-3. The improved wettability can be explained by the interaction between the glass and the more reactive CH_x groups. Analysis of wetting behavior in terms of physical properties,

specifically the surface and interfacial tensions, was restricted by the absence of data concerning reaction products and surface chemistry after wetting.

TABLE 2-1. Glassy Carbon Surface Composition determined by XPS.

Sample	Treatment	% CH_x	% C-O	%C=O	% C = O
a	+2.0V	47	25	13	14
b	-2.0V	65	24	7	4
c	+2.0 to -2.0V	61	25	7	6
d	untreated	53	27	11	9

SUBCONTRACT TO TASK 2

UNIVERSITY OF CALIFORNIA AT SAN DIEGO

ORGANOMETALLIC PRECURSORS TO OXIDATION RESISTANT COATINGS

The goal of our proposed research is to conduct exploratory synthetic studies that will allow us to build molecules that could serve as organometallic precursors to oxidation-resistant coatings for carbon-carbon composite matrix materials. So far our approach has been directed toward constructing molecules that might give rise to metal (M) silicide (M_xSi_y) or ceramic-like ($M_xSi_yO_z$) coatings. Therefore target molecules include simple metal silyls, $M(SiR_3)_x$, or metal siloxides, $M(OSiR_3)_x$. We are pursuing our research objectives in two stages: 1) probing the nature of metal-silicon bonding through examination of simple transition metal silyl complexes, and 2) applying these insights to metal systems of interest, for example silyl complexes of hafnium.

Initial efforts have focused on use of the lithium silyl $(THF)_3LiSi(SiMe_3)_3$ as silylating reagent (Me=Methyl). Reactions of 1-4 equivalents of this reagent with $ZrCl_4$ or $HfCl_4$ have resulted in elimination of LiCl and production ether-soluble complexes which have as yet not been isolated in pure form. We are pursuing isolation and characterization of these materials, and believe that they are zirconium and hafnium silyl species, based on analogous reactions to obtain the closely related compounds $(\eta^5\text{-}C_5Me_5)MCl_2[Si(SiMe_3)_3]$ (1,M=Zr;2,M=Hf;eq1).

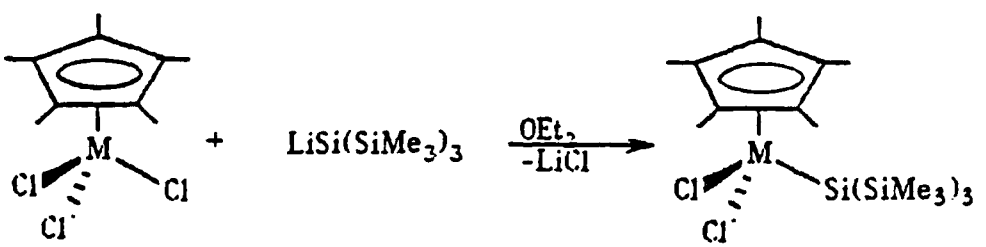

(1)

1. M = Zr
2. M = Hf

Compounds 1 and 2 have been fully characterized by elemental analyses and spectroscopic techniques. In addition, compound 2 has been characterized by X-ray crystallography.

Overall, this general method appears promising, especially since we can isolate simple silyls of the type $M[Si(SiMe_3)_3]_2Cl^-$ and $M[Si(SiMe_3)_3]_2(ether)_2$, where M = Cr, Mn and Fe. We therefore feel that this can be a productive area, and should be applied to other metals that form oxidation-resistant silicides.

A second approach is based on refractory metal siloxide derivatives. The target ceramic monomers are siloxides of early transition metals containing the $^tBu_2FSiO-$ ligand. These molecules contain M-X bonds that can undergo polymerization reactions, e.g.;

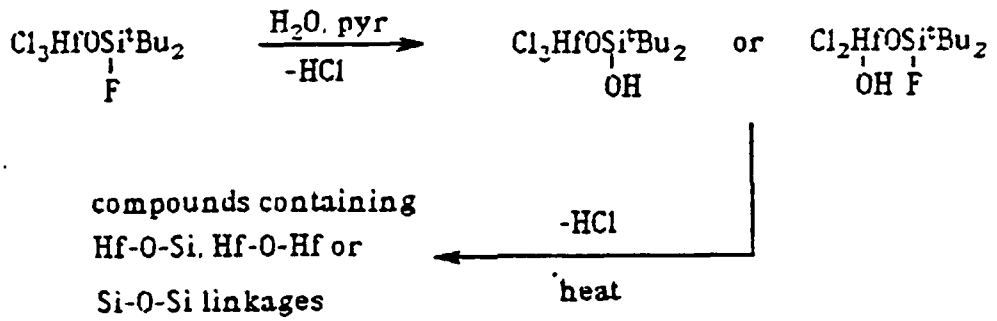

The steric bulk of the ^tBu groups should lead to small aggregates, or small ceramic-type particles, which could serve as precursors to new types of silicates:

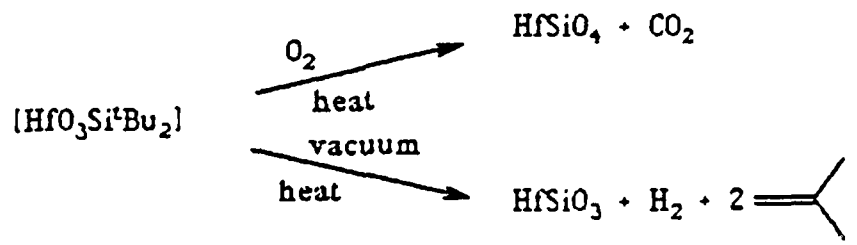

We have found a simple route to siloxides of Zr, Hf, Nb and Ta based on the general equation

$$MCl_x + HOSi^tBu_2 \underset{F}{} \longrightarrow HCl + MCl_{x-1}OSi^tBu_2 \underset{F}{}$$

At present we are working on the characterization of the Zr and Hf examples and exploring possible stoichiometries. With Nb and Ta, we can cleanly obtain the monosiloxides $MCl_4(OSiF^tBu_2)$. In the reaction of $TaCl_5$ with 3 equiv of $HOSiF^tBu_2$, $^tBu_2SiF_2$ is produced along with a tantalum compound which appears to have the structure:

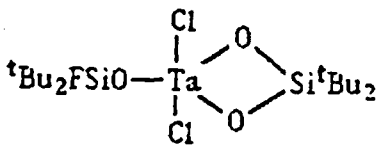

Our efforts to prepare early transition metal silicon compounds for oxidation-resistant coatings are continuing. As likely candidates are obtained, we will investigate their chemical attachment to carbon surfaces, and the oxidation protection that results. We have initiated this part of our study by carrying out reactions to attach hafnium species to a carbon surface. In these experiments, the surface of the carbon material is elecrochemically oxidized to give a high surface coverage of hydroxy groups. This chemically modified surface is then treated with $Hf(CH_2SiMe_3)_4$. We are presently analyzing the resulting carbon materials to evalute this method of attachment of organometallic species to a carbon surface.

REFERENCES

1. Garten V.A. and Weiss D.E., Australian J. Chem.,8,68 (1955).

2. Epstein B.D., Dalle-Molle E. and Mattson J.S., Carbon, 9, 606 (1971)

3. Engstrom R.C., Anal. Chem., 54, 2310 (1982).

TASK 3: CARBIDE AND NITRIDE MATRICES FOR CERAMIC MATRIX COMPOSITES

INTRODUCTION

The objective of this task is to investigate novel inorganic polymers as precursors for the production of high purity carbides and nitrides as matrix materials for ceramic matrix composites. The approach taken to date involves sol-gel processing of alkoxides such as tetraethoxysilane (TEOS) and triethoxyphenylsilane (TREPS) for the preparation of silicon carbide.

The sections below describe gel preparation, thermogravimetric and mechanistic features of silicon carbide formed by pyrolysis of TEOS - TREPS mixtures, and characterization of the pyrolysis products.

GEL PREPARATION

The morphology of the SiC formed during pyrolysis is governed by the polyorganosiloxane polymer formed during hydrolysis and condensation of the precursor materials. Various mixtures of TEOS and TREPS were studied to determine the optimum ratio for SiC formation. All other parameters during gel formation, such as water and ethanol concentration, amount of catalytic HNO_3 and temperature were kept constant.

Four mixtures of TEOS and TREPS were prepared with mole ratios ranging from 100% TREPS to 50% TEOS - 50% TREPS. A summary of these mixtures with their respective Si,O, and C contents is presented in Table 3-1. Assuming no loss of Si during the reaction, it is apparent that there is no need to study mixtures with significantly less than 50% TEOS because of a deficiency of carbon in the system.

Gels were prepared by adding 5ml water, 10ml ethanol, and 6 drops nitric acid to 0.041 moles of siloxanes. Solutions were stirred and heated to ~80°C. After 2-3 hrs. the mixtures had gelled and solidified. No further drying of these samples was performed.

TABLE 3-1

Compositions of the TEOS and TREPS Mixtures

Used in this Study

TEOS - TREPS Mixture (Mole % fractions)	Mole Ratios Si	O	C	Excess moles C*
0.0 TEOS - 1.0 TREPS	1	1.5	6.0	3.5
0.2 TEOS - 0.8 TREPS	1	1.6	4.8	2.2
0.4 TEOS - 0.6 TREPS	1	1.7	3.6	0.9
0.5 TEOS - 0.5 TREPS	1	1.75	3.0	0.25

* Assuming SiC and CO formation only and no loss of Si during the pyrolysis.

THERMOGRAVIMETRIC ANALYSIS

A high-temperature microbalance with product gas monitoring capabilities was set up as diagrammed in Figure 3-1. Samples were heated from room-temperature to 1500°C in argon at 5°C/min, monitoring weight-loss and the effluent gas stream.

The results of a typical microbalance run are shown in Figure 3-2. The three significant weight loss regions are identified in the figure.

During the first part of the temperature ramp, a modest weight drop occurs, due to loss of solvents, i.e. water and ethanol. Between 400°C and 600°C a rapid weight loss is observed. The major constituents of this loss are CO_2, H_2, benzene and other hydrocarbons including methane and ethane indicating a general decomposition of the polymer. After this carbonization step the material remaining is devoid of H and consists exclusively of C, Si and O. This material remains thermally stable until ~1300°C. At this temperature a rapid weight loss is evident accompanied by the emission of CO and formation of SiC.

A summary of the runs is compiled in Table 3-2. High-temperature data to 1500°C has been difficult to obtain, primarily due to breakage of hang-down wires and sample holders. Therefore, these data have not been included in the table at this time. Several features are significant for this set of data. The data are very reproducible between runs and are independent of the temperature ramp rate for the values explored. The higher the TREPS content, the greater the weight loss, due mainly to an increase in loss of CO_2. This is consistent with the data in Table 3-1 which shows a larger excess of carbon for the higher TREPS content.

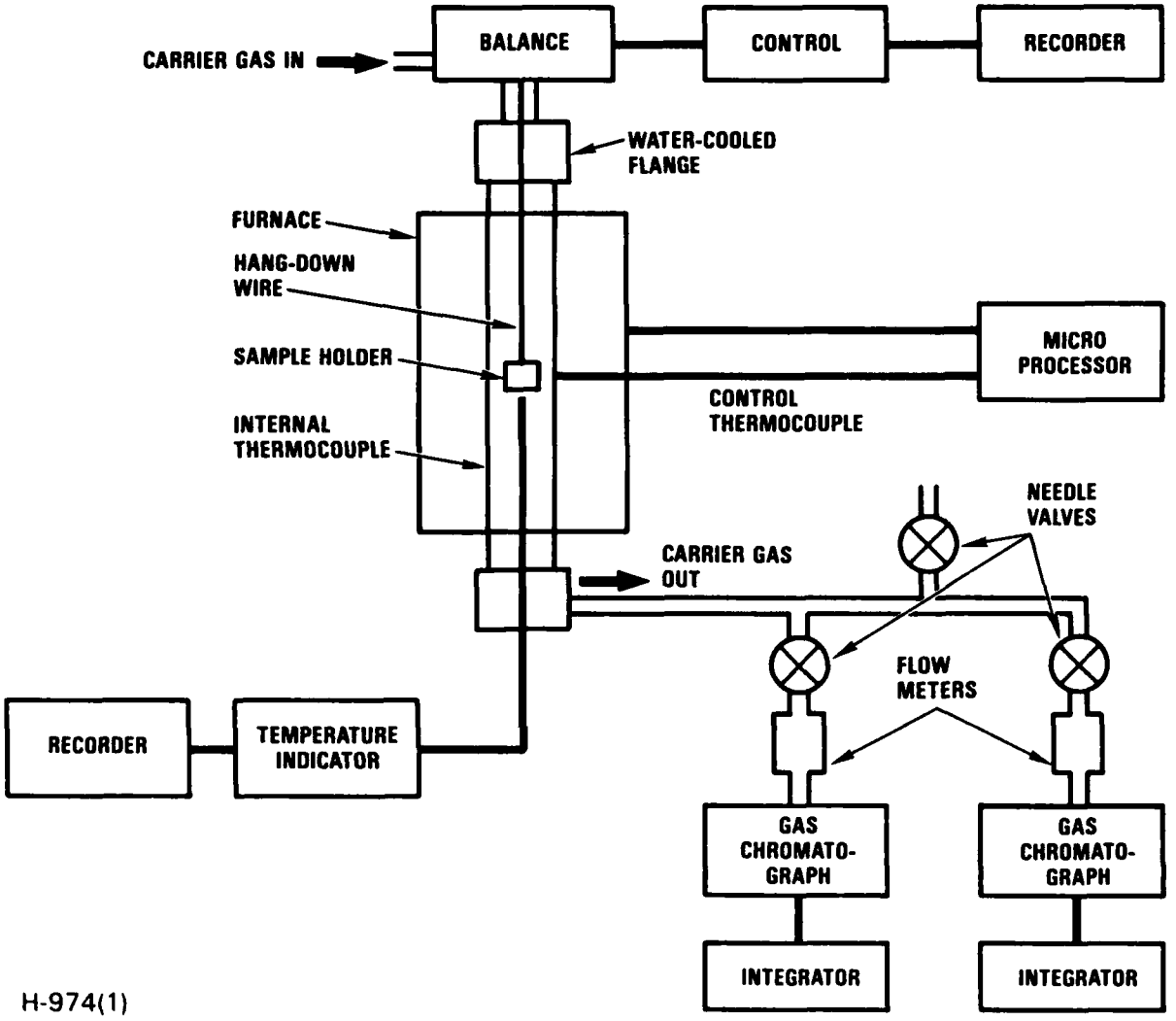

Fig. 3-1 High-Temperature Microbalance Apparatus

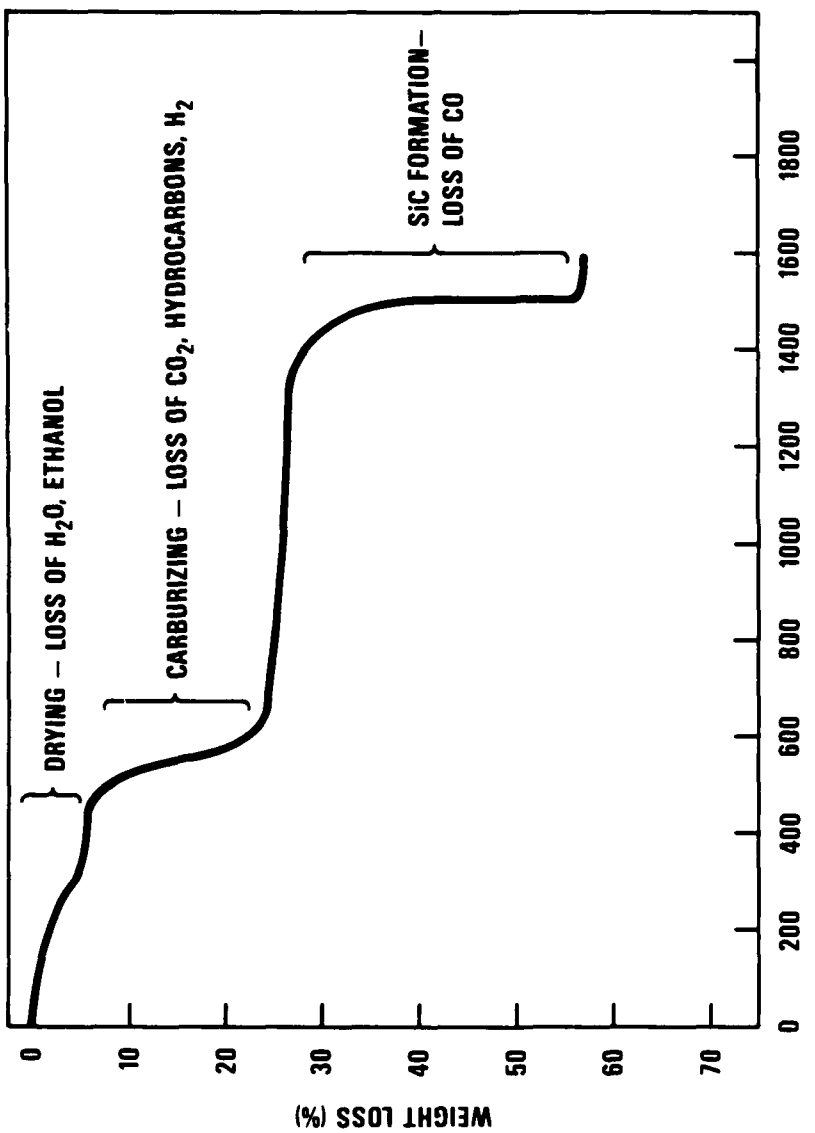

Fig. 3-2 Thermogravimetric Analysis of Treps Polymer, Showing Weight Loss Regions During Temperature Ramp of 5°C/Min in Argon

TABLE 3-2

Weight Loss Upon Heating to 1000°C

MOLE % TREPS	ID NO.	HEATING RATE °C/MIN	INITIAL WEIGHT (mg)	25 - 490°C WEIGHT LOSS (mg)	25 - 490°C WEIGHT LOSS FRACTION	490 - 1000°C WEIGHT LOSS (mg)	490 - 1000°C WEIGHT LOSS FRACTION
100	9604-76	5	986.0	218	.22	286.5	.189
	9331-73	5	498.1	129.2	.26	92.0	.185
	9331-64	5	501.4	128.3	.26	91.2	.182
	9331-16	5	24.81	6.41	.26	4.7	.189
	9331-49	10	525.5	136.1	.25	100.8	.192
	9331-43	10	504.8	128.0	.25	96.3	.191
Average							$.188 \pm .004$
80	9604-61	5	929.1	206.8	.22	155.0	.167
	9331-16	5	31.6	7.76	.24	5.26	.166
	9331-55	10	500.6	119.5	.24	83.1	.166
	9331-17	10	345.2	66.6	.19	55.4	.160
Average							$.165 \pm 0.003$
60	9604-71	5	950.9	197.0	.21	123.5	.130
	9331-16	5	32.62	7.33	.22	4.68	.143
	9331-37	10	500.0	104.9	.21	63.9	.128
Average							$.134 \pm .008$
50	9604-66	5	947.2	180	.19	101.0	.107
	9331-16	5	32.5	6.38	.20	3.70	.114
	9331-25	10	415.0	82.8	.21	45.0	.108
	9331-31	10	508			50.4	.099
Average							$.107 \pm .006$

3-7

PRODUCT CHARACTERIZATION

The pyrolysis product was characterized by several different techniques. X-ray diffraction data are displayed in Fig. 3-3 and reveal the presence of SiC. The shoulder before the (111) peak and the rather weak (200) peak indicate that the material is "disordered" β-SiC. The very low, broad peak centered near 25° is due to residual carbon in the sample. An analysis of the grade of SiC for the various TEOS/TREPS mixtures is in progress.

In an attempt to quantify the amount of the free carbon in the sample, the material was heated in oxygen to convert the carbon to gaseous products. Table 3-3 summarizes the experiments performed to date. In both cases where the gases were monitored the amounts of CO and CO_2 accounted for the total weight loss, indicating that no other reactions were taking place. This validated this method for carbon determination. For samples heated to at least 1400°C, the residual carbon content was in the 20 to 30% range.

Scanning electron micrographs of the SiC from TEOS/TREPS are shown in Fig. 3-4. The SiC was generally present in the form of large, irregularly shaped particles. The submicron whiskers seen in Figs. 3-4c and 3-4d were identified as SiC by selected area electron diffraction and x-ray diffraction. A TEOS/TREPS polymer particle is shown before pyrolysis in Fig. 3-5. Note that the particle morphology remained relatively unchanged during pyrolysis. The intimate mixing of silicon and carbon atoms on an atomic scale is most likely responsible for this phenomenon. For SiC formation, silicon and carbon atoms need to diffuse atomic distances only.

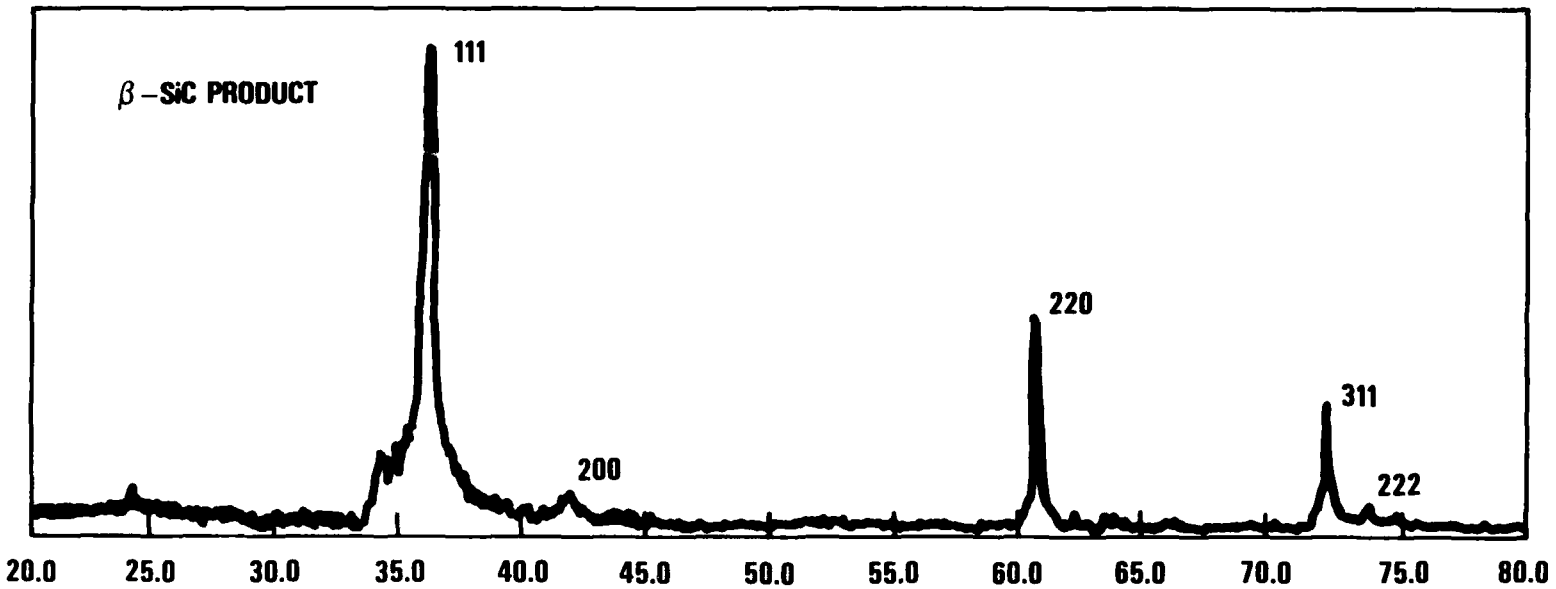

Fig. 3-3 X-ray Diffraction Pattern of Product Obtained from Pyrolysis of Treps Derived Sol Gel

TABLE 3-3

FREE CARBON DETERMINATION

MOLE% TREPS	ANNEALING TEMP (°C)	ANNEALING TIME (HR)	AIR OXIDATION MAXIMUM TEMP (°C)	INITIAL SAMPLE WT (mg)	WEIGHT CHANGE (mg)	WEIGHT LOSS FRACTION	CO EVOLVED (mg)	CO_2 EVOLVED (mg)	TOTAL CARBON LOST (mg)
100	1500	1.08	850	25.73	-8.0	.31			
100	1500	4.8	930	28.48	-7.76	.27			
100	1500	0.37	604	38.60	-6.9	.18	5.39	15.5	6.5
80	1500	1.0	595	30.42	-5.1	.17	2.98	14.9	5.3
80	1495	1.5	750	19.28	-3.8	.20			
50	1440	1.2	995	37.07	-8.68	.23			
50	1500	6.46	800	19.85	+0.3	--			
50	1000	--	900	32.23	-8.90	.28			

3-10

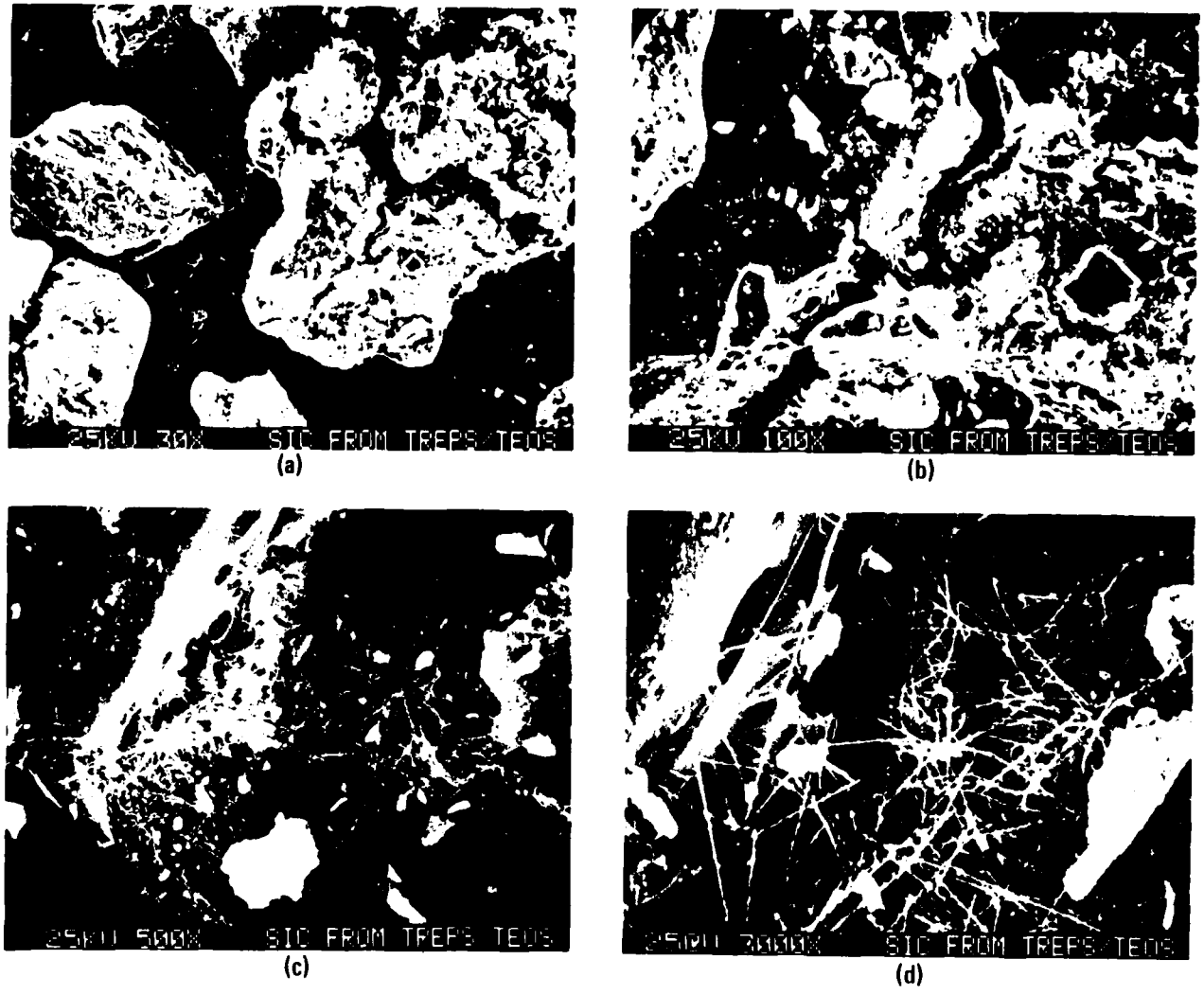

Fig. 3-4 Silicon carbide from TREPS/TEOS

P42-357

Fig. 3-5 Polymer made by mixing TREPS:TEOS: H_2O=1:1:10 (mole ratio) gelling at 80°C, and drying at 150°C/16h (302°F/16h).

One problem with the material produced in the above fashion is that it does not readily form monolithic pieces. Several approaches to overcome this problem are under investigation. One is to add sintering agents at the pyrolysis step. These attempts have been unsuccessful so far.

Adding monomers to the gel in order to fill the pores is a possibility currently under investigation. The monomers polymerize in the pores to fill the void volume and result in a decrease of open porosity.

Control of the drying step might lead to better materials because a lot of the porosity is developed during this step. Studies to confirm this are in progress.

MECHANISTIC FEATURES

Solid reactions have usually been analyzed in terms of structural or distributed models. The former class of models are based on the behavior of the individual grains of a solid matrix. The distributed models are based on an analysis of reaction and diffusion in the solid as a whole.

In practical kinetic investigations of processes involving at least one solid reactant the rate equation is based on the fraction (α) of the sample reacted in the following way:

$$\text{reaction rate } \frac{d\alpha}{dt} = k(T)\ f(\alpha) \quad , \tag{1}$$

where f (α) denotes a function, t is the time and k is the rate coefficient which is a function of the absolute temperature, T.

Many forms of f(α) relating the fraction of reaction of total product formed to the time of reaction have been proposed. Sharp, et al, have divided these equations into four basic categories (Ref. 1). The first is based on "diffusion-controlled reactions" in which the rate is dependent on diffusion of reactants to the raction sites or on diffusion of products away from the reaction site. Typical of this catagory are the models of Carter (Ref. 2) and Gistling and Brounshtein (Ref. 3) which assume that reaction in a sphere is controlled by diffusion through an increasing product layer. Then

$$1 - [2/3\ \alpha\ + (1 - \alpha\ )^{2/3}] = \frac{kt}{2r_o} \quad , \tag{2}$$

where r_o is the radius of the sphere.

In the second category are kinetic equations based on the "concept of an order of reaction." Some solid state reactions fall in this category because they appear to follow first order kinetics. For first

order kinetics

$$\ell n\ (1-\alpha) = -kt \quad . \qquad (3)$$

The third category, "phase boundary reactions," are controlled by movement of an interface at a constant velocity. For this catagory, McKewan (Ref. 4) shows that when the rate of reaction is proportional to the surface area of the unreacted core, equation 4 is obeyed, where ki is the initial rate coefficient.

$$1 - (1 - \alpha)^{1/N} = \frac{k_i t}{r_o} \quad . \qquad (4)$$

The final category is "Avrami-Erofe'ev Equations," in which nucleation and growth of the reactant sites are the limiting processes. As the reactant sites become larger they eventually impinge on each other and growth ceases where they touch. Avrami (Ref. 5) and Erofe'ev (Ref. 6) have given the following equation for this case:

$$\sqrt[N]{-\ell n\ (1 - \alpha)} = k_A\, t \quad . \qquad (5)$$

In the latter two equations the value of N is 2 if the reaction sites are circular disks or cylinders and 3 if reacting if the sites are spheres.

Experimental kinetic data are obtained as tabulations of α versus time. For thermogravimetric data, α is equal to the ratio of the change in weight at any time after the decomposition begins to the total weight change at the completion of the transformation.

By using the reduced time $t/t_{0.5}$, where $t_{0.5}$ is the time to 50% reaction, Eqs. 2-5 can be compared directly to the experimental data. In this way, the category of the reaction mechanism can be selected. Differentiation within each reaction category requires very careful and precise measurements and is usually not possible. In addition, mechanisms based on phase boundary reactions are not easily distinguishable from first-order kinetics.

Shown in Figure 3-6 is the fractional decomposition as a function of the reduced time for the high temperature (1500°C) transformation of a gel derived from TREPS. Along with the experimental data (plotted as O) is the predicted fractional reaction assuming (1) an Avrami-Erofe'ev nucleation and growth mechanism (--); (2) a phase boundary or first order kinetic process (-); and (3) a diffusion mechanism (----). Our data show that the decomposition of the TEOS/TREPS polymers is most consistent with the nucleation and growth mechanism.

The analysis of kinetic data with the reduced time is a technique used under isothermal conditions. We have not measured the rate of decomposition of the TEOS/TREPS polymers under isothermal conditions in the low temperature (400-700°C) carbonizing regime. Several models for obtaining kinetic parameters of transformation occuring in a controlled linear heat rise have appeared in the chemical literature. It is planned to review these models in hopes that more complete mechanistic implications can be obtained for the carborizing decomposition.

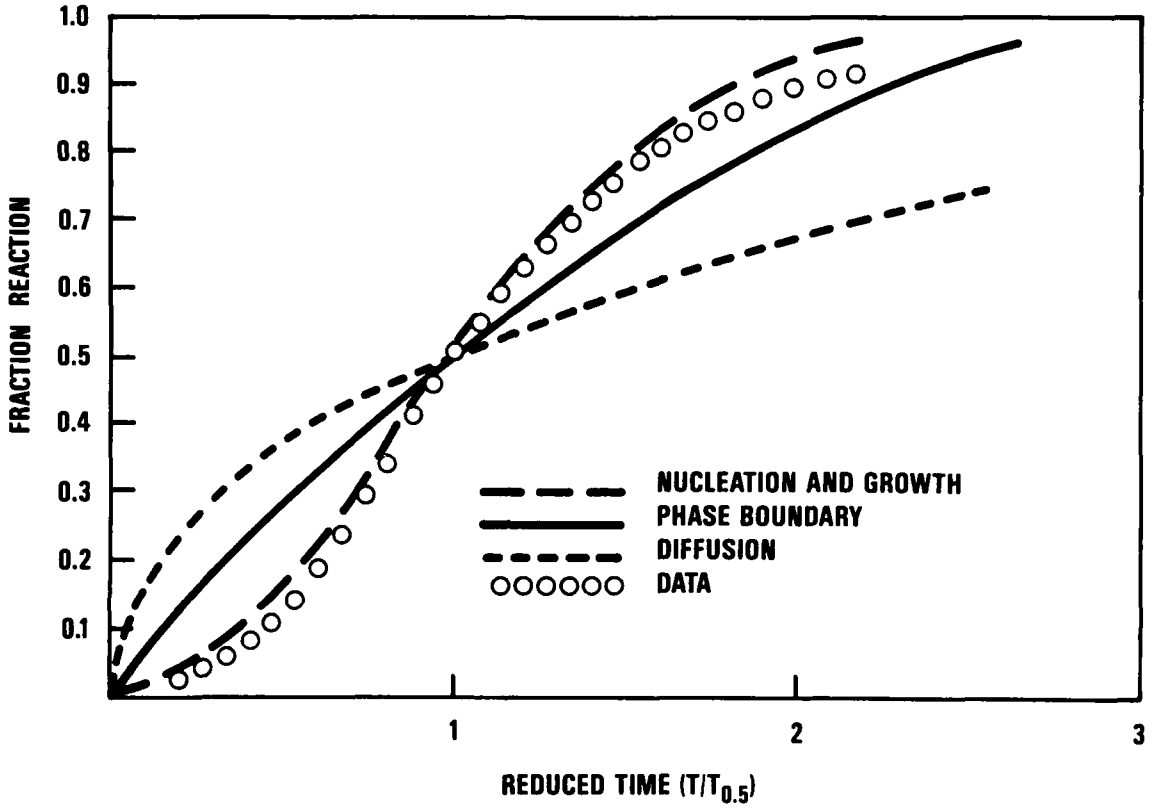

Fig. 3-6 High Temperature Formation of SiC from Polymeric Precursors Follows Nucleation and Growth Mechanism.

SUBCONTRACT TO TASK 3

UNIVERSITY OF CALIFORNIA AT LOS ANGELES SUBCONTRACT

FORMATION OF SILICON CARBIDE BY SOL-GEL METHODS

1. INTRODUCTION

In 1984, UCLA was approached by Dr. George Reynolds of GA Technologies, Inc. to be a collaborator on a research proposal to the U.S. Air Force of Scientific Research entitled "Studies in Support of Oxidation-Resistant Composite Materials." The UCLA program, involving the equivalent effort of only a part-time graduate student under the supervision of Professor J.D. Mackenzie., was to study the possibility of the preparation of silicon carbide by the sol-gel method. The UCLA proposal was approved in 1985 but authorization to commence work was not made until January 1986. This is the final technical report for the one-year research program at UCLA.

2. TECHNICAL APPROACH

The sol-gel method offers a number of potentially useful approaches to the preparation of ceramic matrix composites. First, a starting liquid solution of fairly low viscosity can be used as a precursor for injection into an array of ceramic fibers. The solution can be rendered into a gel at low temperatures (room temperature, for example) and later fired at relatively low temperatures. Porosity can be minimized by back-fill and/or by pressure. Almost all sol-gel processes involve the use of alkoxides such as a tetraethoxysilane (TEOS), which after gelation and firing forms SiO_2. In order to prepare SiC, alternative approaches must be used. Because this was only a small exploratory program, the approach had to be simple and would have to furnish some definitive results within a year. It was therefore proposed to identify and to use a readily available metal-organic precursor as a starting raw

material. Diethoxydimethylsilane, $(CH_3)_2Si(OEt)_2$(DEDMS) was readily available from Alfa Products, Inc. It was thus selected for our preliminary experiments. It would be hydrolyzed and then polymerized via the two ethoxy groups. Silicon-carbon bonds were already present at the Si-Me sites. The resulting gel would then be pyrolyzed in vacuum or in an inert atmosphere. It was understood that the formation of SiC from this reaction is a highly complex process. However, the results obtained would provide a guidance for further work.

3. RESEARCH PERFORMED

3.1. SOLUTIONS FROM DIETHOXYDIMETHYLSILANE (DEDMS)

Theoretically, solutions containing DEDMS, water ethanol and a catalyst should react to yield a gel after polycondensation. However, after a number of attempts, gelation was not obtained. The compositions of the various liquids studied are given in Table 1. Even after prolonged overnight stirring, all these solutions separated into a two phase system, with a viscous liquid layer at the bottom and a fluid liquid layer on top. The top layer contained mostly ethanol and water. The bottom layer of viscous liquid was separated for further aging and heat treatment. Aging, however, did not "solidify" this viscous liquid even when excess amounts of water were used, indicating gelation did not occur because of insufficient hydrolysis and polymerization. The reason for the lack of gelation had to be the bi-functional nature of the diethoxydimethylsilane. During pyrolysis, the viscous liquid evaporated, and only minor amounts of residual solids remained.

Several more solutions were prepared to further explore the possible existence of a miscible region in the DEDMS-Ethanol-Water ternary system. It was found that most of the combinations of these three components were immiscible in this ternary system (Fig. 1., solid circles). Only combinations with small amounts of water gave homogenous solutions (Fig. 1, open circles). However, at these low concentrations of water, it was not possible for the hydrolysis reaction to proceed to completion. Even for these apparently homogeneous solutions only

Table 1. Experimental conditions for the preparation of SiC from diethoxydimethylsilane (DEDMS) .

MOLAR RATIO	DEDMS	1	1	1	1	1
	EtOH	1	2	3	4	8
	H_2O	2	2	2	2	2
HCl						
0.03		#11203	#12203	#13203	#14203	#18203
0.1		#11210	#12210	#13210	#14210	#18210

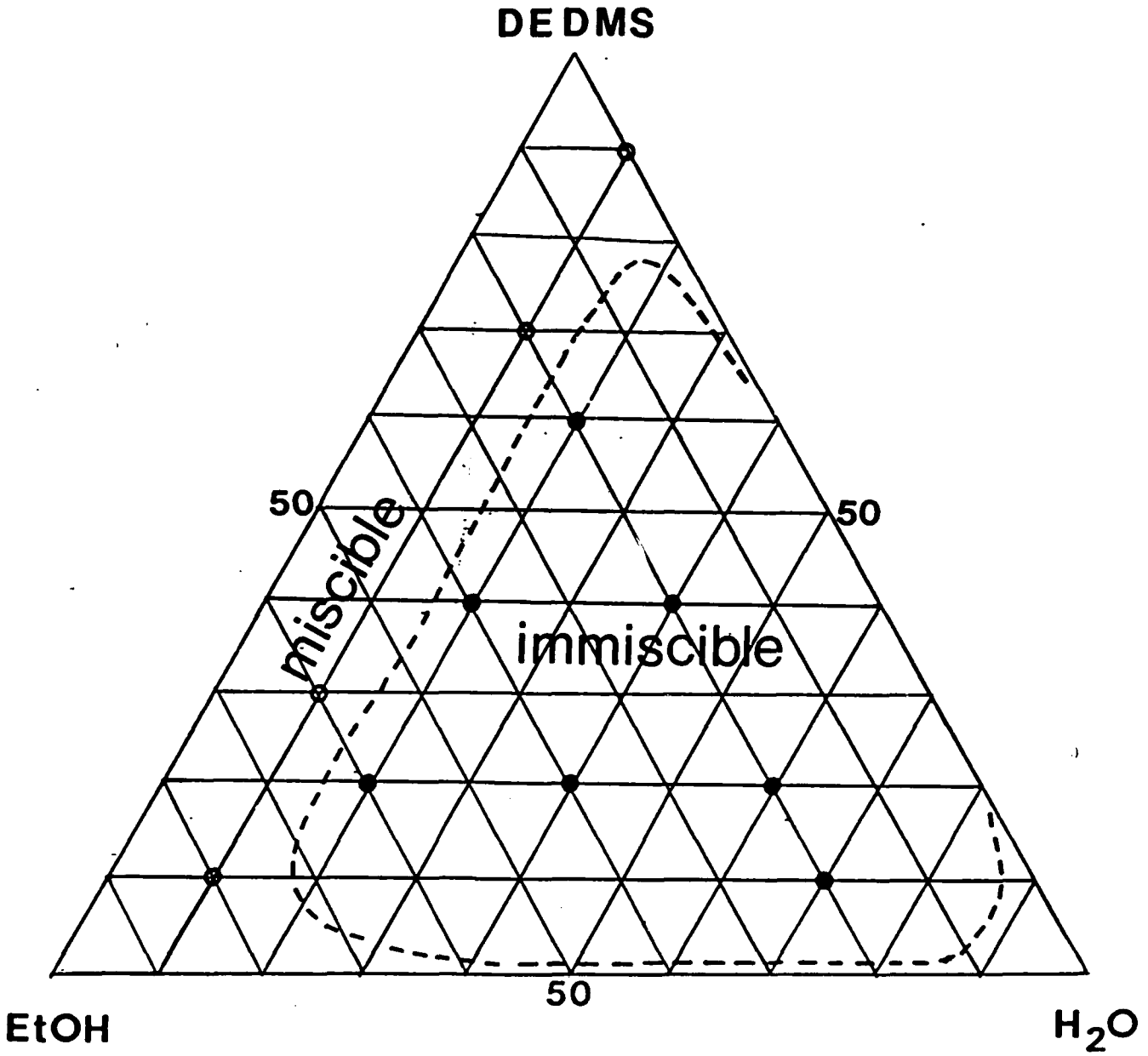

Figure 1: Homogenous miscible region in diethoxydimethyl silane-ethyl alcohol and water ternary system.

viscous liquids were obtained after aging for three months. Therefore, it was concluded that DEDMS by itself could not be used to form bulk gels.

To better understand the reason for the absence of gelation in the system based on DEDMS, the structure of the viscous liquids obtained from hydrolysis was examined in infrared absorption. The spectra obtained were similar to that of polydimethylsiloxane, a silicone oil (Fig. 2). The spectra showed the Si-CH_3 vibration of 1260 cm^{-1} and Si-O-Si stretching vibration at 1015 and 1090 cm^{-1}, $Si(CH_3)_2$ vibration at 800 cm^{-1} and Si-O-Si bending vibration at 390 cm^{-1}. This material was reported to have approximately 40% octamethylcyclosiloxane as a major constituent (1). This octamer evaporated and decomposed when heated at 900°C under nitrogen atmosphere yielding no solid residue. We then decided to examine a precursor with three ethoxy groups. Triethoxyphenylsilane (TREPS) was selected.

3.2. SOLUTION FROM TRIETHOXYPHENYLSILANE (TREPS)

Triethoxyphenylsilane solutions readily gave solid, clear gels for the conditions studied (Table 2). However, when the gels were heated, they first melted, and after the liquids thermally decomposed only black foamy solids remained. Because of the melting TREPS could not be used by itself. This melting was unexpected for a three functional group molecule. This phenomenon could be explained by the bulky benzene rings which prevented complete polymerization.

One possible way to overcome melting of the TREPS and to obtain gelation of the DEDMS might be to add tetraalkox ysilanes, such as tetraethoxysilane TEOS to increase the "rigidity" of the gels. This would occur because a molecule of the DEDMS has only two reactive (ethoxy) functional groups; hence, even with complete hydrolysis and polymerization only linear and cyclic oligomers or polymers are possible, and no three dimensional extended gel network structure can be achieved. With the addition of a tetrafunctional TEOS, the inorganic-organic polymer becomes branching, and a rigid three

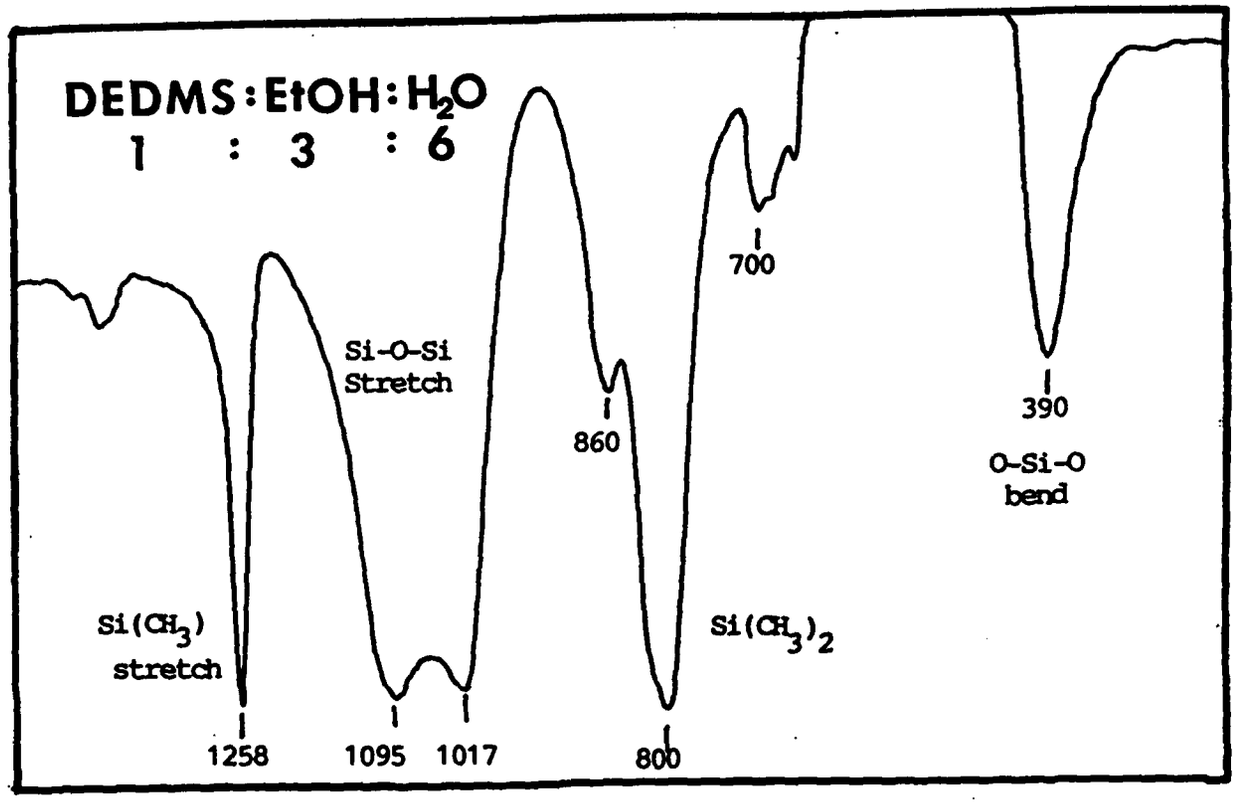

Figure 2: Infrared spectra of the polydimethylsiloxane prepared from the hydrolysis and polymerization of diethoxydimethylsilane

Table 2. Experimental conditions for the preparation of SiC from triexthoxyphenylsilane (TREPS).

MOLAR RATIO	TREPS	1	1	1	1	1	1	1
	EtOH	0	0	1	1	1	2	4
	H_2O	2	4	2	3	4	2	2
HCl								
0.00		#10200	#10400	#11200	#11300	#11400	#12200	#14200
0.01		#10201	-	-	-	-	-	-
0.05		#10205	-	-	-	-	-	-

dimensional structure might be obtained. The same considerations also apply to TREPS.

3.3. SOLUTIONS FROM TRIETHOXYVINYLSILANE (TREVS)

Gels were readily obtained from triethoxyvinylsilane. Therefore, studies were performed on this compound (Table 3). It was found that excess ethanol aided homogenous mixing. While an HCl catalyst also aided mixing, large amounts of acid (larger than 0.1 molar ratio of catalyst to starting compound) caused immediate precipitation of a white solid phase. These white precipitates settled as a layer at the bottom of the clear gel. The clear gel hardened and turned yellowish upon drying. These gels were subsequently heat-treated at elevated temperatures to see if crystalline silicon carbide could be obtained.

3.4. SOLUTIONS OF MIXTURES OF DIETHOXYDIMETHYLSILANE AND TETRAETHOXYSILANE

The addition of TEOS to DEDMS in 1 to 1 molar ratio, as expected, gave rigid clear gels. Even without the addition of the HCl catalyst, gelation could be achieved. Monolithic gels were easily obtained. These gels were eventually heat treated at temperatures up to 1550°C to obtain silicon carbide. The compositions of the solutions studied are shown in Table 4.

3.5. CONVERSION OF GELS TO SiC

The conversion of the gels into SiC was carried out in a controlled-atmosphere, high-temperature furnace. This furnace was specially constructed for this research project and has the capability of firing samples up to 1600°C under a nitrogen or argon atmosphere. The furnace is shown in Fig. 3.

From the solution and gelation study, it was found that the bulk gel can be successfully prepared by the use of DEDMS and TEOS in 1/1 and 2/1 (i.e. 1/0.5) molar ratios as described in the previous section. Fig. 4

Table 3. Experimental conditions for the preparation of SiC from triethoxyvinylsilane (TREVS).

MOLAR RATIO	TREVS	1	1	1	1	1	1	1
	EtOH	0	0	1	1	2	3	5
	H_2O	2	3	2	3	2	2	2
HCl								
0.00		#10200	-	#11200	-	-	#13200	#15200
0.007		#102007	-	-	-	-	-	-
0.01		#10201	-	#11201	-	-	#13201	#15201
0.05		#10205	#10305	#11205	#11305	#12205	#13205	#15202
0.08		#10208	-	#11208	-	-	-	-
0.10		-	-	#11210	-	-	-	-
0.15		#10215	-	#11215	-	-	-	-
0.20		#10220	-	-	-	-	-	-

Table 4. Experimental conditions for the preparation SiC from the mixtures of diethoxydimethylsilne (DEDMS) and tetraethoxysilane (TEOS).

MOLAR RATIO	DEDMS	1	2	1	2
	TEOS	1	1	1	1
	H_2O	10	10	6	8
HCl					
0.00		#111000	#211000	#11600	#21800
0.01		-	-	-	-

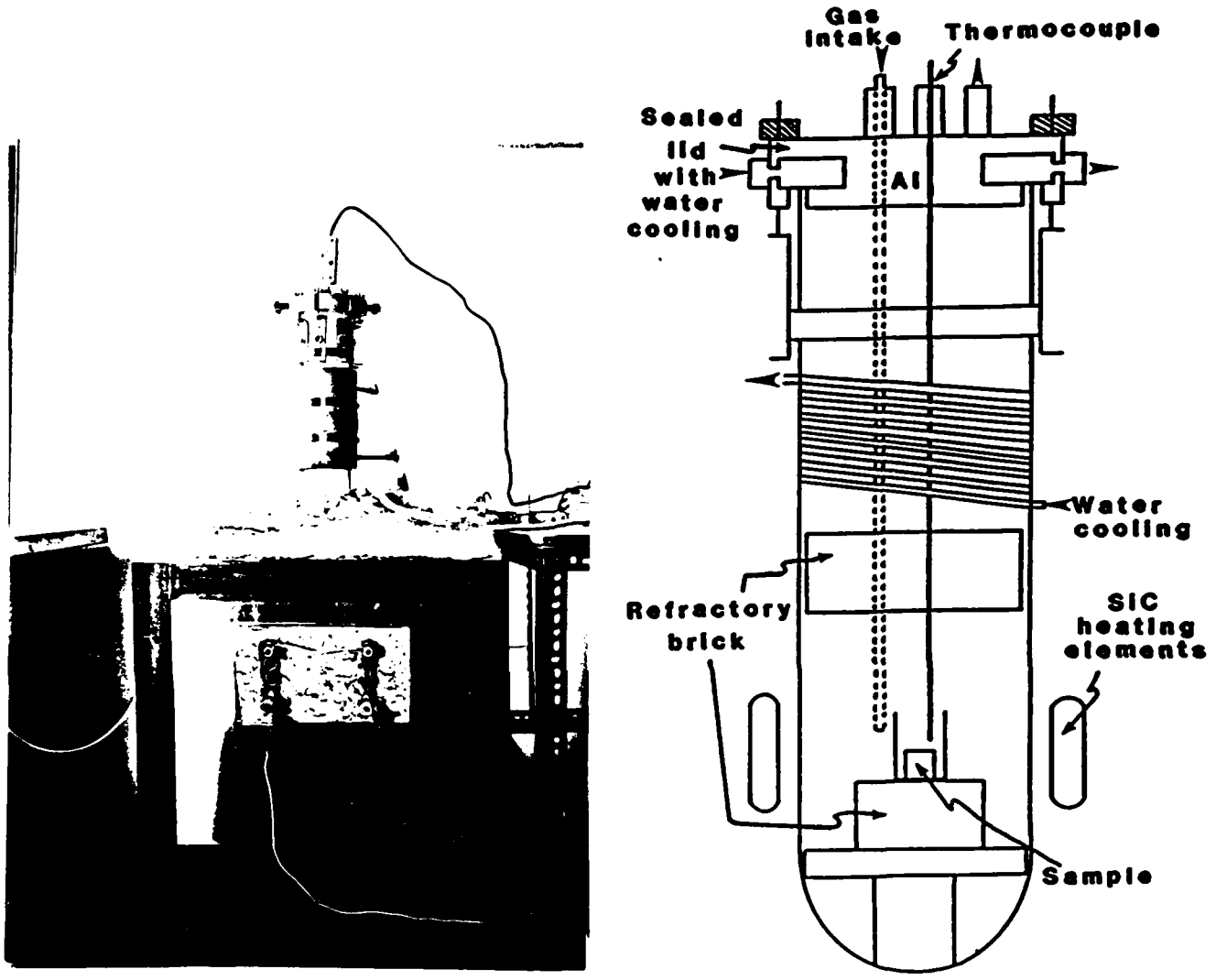

Figure 3: A controlled atmosphere, high temperature furnace designed and built at UCLA.

shows a monolithic gel piece of the 2/1 composition. The gel retained its shape with little shrinkage and was mechanically strong after annealing at 1600°C for 10 hours. X-ray diffraction indicated the presence of beta-silicon carbide in this material.

3.6. CRYSTALLIZATION OF TRIETHOXYPHENYLSILANE AND TETRAETHOXYSILANE IN 1/1 MOLAR RATIO

The mixture of TREVS and TEOS in a 1/1 molar ratio, which formed a clear bulk gel, was heat treated stepwise at 200°C for 5 hours, 300°C for 14 hours, 500°C for 12 hours, 700°C for 12 hours, 900°C for 2 hours and finally at 1300-1600°C for different periods of time. Despite the large amount of carbon in a benzene ring, no crystalline silicon carbide phase was detected, as shown in Fig. 5. This indicated that the benzene ring easily broke away from the gel structure so that excess carbon was not retained in the gel structure. This phenomenon has also been observed by the research group at GA Technologies, Inc, San Diego. In their work, they have shown that more than 1 to 1 molar ratio of TREPS to TEOS was needed for SiC formation on pyrolysis. The ease of splitting of the phenyl group could be clearly seen from the infrared study of the heat-treated gels.

3.7. CRYSTALLIZATION OF DIETHOXYDIMFTHYLSILANE AND TETRAETHOXYSILANE IN 1/1 AND 2/1 MOLAR RATIOS

In gels prepared from DEDMS and TEOS, silicon carbide (beta form) was first observed after 1 hour of heat treatment at 1550°C in N_2 where small amounts of beta-SiC and an amorphous broad peak located at about 21° were observed in X-ray diffraction (see Fig. 6). This indicated that silicon carbide had begun to nucleate from the amorphous phase. Therefore, a higher annealing temperature or a longer heat treatment time was necessary to obtain more SiC. The gel was thus further heat treated for one more hour (total of 2 hours), and the amount of SiC did increase. However, some other minor phase(s) also appeared. The new diffraction peak positions were near to, but not exactly at, the peak positions for Si_2N_2O and Si_3N_4. Further study will be needed to

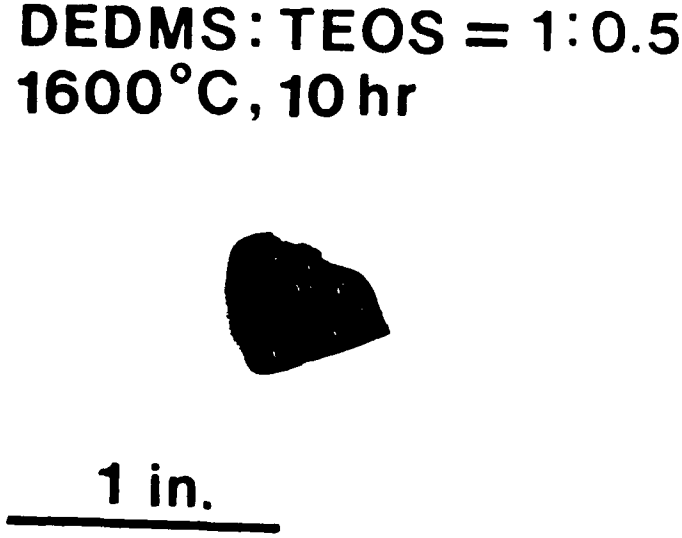

Figure 4: Monolithic β-silicon carbide obtained from the pyrolysis of diethoxydimethyl silane and tetraethoxy silane at a 1:0.5 mole ratio heat treated at 1600°C for 10 hours.

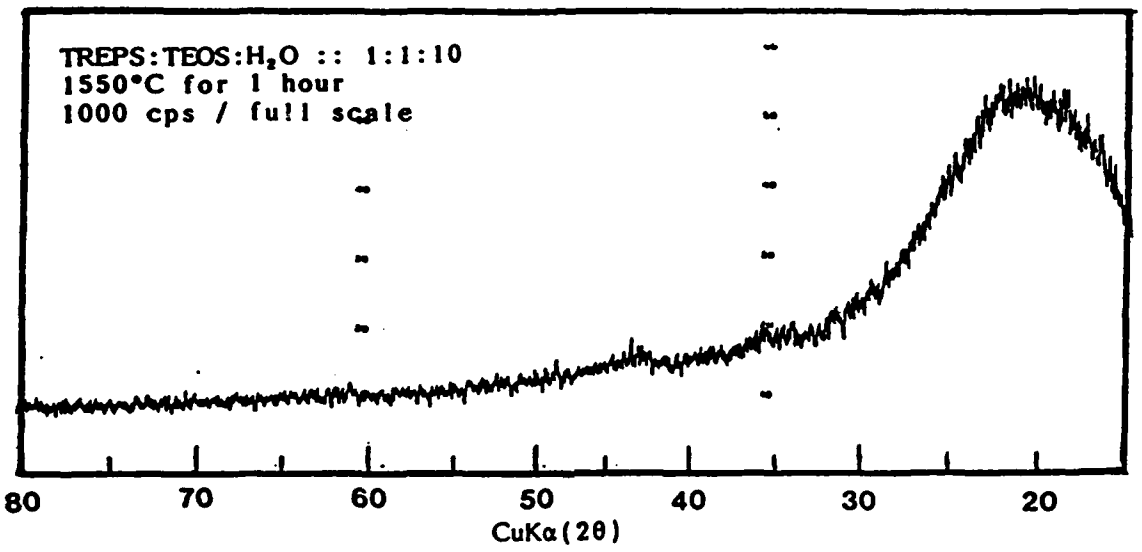

Figure 5: X-ray diffraction pattern of triethoxy(phenyl) silane and tetraethoxy silane in a 1:1 mole ratio heat treated at 1550°C for 1 hour.

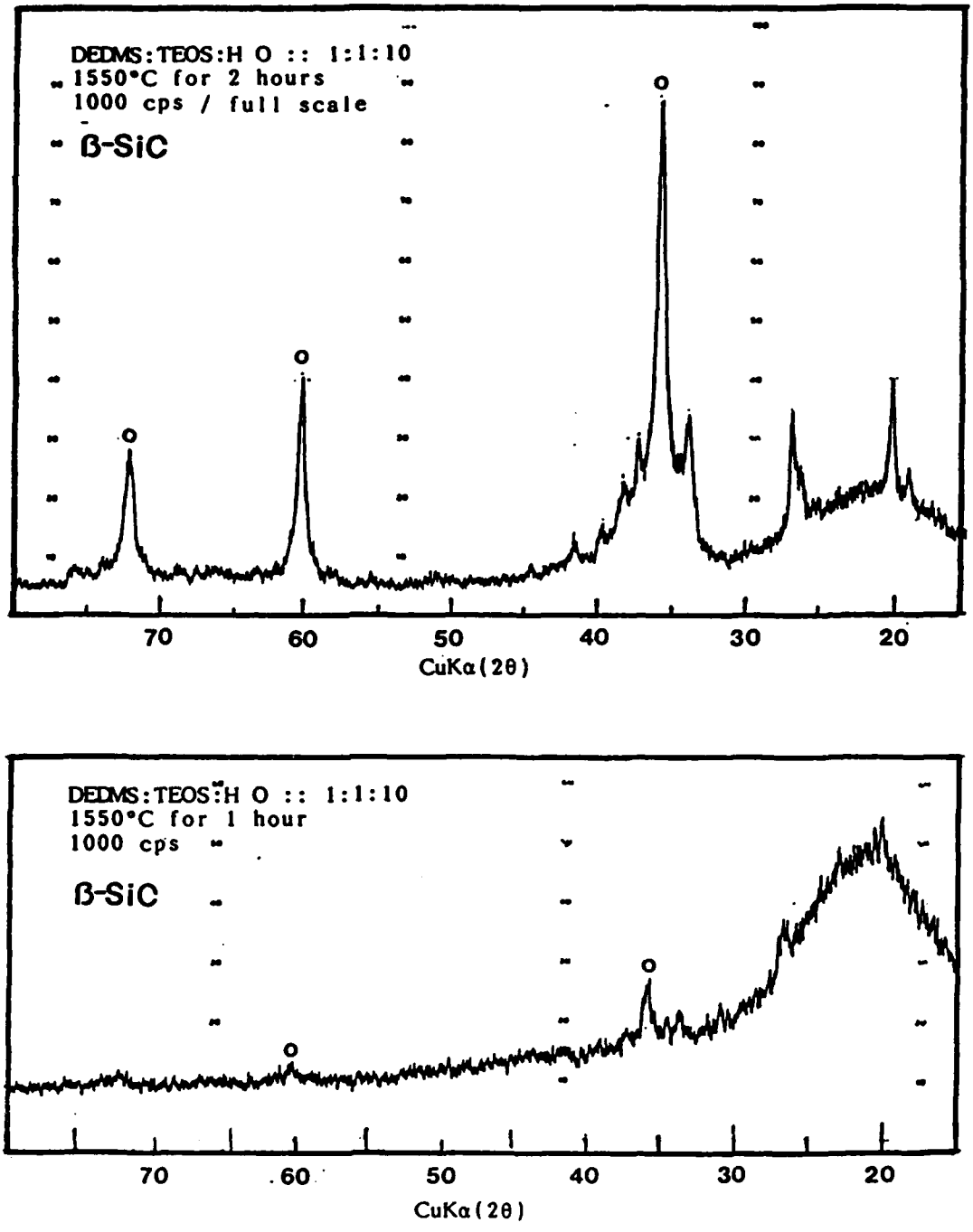

Figure 6: X-ray diffraction pattern of diethoxydimethyl silane and tetraethoxy silane in a 1:1 mole ratio heat treated at (a) 1550°C for 2 hours and (b) 1550°C for 1 hour.

identify these phases. If the phases are indeed nitrogen containing compounds, they probably were produced by the use of a nitrogen atmosphere during annealing.

In order to increase the yield of SiC, it was desirable to decrease the oxygen content of the gel structure. Therefore, the ratio of DEDMS to TEOS was increased to 2:1 (i.e. 1:0.5). This solution was homogenous and formed a bulk gel after drying. After calcining at 1600°C for 10 hours, the amount of beta SiC was unexpectedly (Fig. 7) lower than that of the 1:1 ratio solution, and a considerable amount of amorphous phase was still present. The reason of this discrepancy is not clear. From the broadening of the X-ray diffraction peaks, the SiC crystal size was also smaller than that of the 1:1 sample.

3.8. INFRARED STUDY OF THE TRANSFORMATION OF GELS TO SILICON CARBIDE

In order to understand the influence of the starting compounds on the gels structure after drying and after heat treatment, infrared studies on gels were initiated. In this study the decomposition of the organic functional groups, such as methyl and phenyl, and the formation of the Si-C bonding were monitored.

3.8.1. TRIETHOXPHENYLSILANE (TREPS) AND TETRAETHOXYSILANE (TEOS) SYSTEM

The infrared spectra of TREPS and TEOS in equal molar ratio with an excess amount of water (7 mole per mole of TREPS) are shown in Fig. 8. At the dried stage, curve (A), the existence of phenyl groups can be clearly seen at 1430s, 1130-1100s, 1030w, 995w, cm^{-1} for the Si-(C_6H_5) (s: strong, m: medium, w: weak), and polysiloxanes are seen at 735s and 697s cm^{-1}. These bands are marked by a * in the figure. The 1130-1110 cm^{-1} band also overlaps with the Si-O-Si stretching vibration. The broad Si-O-Si absorption band indicates that the siloxane chain is long or branched. The 950 to 810 cm^{-1} absorption bands arise from Si-OH stretching or from Si-O stretching. The band located at 800 cm^{-1} is attributed to the ring structure of tetrahedral (SiO_4).

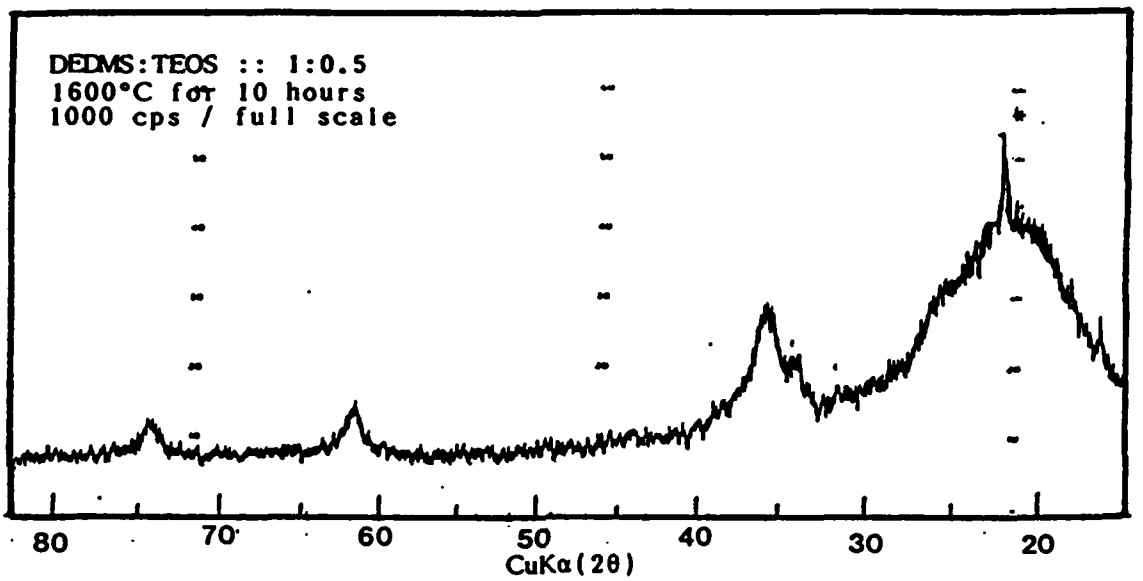

Figure 7: X-ray diffraction pattern of β-silicon carbide from the pyrolysis of diethoxydimethyl silane and tetraethoxysilane prepared at a 1:0.5 mole ratio heat treated at 1600°C for 10 hours. (*cristobalite)

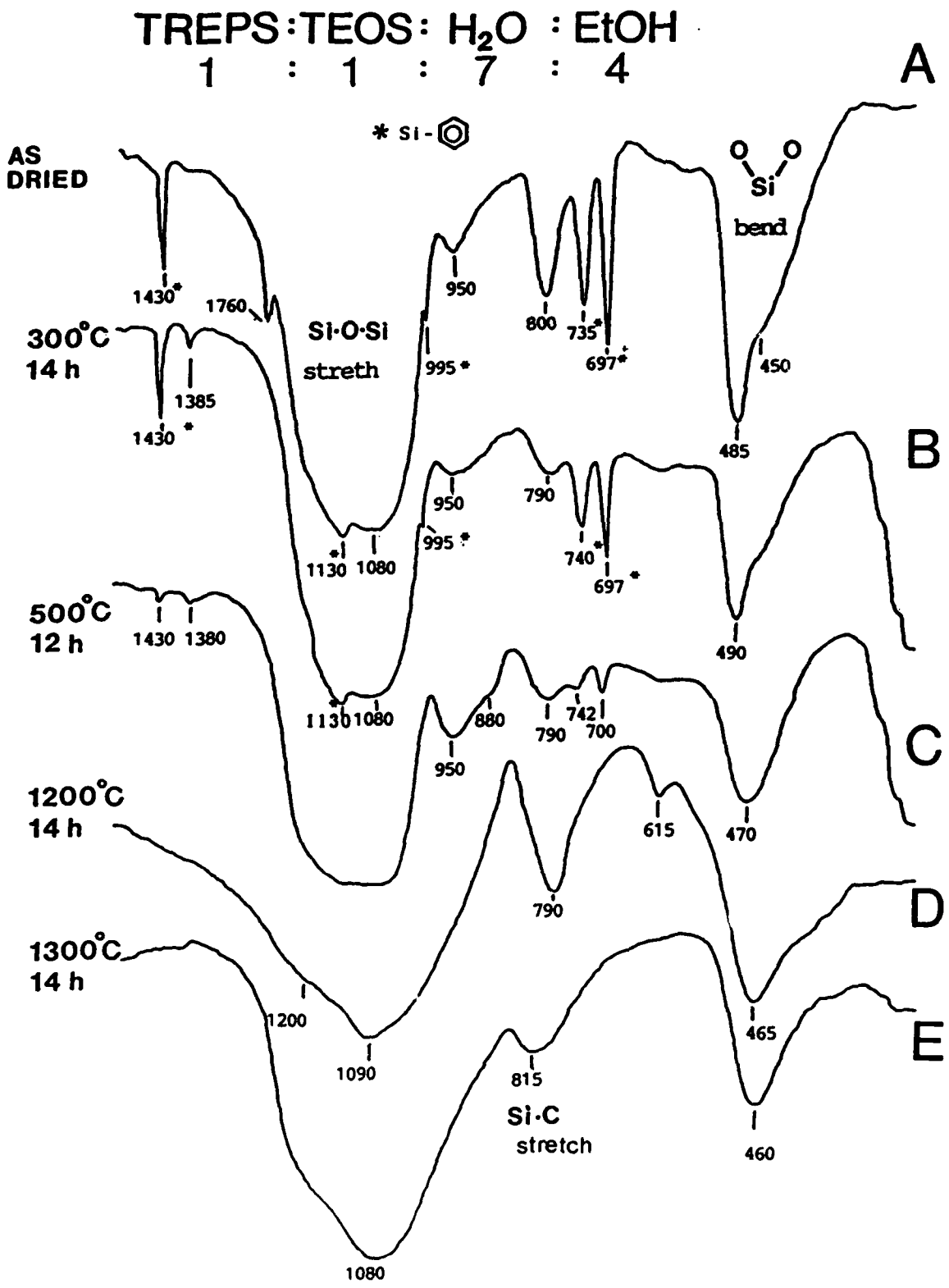

Figure 8: Infrared spectra of gels heated at different temperatures and times.

After 14 hours at 300°C, the gel structure still contained phenyl vibrations. Thus, the decomposition of the phenyl group was not significant (Curve B). For the 500°C sample, the intensities of the absorption bands of phenyl groups had decreased, and the 950 cm^{-1} band intensity had increased. However, the expected Si-C vibration center around 815-800 cm^{-1} did not appear. Therefore, most of the phenyl groups had probably been released as intact benzene rings. But not all the phenyl groups were lost since the Si-C vibration did appear in the 1300°C, 14 hours sample (Curve E). Furthermore, the sample remained black in color indicating the existence of some carbon in the gel structure. At an intermediate temperature of 1200°C (Curve D) the gel still showed strong absorption bands for Si-O-Si at 1090 cm^{-1}, 950 cm^{-1} and 485 cm^{-1}. This means the oxygen was not successfully removed from the structure by decomposition of the phenyl group. It is interesting to note that in curve (A) the 485 cm^{-1} band shifted to 460 cm^{-1} in curve (E). The final position at 460 cm^{-1} is identical to the Si-O bending vibration in fused silica. The shifting to 485 cm^{-1} at the dry gel state indicates the local influence of Si-(C_6H_5) in the vibration. Hence intimate mixing at the molecular level had been achieved. In curve E, except for the medium intensity 815 cm^{-1} band of Si-C, the entire spectra was essentially the same as that of silica gel (8).

To better understand the effects of the addition of excess amounts of water, we also studied one series of TREPS/TEOS in equal molar ratio with 10 moles of water per mole of TREPS instead of 7 moles (Fig. 9). The decomposition of phenyl at around 700°C was still visible. At 900°C, the spectra was the same as that of silica gel. However, at 1500°C - 1550°C, crystallization occurred as shown by the bands located at 500-300 cm^{-1} for cristobalite. It was concluded that excess amounts of water would enhance the crystallization of the silica phase.

3.8.2. DIETHOXYDIMETHYLSILANE (DEDMS) AND TETRAETHOXYSILANE (TEOS) SYSTEM

Figure 10 shows the infrared spectra of gels from DEDMS and TEOS in a 1 to 1 molar ratio. The bands at 1275, 830 and 790 cm^{-1} are attributed to

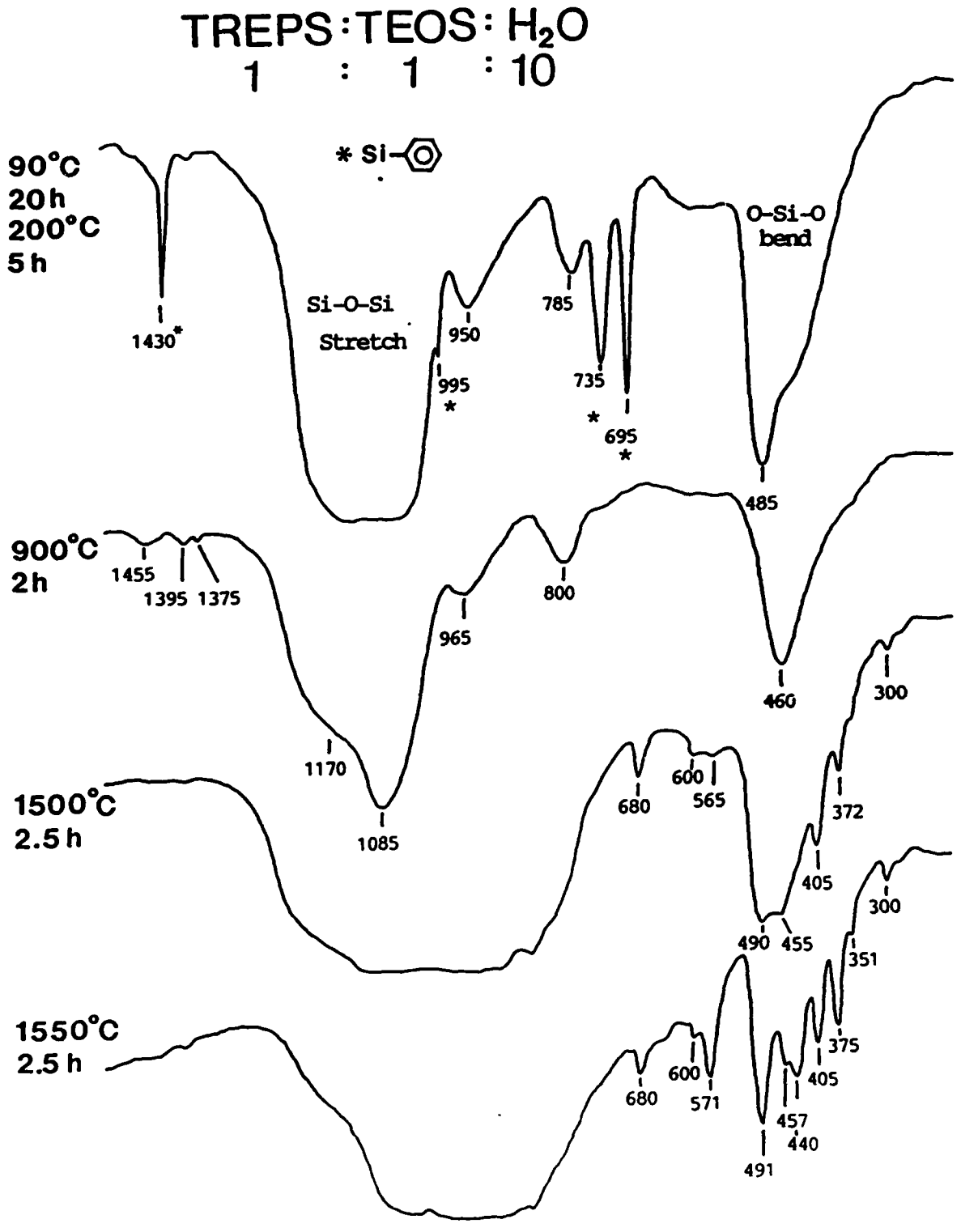

Figure 9: Infrared spectra of gels heated at different temperatures and times.

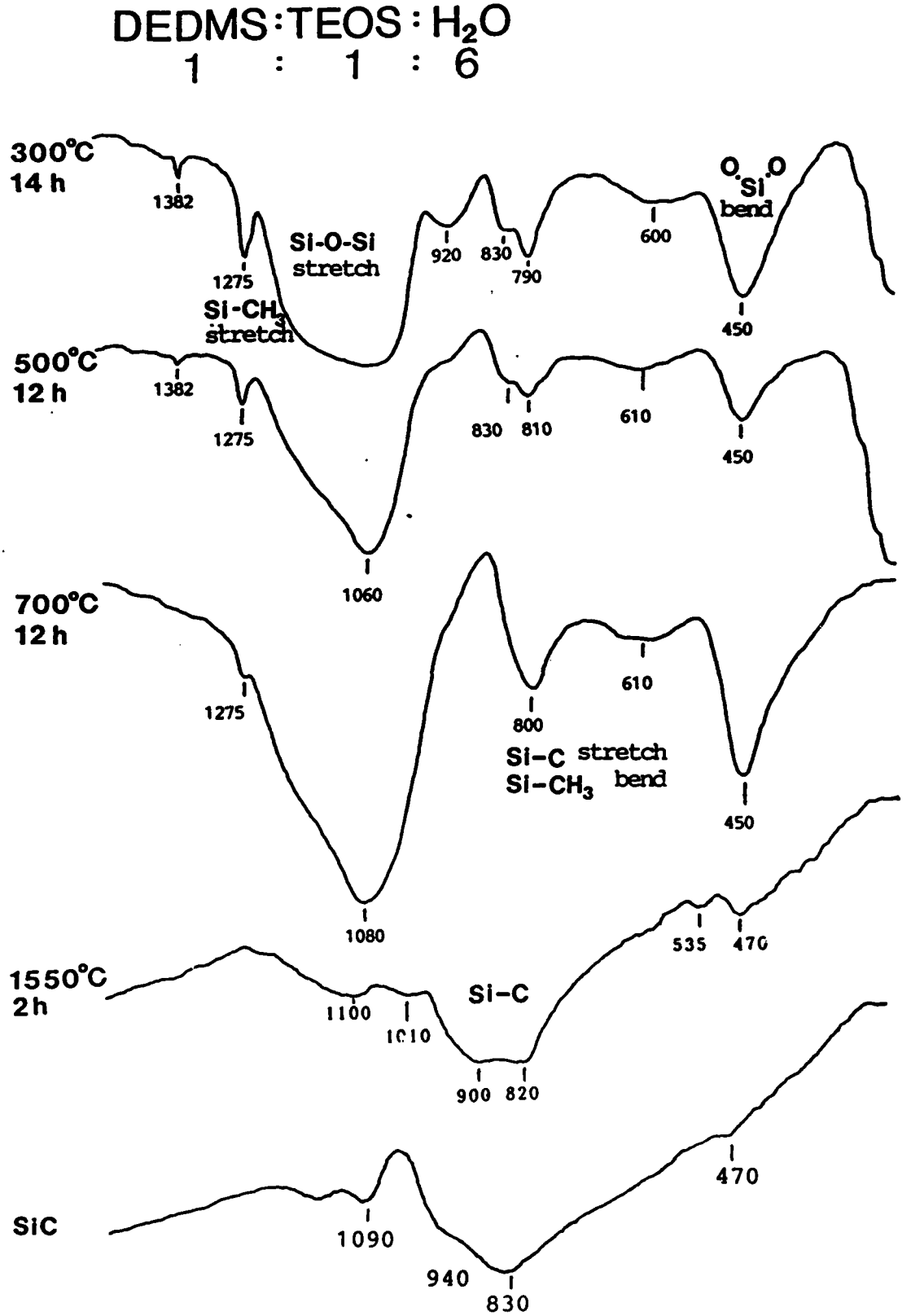

Figure 10: Infrared spectra for heated gels of the DEDMS:TEOS system.

the $Si-CH_3$ group. The $Si-CH_3$ group is usually recognized from its strong sharp band at about 1260 cm^{-1}. In our samples this band had shifted 15 cm^{-1} to a higher frequency due to the linkage of Si-0. Again we see that molecular mixing had been achieved. The bands of Si-0 also appeared at the usual positions (1200-1000 cm^{-1} for Si-0 stretching, 920 cm^{-1} for Si-0 ring stretching, and 450 cm^{-1} for Si-0-Si bending).

After calcining at 700°C for 12 hours, some $Si-CH_3$ bands were still observable at 1275 cm^{-1}. The intensity of the band at 800 cm^{-1} had increased. As previously described this band is assigned to Si-C stretching vibrations. Thus for the DEDMS/TEOS system the transformation of gel to silicon carbide probably started at around 700°C. After heating at 1550°C for 2 hours in a nitrogen atmosphere the Si-C band had become even more intense and the Si-0-Si bands at 1100 and 450 cm^{-1} had decreased. The spectra resemble that of chemically obtained SiC.

3.9 MICROSTRUCTURE OF CRYSTALLIZED GEL FROM DEDMS/TEOS IN 1/1 MOLAR RATIO

X-ray diffraction showed the presence of considerable amounts of beta-SiC in the 1/1 molar ratio sample of DEDMS and TEOS after heating at 1550°C for 2 hours in a N_2 atmosphere. Scanning electron microscopy was also used to examine the microstructure and the crystal size in the sample. Figure 11 shows the crystal size to be of the order of 500-1000 Å. Some porosity still existed. This sample was easily etched with HF, indicating the presence of some amorphous phase between the crystallites, probably silica.

3.10. YIELD OF SILICON CARBIDE FROM THE DEDMS/TEOS 1/1 MOLAR RATIO SYSTEM

The largest amount of beta-SiC observed in a pyrolyzed gel in this study was in the DEDMS/TEOS sample (1/1) heated at 1550°C for 2 hours. In order to perform a quantitative analysis of the yield of SiC a calibration curve was first obtained. The dried gel was pre-weighed and

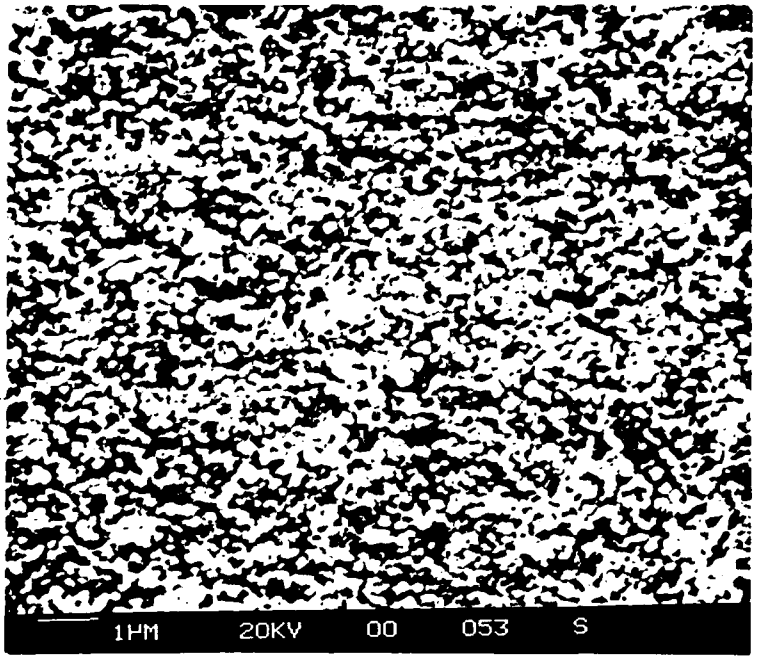

Figure 11: Electron micrograph of β-SiC prepared by pyrolysis of diethoxysimethylsilane and tetraethoxysilane at 1550°C for 2 hours. (Polished and 2% HF, 10 seconds etched surface).

calcined stepwise up to 700°C. The weight loss at this temperature was 60%, i.e., only 40% of the original material remained. This amorphous phase was then mixed with different amounts of crystalline silicon carbide obtained from a vendor (2%, 3%, 5%, 10%, 20%, 30%, 50%, 70%, and 90% by weight). A calibration curve was obtained from the X-ray diffraction of these samples, pre-mixed with CaF_2 as an internal standard. The final amount of the silicon carbide in the DEDMS/TEOS sample was then determined by the relative peak intensity, and was calculated to be 30% by weight. This corresponds to a 12% yield if the dried gel was considered to be the starting material. Since only two formula weights of silicon carbide (formula weight: 40:10) can be obtained from one molecule of DEDMS (formula weight: 148:28) and one molecule of TEOS (formula weight: 208.33), the theoretical yield will be 22.5% (= 2 x 40.10/(148.28 + 208.33)). Therefore, we had obtained about 50% of the maximum amount of SiC possible.

4. SUMMARY AND CONCLUSIONS

Several silicon containing metal organic compounds were evaluated for their ability to form homogenous solutions and gels. Homogenous solutions and gels were successful obtained from the three systems of triethoxyvinylsilane, triethoxyphenylsilane/tetraethoxysilane and diethoxydimethylsilane/tetraethoxysilane. Only the systems of diethoxydimethylsilane/tetraethoxysilane with 1 to 1 and 2 to 1 mole ratios crystallized into silicon carbide. These monolithic gels retained their shapes up to 1600°C with crystalline beta-silicon carbide as the major phase. The crystal sizes in these samples were greater than 1000 Å. The maximum silicon carbide obtained was about 50% of the theoretically possible value. The transformation of the gel structure into the silicon carbide was studied by infrared absorption analysis.

This small research effort has indicated that SiC can indeed be prepared from sol-gel compositions. It is probable that a significant increase in the yield of SiC can be achieved from further research on improved sol-gel compositions. Despite the somewhat low yield of SiC from the starting solutions, this technique may be effective for the protection

of carbon fibers. Tests on the oxidation of carbon fibers after coating by the solutions studied in this project are in progress.

5. PERSONNEL

This project was under the supervision of Professor J. D. MacKenzie. Research was conducted by Mr. Kevin Thorne (undergraduate laboratory assistant) and Mr. K. C. Chen (graduate research assistant).

AD-A193 320 STUDIES IN SUPPORT OF OXIDATION-RESISTANT COMPOSITE MATERIALS(U) GENERAL ATOMICS SAN DIEGO CA J L KAAE ET AL. 01 FEB 88 GA-A19195 AFOSR-TR-88-0284 2/2

UNCLASSIFIED FF9620-86-C-0011 F/G 11/4 NL

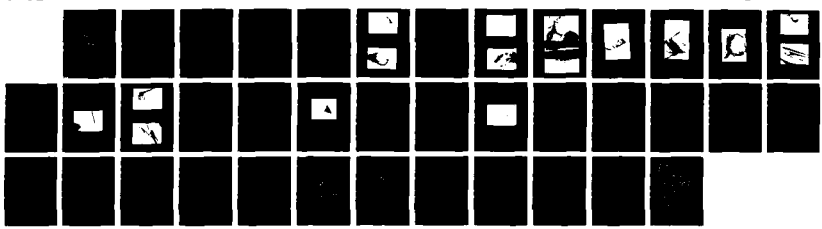

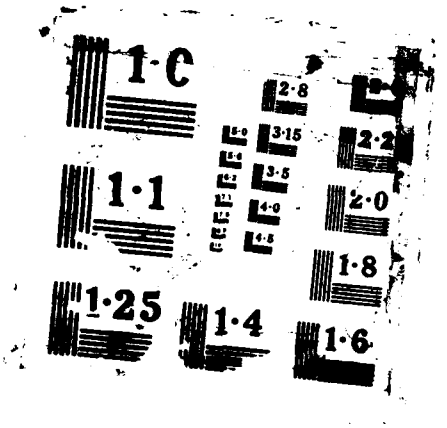
1·C
2·8
3·15
3·5
4·0
4·5
2·2
2·0
1·8
1·1
1·25
1·4
1·6

REFERENCES

1. Sharp, J. H., Brindley, G. W., and B. N. Narahari Achar, "Numerical Data for Some Commonly Used Solid-State Reaction Equations," Journal American Ceramic Society, 49 (7), 379, 1966.

2. Carter, R. E., "Kinetic Model for Solid-State Reactions," J. Chem. Phys. 34 (6), 2010-15 (1961).

3. Ginstling, A. M. and B. I. Brounshtein, "Concerning the Diffusion Kinetics of Reactions in Spherical Particles," J. Appl. Chem. USSR (English Transl.), 23 (12d), 1327-1338 (1950).

4. McKewan, W,. M. "Kinetics of Iron Oxide Reduction," Trans. Met. Soc. AIME, 2, (1960).

5. Avrami, M., "Kinetics of Phase Change: I, "J. Chem. Phys. 7 (12), 1103-12 (1939); "II" ibid., 8 (2) 212-24 (1940), "III" ibid., 9 (2), 177-84 (1941).

6. Erofe'ev, B.V., "Generalized Equation of Chemical Kinetics and Its Application in Reactions Involving Solids," Compt. Rend. Acad. Sci. ISSR, 52, 511-14 (1946).

7. Rochow, E. G., "An Introduction to the Chemistry of the Silicons, 2nd Ed., Chapman and Hall, p. 80.

8. Bertoluzza, A., C. Fagnano and M.A. Morelli, "Raman and Infrared Spectra on Silica Gels Toward Glass, J. Non-Cryst. Solids, 48, 117-128 (1982.

TASK 4: INTERCALATION OF GRAPHITE FIBERS FOR IMPROVED OXIDATION RESISTANCE

INTRODUCTION

The broad goal of this task is the development of oxidation resistant fibers by using intercalated graphite fibers as precursor fibers. The work to date has proceeded along two lines. First, hydrolysis of a metal chloride species within the graphite layers produces a metal oxide or hydroxide at the surface edges of the graphite layers. It is hoped that high temperature oxidation of graphite, which occurs preferentially at these edges, will be impeded by these deintercalated materials on the surface. Some initial hydrolysis of graphite-aluminum chloride fibers have been performed. The second line of research was unanticipated, but has produced a variety of refractory fibers. When the intercalated graphite-metal chloride fibers are heated in air, without a hydrolysis step, the carbon is burned away and a metal oxide fiber remains. Fibers of Al_2O_3, ZrO_2, and HfO_2 have been produced. The ceramic fibers appear to have the general morphology and size of the original graphite fiber. Fibers of mixed composition can be produced, as demonstrated by an Al_2O_3-ZrO_2 fiber. Under appropriate conditions, hollow fibers of Al_2O_3 can be produced. The hollow fibers have a wall thickness of 1-2 μm, and an inner diameter of ~5-10μm.

SYNTHESIS OF CERAMIC FIBERS

In all the work described below, Union Carbide P-100 fibers were used. There are 2000 graphite fibers in a tow, and the graphite tow is continuous. The fibers were heated at ~300°C in air to remove a sizing. Approximately six-inch long lengths were put in a pyrex tube, to which a known quantity of metal chloride was added. A stoichoimetric amount of chlorine gas (1:2 of Cl_2 and MCl_x) was frozen in the tube, and the tube was sealed under vacuum. The sample was then heated to generate sufficient vapor pressure of metal chloride. After 1-3 days, the tube was cooled and opened in a drybox. The intercalated fibers were placed in a quartz tube which was open to the air and then heated to 800°C. Within 1-3 h, all the graphite was burned off, and the ceramic fiber tow remained.

Alumina Fibers

Graphite fibers were intercalated with $AlCl_3$, at 150-180°C for 1-3 days to form material of nominal compositions $C_{36}^{+}AlCl_4^{-}$, $C_{60}^{+}AlCl_4^{-}$ and $C_{12}^{+}AlCl_4^{-}$. EDAX showed a ratio of Cl/Al~4 in the two more dilute materials, and Cl/Al~3-3.5 in the "$C_{12}^{+}AlCl_4^{-}$" material. X-ray diffraction showed the $C_{12}^{+}AlCl_4^{-}$ to be first stage and the $C_{36}^{+}AlCl_4^{-}$ to be second stage.

The Cl/Al ratio is significant as a measure of the amount of ions inside the graphite as compared to the amount of neutral molecular species. A ratio of 4 indicates total $AlCl_4^{-}$ while a ratio of 3.5 implies $Al_2Cl_7^{-}$. Ratios below 3.5 imply $Al_nCl_{3n+1}^{-}$ ($n > 2$).

$$Al_nCl_{3n+1}^{-} \longleftrightarrow AlCl_4^{-} + (n-1)AlCl_3$$

Because the ion can dissociate to create a smaller ion plus neutral $AlCl_3$, it is not proven that only ionic species exist within the graphite planes. Thus, for ratios below 4, it is ambiguous whether all the aluminum species are one ion or only some species are ionic.

This ambiguity was apparent in the growth of the alumina fibers from the intercalated fibers. When the $C_{12}^{+}AlCl_4^{-}$ was first put in the oven at 800°C, white fumes formed and deposited on the cool walls within 30 s. For "$C_{12}^{+}AlCl_4^{-}$" where the Cl/Al ratio is closer to 3-3.5, there are molecules of neutral $AlCl_3$ or larger ions which decompose at higher temperatures to $AlCl_4^{-}$ plus $AlCl_3$. Presumably, the fumes were from neutral $AlCl_3$ inside the graphite, since bulk $AlCl_3$ boils below 200°C. Even with this loss of $AlCl_3$, white fibers grew over the next three hours. The $AlCl_4^{-}$ ions should not volatilize at 800°C, but they can be converted to Al_2O_3. By contrast, there are predominantly $AlCl_4^{-}$ ions in the $C_{36}^{+}AlCl_4^{-}$ lattice where the Cl/Al ratio is almost 4. No white fumes were observed from $C_{36}^{+}AlCl_4^{-}$.

The alumina fiber tow produced by this 800°C treatment had the following characteristics. The tow was light and flexible. The cross section of the tip showed layer planes aligned down the fiber axis identical to those of the precursor graphite fiber. (See Fig.4-1.) (To our knowledge, this is the first control of alumina fiber morphology.) X-ray diffraction showed the alumina to be the gamma phase, with no obvious preferred orientation. From estimates of the fiber cross section, length, and mass, the density of the fiber was less than 1g/cc (~0.6g/cc). This value is much lower than the bulk density ~3g/cc of Al_2O_3. We surmise the porosity is due to escaping CO_2 and Cl_2 as the fiber is oxidized at 800°C. EDAX shows the complete loss of carbon and chlorine, and the presence of only aluminum and oxygen.

Gamma Al_2O_3 is converted to alpha Al_2O_3 (hexagonal corundum) above ~1200°C. The Al_2O_3 fibers were heated in air at 1250°C or 1400°C for 6-12 h to effect this phase change and hopefully to densify the fibers. The resulting fibers were alpha Al_2O_3, but they maintained a porous,

Fig 4-1(a) Gamma Al_2O_3, fiber fracture surface

Fig 4-1 (b) Initial P-100 graphite fiber fracture surface

vermicular layered structure. (See Fig 4-2.) Domains of ~0.5 μm were clearly visible as the densification caused the domains to separate. X-ray diffraction showed the (110), (113), and (116) planes were preferentially aligned down the fiber axis.

It appears that the gamma Al_2O_3 must be avoided in order to avoid the vermicular structure in alpha Al_2O_3. To test this hypothesis, intercalated fibers were heated immediately to 1250 or 1400°C, in order to make the alpha Al_2O_3 directly. The 1250°C heating produced more dense, and non-vermicular fibers (Fig 4-3). Small pores (~0.1-0.3μm) were visible on the surface. In addition, layering was much less pronounced. The 1400°C heating produced a very different morphology (Fig 4-4). The fibers appeared very segmented along their length. A skin of Al_2O_3 was present in place of the original graphite fiber surface. This skin had small pores, and appeared like a rolled scroll. The inside of the fiber was not hollow, but was not dense. The inside material appeared "fluffy". In this 1400°C heating, the outer skin apparently formed rapidly, in a near continuous manner. The gases escaping from the inside flowed out of the ends of the fiber, leaving the "fluffy" interior. As anticipated, avoiding the gamma Al_2O_3 formation led to a non-vermicular alpha Al_2O_3 fiber. Heating to ~1250°C produced a visibly more dense fiber, while sudden heating of the surface resulted in an Al_2O_3 skin, but a structurally weak fiber.

Hollow Alumina Fibers

Boric acid was suggested as a sintering aide to densify the alumina. Some gamma Al_2O_3 tows were put in 10^{-3} M H_3BO_3 for ~12h, dried briefly at 150°C and then heated to 1250°C for ~12h. The resulting alpha Al_2O_3 fibers were tubes. (See Fig.4-5.) The hollow fibers were ellipsoidal, with major and minor axes of 5 and 10 μm respectively. The wall thickness was 1-2 μm. The tubes appeared hollow for long distances (>100 μm). Many of the fibers were cracked open far from the point of fracture. Some fibers also had holes in their walls. X-ray diffraction of the hollow tubes indicated only alpha Al_2O_3, with the same preferred orientation as the fibers not dipped in boric acid.

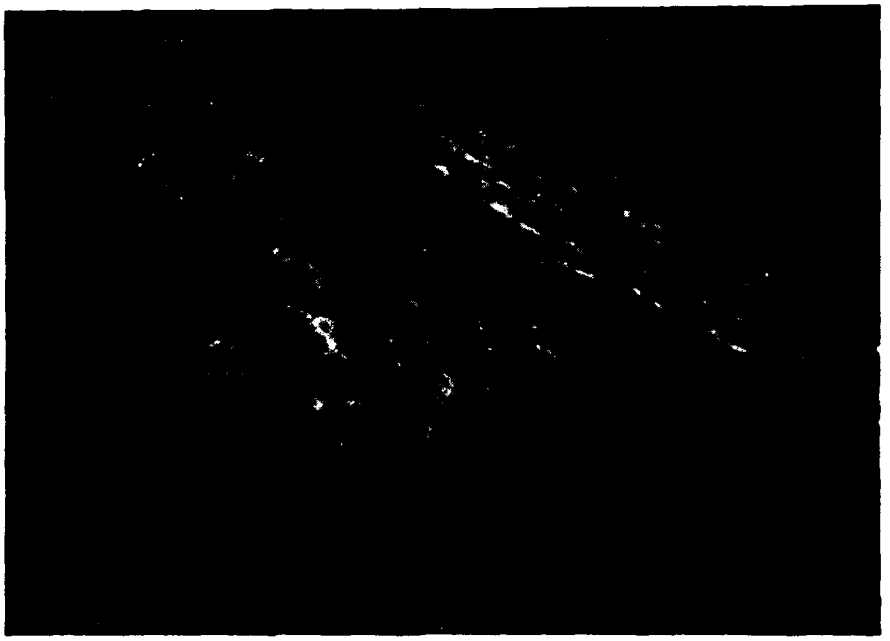

Fig 4-2 Alpha Al_2O_3 fiber

(a)

(b)

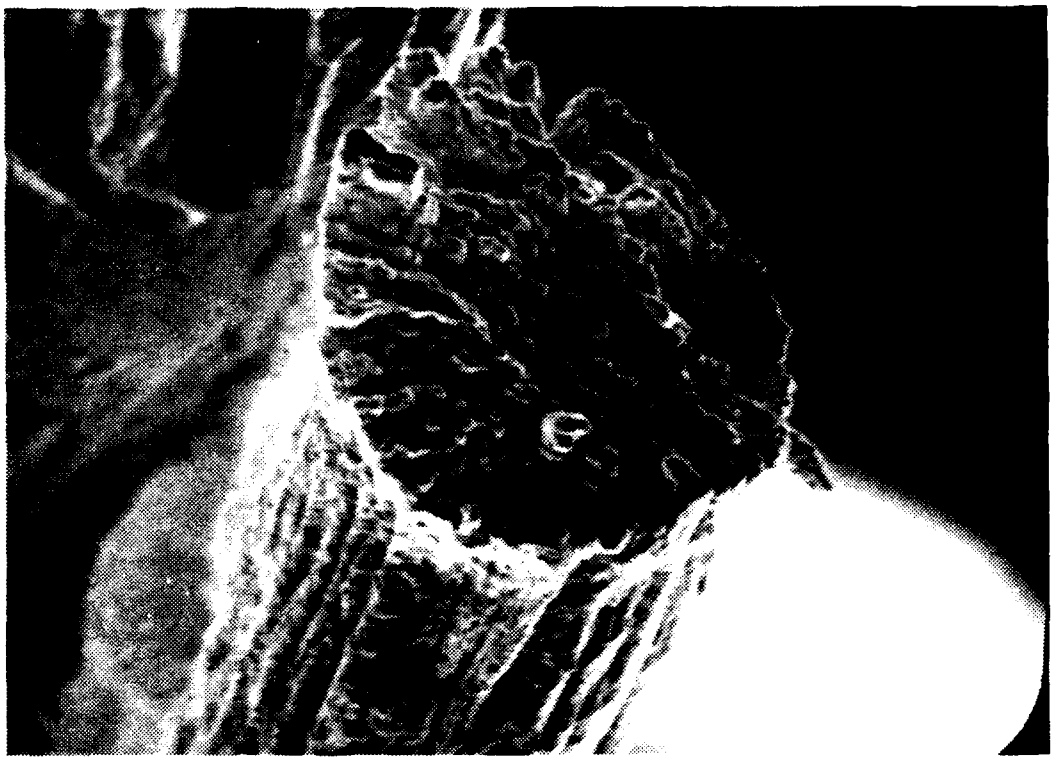

Fig 4-3 An alpha aluminum fiber produced by heating C+$AlCl_3$ in air at 1250°C. The fiber is more dense, and the fiber body has some small pores

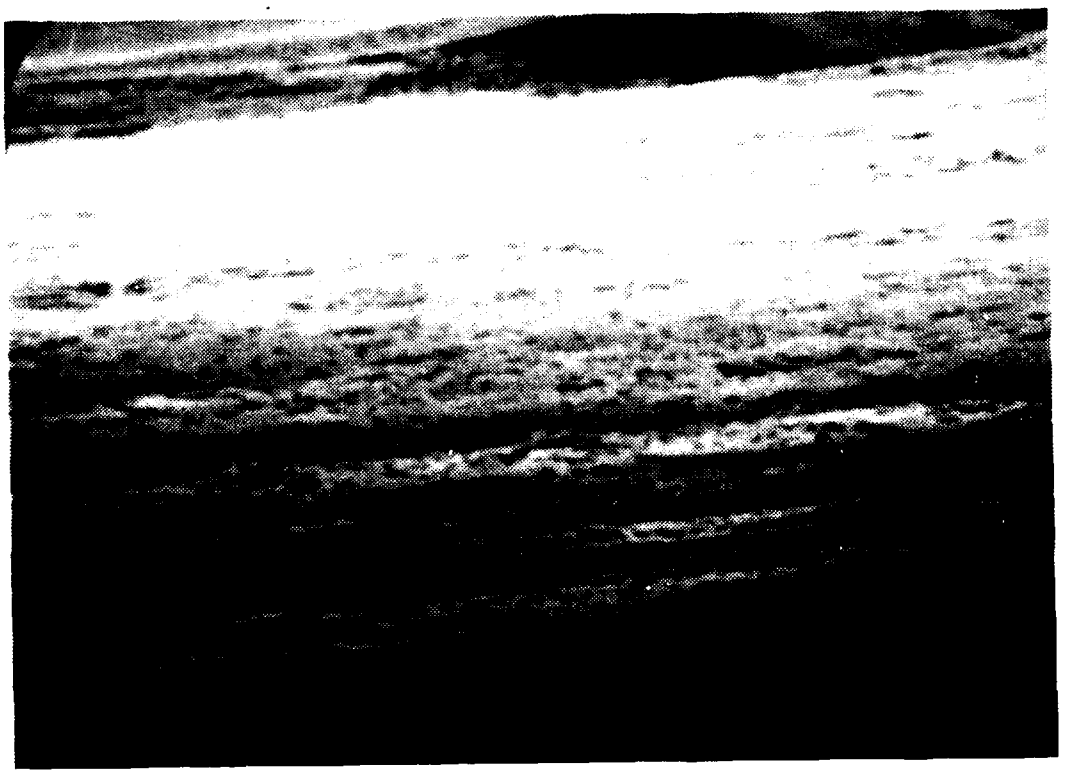

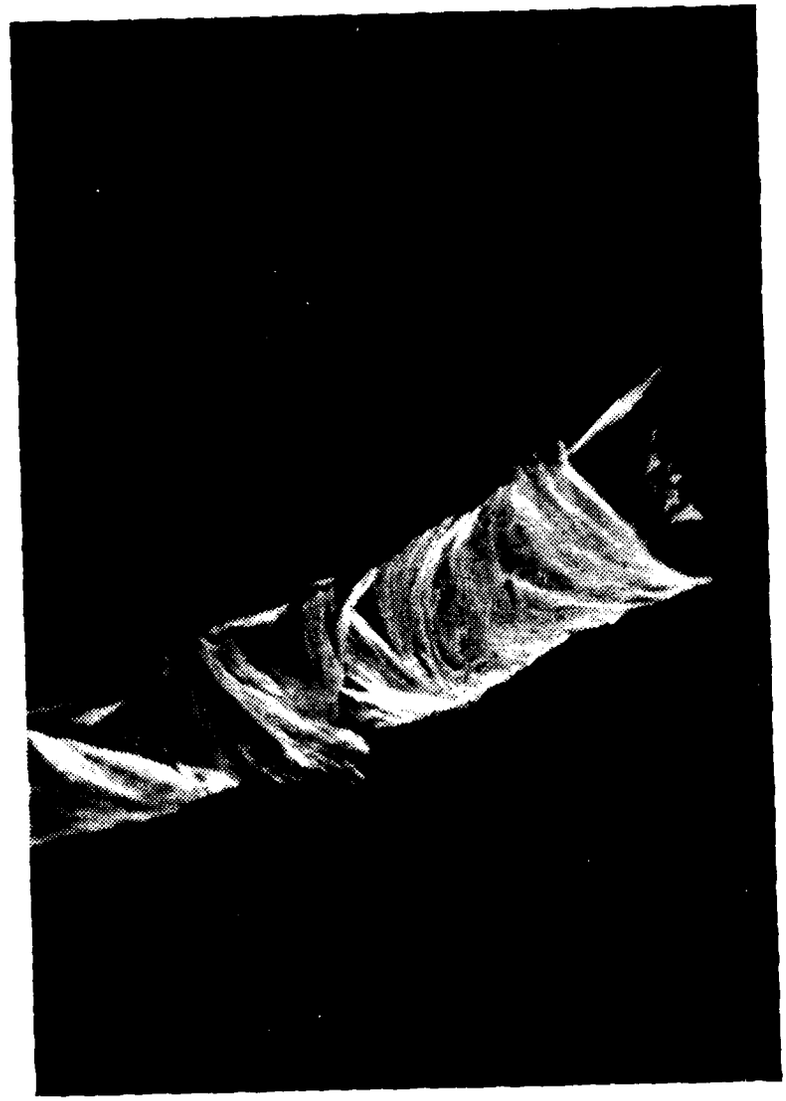

Fig 4-4 Alumina fiber produced by burning $C_n^+AlCl_4^-$ at 1400°C:
(a) Shows the segmented fiber body

Fig 4-4 Alumina fiber produced by burning $C_n^+AlCl_4^-$ at 1400°C:

(b) Shows the pores in the surface skin

Fig 4-4 Alumina fiber produced by burning $C_n^+AlCl_4^-$ at 1400°C.
(c) Shows the degree of "hollowness" of the fiber

Fig 4-5 (a) Hollow alpha Al_2O_3 fibers

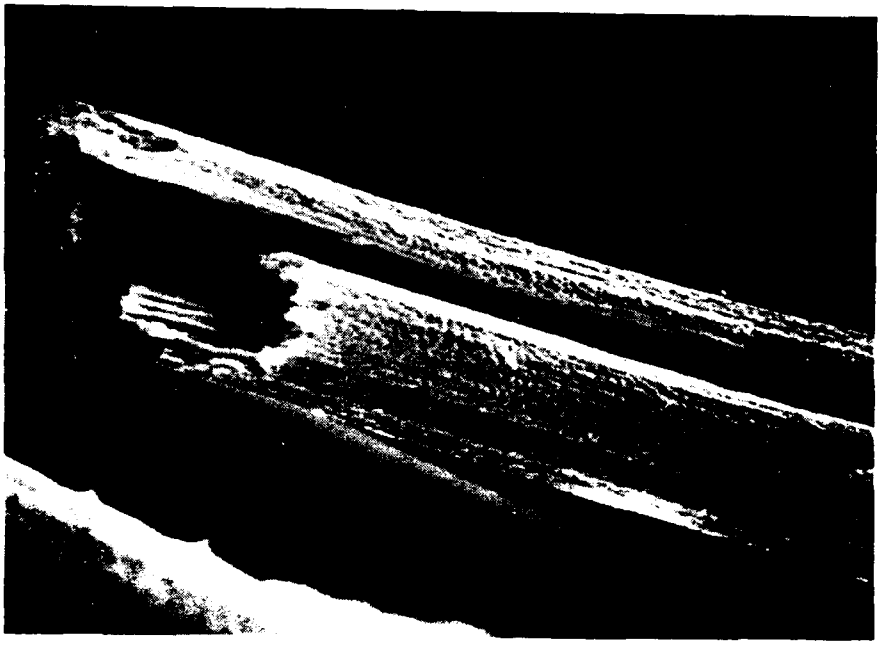

Fig 4-5 (b) Cracked alpha Al_2O_3 fiber showing continuity of the central hole

Gamma Al_2O_3 fibers dipped in 10^{-2} M H_3BO_3 and heated to 1250°C had the same hollow structure and the same Al_2O_3 pattern as those treated with 10^{-3}M H_3BO_3.

Gamma Al_2O_3 dipped in 10^{-2}M H_3BO_3 and heated to 800°C assumed the shape of very flattened tubes. (See Fig. 4-6.) The correlation of the different morphologies with the different heat treatments is unclear. Perhaps, at 1250°C, some B_2O_3 was volatilized. Thus, any liquid phase which might densify the solid would lose B_2O_3 from the outer surface. The liquid phase would not be able to propagate through the fiber, so it would always be maintained near the outer surface. Alumina from the center would then be drawn toward the outer surface and the tube would be formed. At 800°C, a liquid phase could also form, but the lower volatility of B_2O_3 may have permitted propagation of the liquid throughout the fiber. Thus, the walls could collapse down together.

Other Metal Oxide Fibers

To demonstrate that this method of growing ceramic fibers is not unique to alumina, other oxide fibers have been prepared.

Fibers of ZrO_2 and HfO_2 can be made by burning graphite fibers intercalated by the metal tetrachloride plus chlorine. (See Fig. 4-7.) The exact stoichiometry of the intercalated ions is unclear. EDAX showed a Cl/Zr ratio ~4.31, while the ion $Zr_2Cl_9^-$ was implied by weight gain upon intercalation coupled with the weight of ZrO_2 produced upon burning ($C^+_{63.5}Zr_2Cl_9^-$). Apparently, for C_nZrCl_{4+x}, simple ions such as $ZrCl_5^-$ or $ZrCl_6^{-2}$ are not formed. (EDAX of the C_nHfCl_{4+x} has not been performed.)

The kinetics of the ZrO_2 and HfO_2 fiber growth were significantly faster than those of Al_2O_3 fibers. Burning C_nZrCl_{4+x} (n~36) or C_nHfCl_{4+x} (n~80) produced white fibers in ~1 h, rather than the three hours for $C^+_nAlCl_4^-$. For ZrO_2 air oxidation may be rapid because the diffusivity of oxygen in ZrO_2 is high, and thus transport of oxygen through the ceramic to the interior carbon is rapid.

Fig 4-6 Flattened gamma-Al_2O_3 fiber

Fig 4-7 (a) ZrO_2 Fiber

Fig 4-7 (b) HfO_2 Fiber

Both ZrO_2 and HfO_2 fibers had monoclinic unit cells, which is consistent with the 800°C temperature at which they were formed. The ZrO_2 fibers had a strong preferred orientation of the $(11\bar{1})$ planes along the fiber axis. The HfO_2 fibers had no preferred orientation.

The formation of yttria (Y_2O_3) has been attempted several times, via intercalation of YCl_3. However, an unambiquous synthesis of yttria fibers has not yet been completed, due to several complications. First, the intercalation reaction is slow, even at ~900-1000°C, where YCl_3 has a vapor pressure of about one torr. Reactions of several days have yielded little intercalation. Second, we have found that liquid YCl_3 wets the graphite fibers. If the graphite fibers are in contact with the liquid, the liquid wicks along the fibers, filling the volume between the fibers of the tow. Burning this wetted tow produced an interconnected yttria matrix, with holes in it. The holds resulted from the combustion of the graphite fibers. Thus, a porous yttria matrix resulted, but not yttria fibers. In this work, x-ray diffraction did show some lines attributable to intercalation. However, the YCl_3 coating does complicate the x-ray pattern. Further work is planned, to obtain pristine yttria fibers.

Binary Oxide Fibers

Stronger and tougher ceramics can be made by incorporating a second phase in a primary phase. To demonstrate that binary oxide fibers could be synthesized, a mixture of graphite, $AlCl_3$, $ZrCl_4$, and Cl_2 was mixed to attempt a synthesis of

$$C_{36}^{++}AlCl_4^-.ZrCl_5^-.$$

The material was heated to 250°C for 4 days and all the metal chloride intercalated. When the fiber was heated at 800°C, some white fumes formed initially, but the white ceramic fibers showed Al/Zr=2.8. Thus, since the starting intercalated fiber had Al/Zr=1.0, more $ZrCl_4$ was volatilized than $AlCl_3$. The ceramic fibers were 9-13 μm in diameter.

X-ray diffraction of the ceramic phase showed the tetragonal phase of ZrO_2 in the presence of gamma Al_2O_3. (Actually, the gamma Al_2O_3 was inferred because it produces a very weak pattern. The ZrO_2 dominated the pattern.) Pure tetragonal phase ZrO_2 is stable only above ~1000°C, yet in these fibers which were never heated above 800°C, this tetragonal phase was present.

A second binary oxide fiber was made by cointercalating $AlCl_3$ and $FeCl_3$. This reaction was chosen for several reasons:

- Fe_2O_3 has the α-Al_2O_3 structure, with lattice constants about 7% larger than α-Al_2O_3. It was hoped that Fe_2O_3 would nucleate growth of α-Al_2O_3 at 800°C, and be an agent for densification of α-Al_2O_3.

- Intercalation of $AlCl_3$ requires the presence of Cl_2. $FeCl_3$ intercalates by vaporizing $FeCl_3$, and generating Cl_2. The Cl_2 produced by $FeCl_3$ could help intercalate $AlCl_3$. This approach avoids the direct handling and addition of Cl_2.

- $AlCl_3$ and $FeCl_3$ can complex each other, to form $FeAlCl_6$ in the gas phase. In a way, they carry each other into the graphite in an intimate mixture. ($AlCl_3$ can complex many other metal chlorides of low volatility, in order to intercalate multiple species.)

An excess of $AlCl_3$ and $FeCl_3$ was sealed under vacuum with P-100 fibers, and initially heated to ~200°C. Very little material was transported over 24 hours. The temperature was gradually increased over ~ 5 hours to 300°C. Loss of $AlCl_3$ and $FeCl_3$ was evident by the end of the 5 hours. The fibers were removed, and then heated in air at 800°C. After 3 hours, the fibers were rusty-red on one end and white on the other end. The fibers at the rusty-red end were hollow and were about 7-12μm in diameter. (Fig 4-8) EDAX showed these red fibers were ~22%Fe and 78% Al [$(Fe_{0.22}\ Al_{0.78})_2O_3$]. X-ray diffraction showed γ-Al_2O_3 and a pattern similar to α-Al_2O_3 (presumably α-Fe_2O_3). The composition at the white end was 1-2% Fe in a γ-Al_2O_3 matrix. No α-Al_2O_3 was distinctly

Fig 4-8 Hollow Al_2O_3:Fe_2O_3 Fiber

$(Al_{0.78}Fe_{0.22})_2\ O_3$

present.

The synthesis of the hollow Al-Fe oxide fibers is intriguing, because the fibers were obtained in a one-step process compared to the two steps required for production of the hollow α-Al_2O_3 fibers. It remains undetermined whether the mechanism for growth of the red hollow fibers is similar to that for growth of the hollow α-Al_2O_3 fibers.

HYDROLYSIS OF $C_N^+ALCL_4^-$

Another direction of this research was the controlled hydrolysis/deintercalation of a graphite fiber, in order to deposit a metal oxide on the edges of the graphite. Sufficient $AlCl_3$ and Cl_2 were added to graphite fibers to make ~$C_{36}^+AlCl_4^-$. EDAX of the ultimate fibers showed a Cl/Al~3.8-3.9. (This ratio is the highest known in the C $AlCl_3.Cl_2$ literature.) Nitrogen gas was bubbled through water and then over the intercalated fibers in an oven at a given temperature for several hours or days. The resulting deintercalated fibers were studied by SEM and EDAX.

The intercalated $AlCl_4^-$ should act like $AlCl_3$ and form AlOCl at low temperatures as is shown in the equation below. Then AlOOH should form fairly readily at temperatures above 400°C, and Al_2O_3 will form at temperatures above 600°C.

$$AlCl_3 \xrightarrow[25\text{-}250°C]{+H_2O} AlOCl \xrightarrow[\sim 500°C]{+H_2O} AlOOH \xrightarrow[>600°C]{} Al_2O_3$$

By initially performing a low temperature hydrolysis, the AlOCl should remain at the graphite edges and will convert to Al_2O_3 at higher temperatures.

The intercalated fibers were hydrolyzed at 100°C, 250°C, and 400°C for 1-4 days at a time and were observed under SEM after each step. (See Fig.4-9.) Differing Cl/Al ratios were obtained by EDAX for crystals growing on the fiber surface, for a clean fiber surface without crystals, and for an overall average region of the tow. As is shown in Fig. 4-10, the Cl/Al ratio of the heat-treated fibers decreased dramatically from that of the pristine intercalated sample. In the range of 100-250°C, the material on the surface had a Cl/Al ratio of ~1, which is indicative of AlOCl. Above 250°C, the Cl/Al ratio of the

fig 4-9

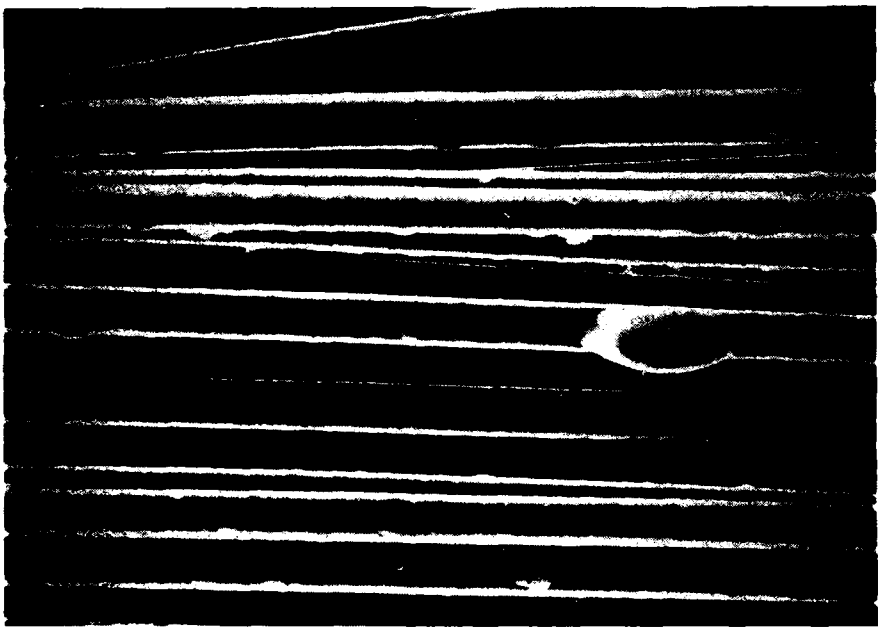

Fig 4-9 Hydrolysis Products (AlOCl, AlOOH) on Graphite Fibers

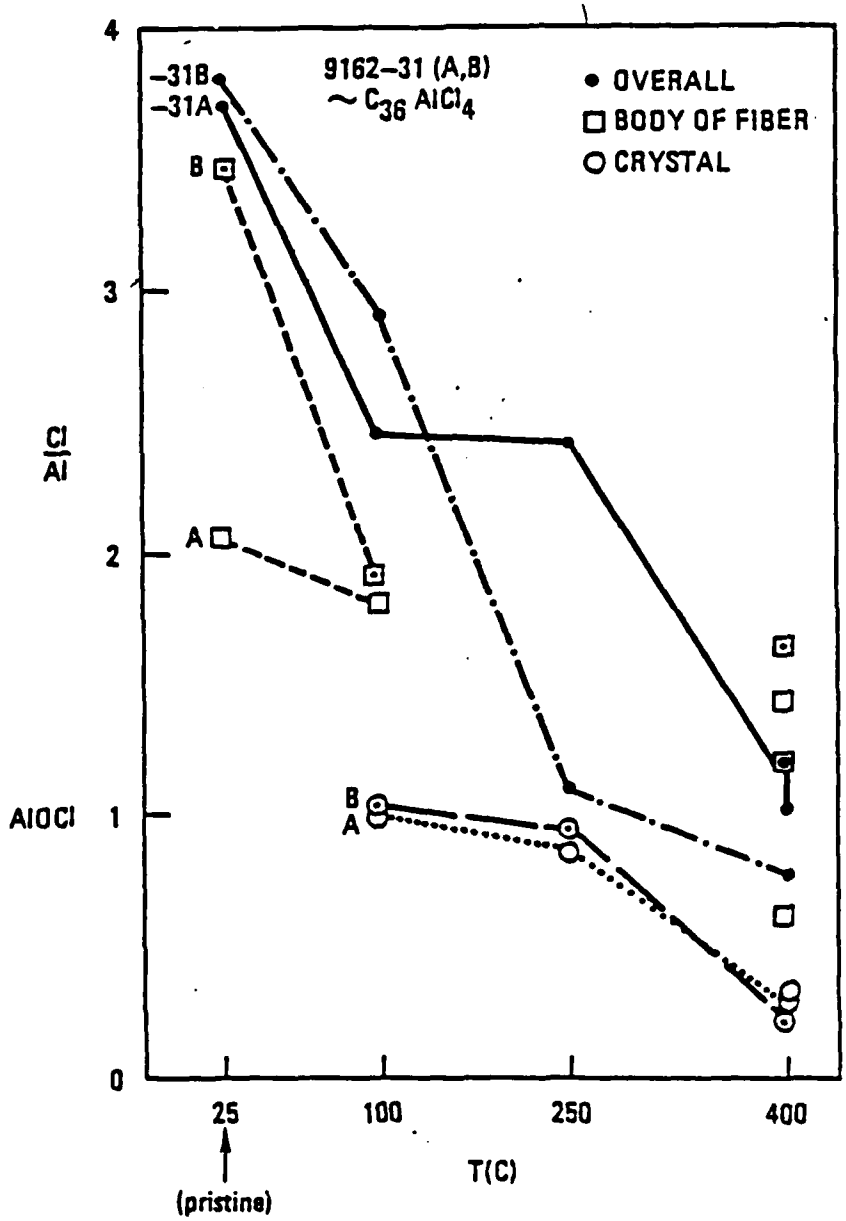

Fig 4-10 Ratio $\frac{Cl}{Al}$ for hydrolysis products

surface materials decreased as the last chloride was removed. In all cases, the Cl/Al ratio was lower for the surface material than for the fiber surface.

At 600°C and above, the intercalated fibers were totally oxidized to form alumina fibers. The materials formed during hydrolysis were still on the surface of the alumina fibers. However, these surface materials did not appear to be strongly bonded to the fibers. In several locations, fibers had clearly pulled away from the surface oxide. This weakness of bonding may permit oxidation of the carbon.

CONCLUSIONS AND FUTURE WORK

The growth of ceramic fibers from intercalated graphite fibers was totally unanticipated and may prove very useful. That the morphology of alumina fibers (layered, hollow tubes, and plates) can be controlled is very novel. In particular, the hollow or porous αAl_2O_3 may be impregnated with other materials.

One direction for the future is to continue trying to densify the Al_2O_3 fibers in order to obtain a higher strength. Measurement of their mechanical properties is required. Lastly, synthesis of more mixed oxides, such as zirconia toughened materials, appears to be a fruitful avenue of research.

SUBCONTRACT TO TASK 4

MASSACHUSETTS INSTITUTE OF TECHNOLOGY SUBCONTRACT

RAMAN SCATTERING OF INTERCALATED CARBON FIBERS

This section summarizes the work that has been conducted on Raman measurements of $AlCl_4$-intercalated graphite fibers and the fibers related to them.

1. PRISTINE P-100 FIBERS

Both conventional Raman spectroscopy and Raman microprobe measurements have been performed to examine P-100 fibers. The motivation for conducting these experiments is as follows:

1. To evaluate the degree of structural ordering of the host materials before intercalation by using the intensity ratio for the disorder-induced line near 1355 cm^{-1} to the Raman-active E_{2g_2} mode at 1582 cm^{-1}.

2. To obtain experimental evidence that the microstructure of the fiber cross-section has a radial distribution of graphite planes by using different polarization-orientations of the incident light.

3. To test and verify the experimental techniques, especially the Raman microprobe, for application to the $AlCl_4$-intercalated fibers and the fiber species derived from these fibers.

We have recorded Raman spectra for several spots on a single fiber as well as on different fibers, using the technique schematically shown in Fig. 1a. The spectra from both the conventional and the Raman microprobe systems consistently show only the peak corresponding to the E_{2g_2} Raman-allowed mode, but no pronounced peak associated with disordering, so that the intensity ratio R = I(1355)/I(1582) = 0/constant = 0.

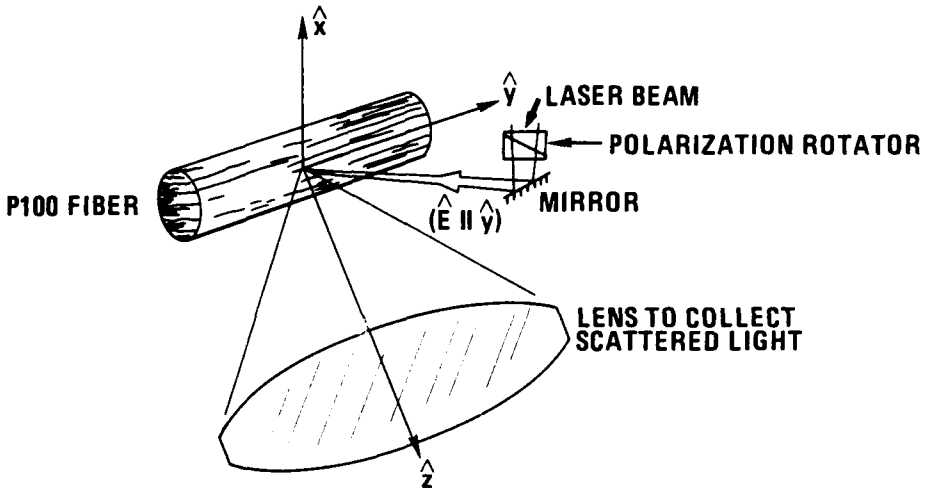

FIGURE 1(a)

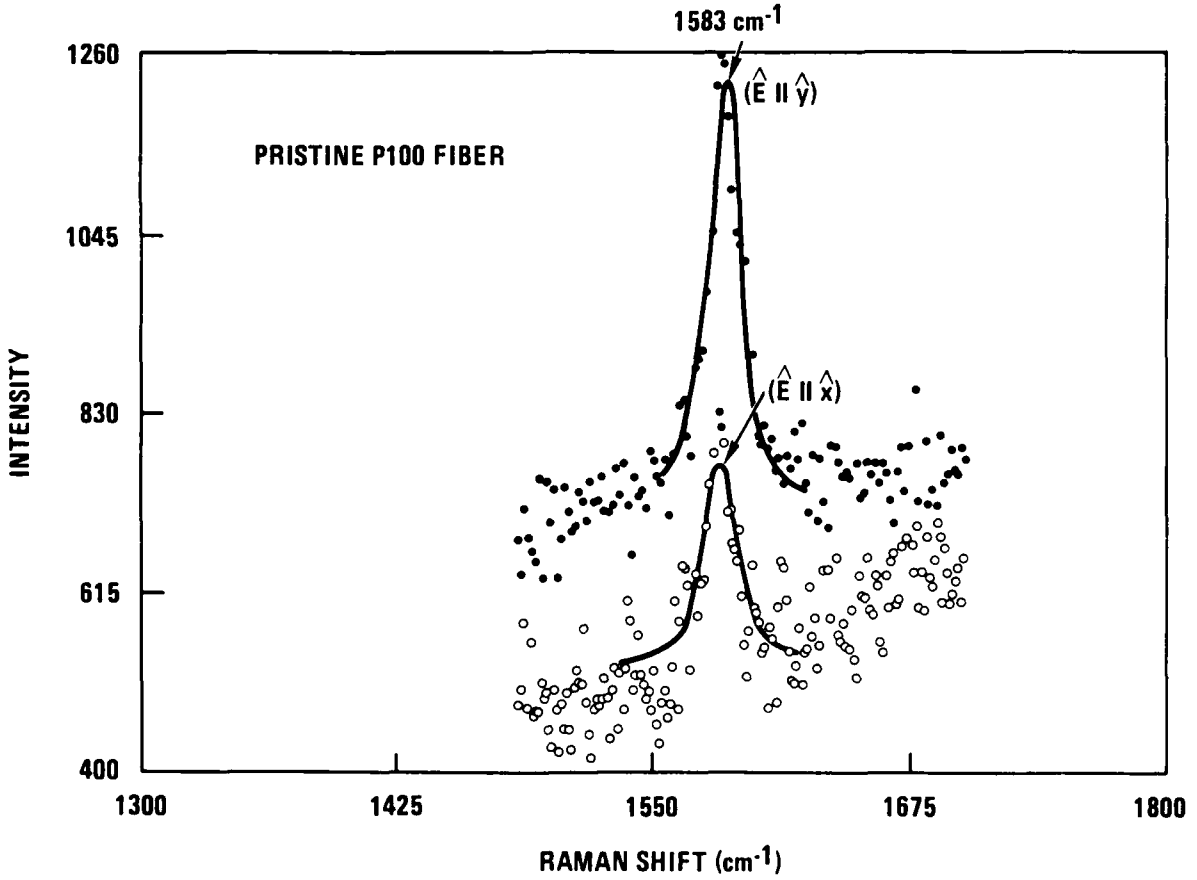

FIGURE 1(b)

FIGURE 1 (a) Polarization scheme.
(b) Raman spectra of pristine P100 fiber for incident light at different orientations.

Since this ratio has been shown to be inversely proportional to the in-plane crystal size L_a, it can be concluded that the structure of the P-100 fiber host material, has a high degree of microcrystalline ordering.

The results of the Raman measurements, shown in Fig. 1(b), using different polarization orientations, are exactly as expected, i.e., the Raman peak when the incident light is polarized along the fiber-axis is stronger than when the incident light is polarized perpendicular to this axis. This observation is in agreement with our expectations that the Raman-active E_{2g2} mode can only be excited by incident light polarized in the basal plane. This condition is satisfied if the geometric configuration of the experiment is arranged in such a way that the incident light is polarized along the fiber-axis. However, when the incident light is polarized perpendicular to the fiber-axis, the polarization vector has to be projected onto the layer plane to excite the E_{2g_2} mode. Consequently, the Raman peak for this polarization-orientation was expected to be much weaker. For this latter configuration of the incident light, we expected to observe a zero intensity for the Raman peak when the polarization was aligned not only perpendicular to the fiber-axis but also perpendicular to the layer plane of the fiber crystal structure. Due to the experimental difficulties we could not completely align the polarization in this way. Thus, a Raman peak of reduced intensity, rather than zero intensity, was observed.

The effect of the glass tubing on the Raman microprobe measurements was qualitatively estimated using the P-100 fiber. The results showed negligible distortion of the Raman peak though the glass tubing significantly reduced the peak intensity and increased the background noise.

2. INTERCALATED GRAPHITE FIBERS

In previous work, we demonstrated that Raman spectroscopy could be used to characterize the intercalation stage of HOPG for a variety of intercalants. The Raman active E_{2g_2} vibrational mode increased in energy from 1582 cm^{-1} upon intercalation of acceptor species. The single absorption becomes two different vibrational modes, arising from the graphene layers adjacent to the intercalant, and from graphene layers interior to these bounding layers.

The bounding layers are shifted to higher energy than the interior layers and both absorptions increase in energy as the stage parameter (1/n) increases. We sought to compare these data on HOPG intercalated graphite with the P-100 intercalated graphite fibers.

Besides conventional Raman spectroscopy, Raman microprobe spectroscopy of individual fibers was carried out. With this latter technique, the argon ion-laser is focussed onto a small spot (~1-2 μm), and a silicon photodiode array records an entire spectral region simultaneously, so that data can be acquired quickly at high spatial resolution.

Samples of composition $C_{61.7}AlCl_4$, $C_{48}AlCl_4$, $C_{36}AlCl_4$ and $C_{12.75}AlCl_4$ were studied. The first three, more dilute compositions arrived first, in sealed glass tubes. Dr. McQuillan anticipated that the samples would be moisture sensitive, although he had not visually observed any decomposition in air over a matter of hours at room temperature. (Decomposition of C_2FeCl_3 is visible in a matter of minutes, with red spots growing on the fiber surface).

The sample $C_{36}AlCl_4$ was run in the Raman microprobe, in air, anticipating the sample would have some kinetic stability. Only the data of the very first few Raman microprobe measurements showed any useful spectra. These data vaguely showed two overlapped peaks, indicating that the stage index was greater than 2. The sample was very unstable and deintercalated rapidly in air. After a number of days, these lines disappeared and the spectra of this sample became the same as that of the P-100 fibers. The sample $C_{61.7}AlCl_4$ underwent the same behavior. The Raman microprobe results clearly demonstrated that these materials were air sensitive.

The sample $C_{48}AlCl_4$ was studied inside the original sealed glass tubing, using the conventional Raman setup. Only the bulk fiber tow, rather than individual fibers, could be studied. The spectrum showed no shift in the Raman frequency from that of the pristine fibers. This result may indicate that the sample had been poorly intercalated.

The sample $C_{12.75}AlCl_4$ tow was received in a thin (~300μm) quartz capillary

tube, which is especially well suited for Raman microprobe measurements. The spectrum showed a single up-shifted Raman peak, typically at ω = 1628 cm^{-1} with a half width Γ = 10 cm^{-1}. This spectrum is shown in comparison to that of the pristine fiber in Figure 2. This observed up-shifted peak is attributed to the Raman active E_{2g_2} mode of the stage 1 intercalation compound, on the basis of spectra taken on a large number of different intercalation compounds (see Fig 3).

Measurements have been taken on several spots along the fiber length and for different fibers in the same batch, in order to identify inhomogeneities in the intercalation. The data for the Raman shift and for the half width have been plotted against the positions along the fiber length in Fig 4. The results indicate good homogeneity of the staging in this sample.

3. γ- Al_2O_3 AND α- Al_2O_3 FIBERS

A sample of $C_{36}AlCl_4$ was heated at 800°C in air. Within ~3 hours, the fibers had turned white. After 20 hours of heating at 800°C, the white flexible fibers were removed. X-ray diffraction showed lines characteristic of γ-Al_2O_3.

Raman spectra were taken in air, on individual fibers. Several spots on a single fiber, as well as on different fibers have been examined. They all showed the same characteristic of a very broad peak at ω ~ 1000cm^{-1} with a half width of Γ ~ 100 cm^{-1} (see Fig. 5). Gamma alumina is known to contain OH groups on its internal surface. (1) Infrared spectra of bayerite ($Al(OH)_3$) and diaspore (AlO(OH)) show two strong peaks at (bayerite: 1016, 975) and (diaspore: 1069, 960) cm^{-1}, which are assigned to OH bonds. (2,3) Thus we interpret the low broad Raman peak at ~1000 cm^{-1} to be indicative of some OH content in the γ - alumina.

A sample of γ - alumina was heated for several hours at 1250 C in air. The resulting α - Al_2O_3 was porous and brittle. Raman spectra taken between 200 and 2000 cm^{-1} showed no pronounced peaks. The absence of peaks is puzzling, since the material was very crystalline.

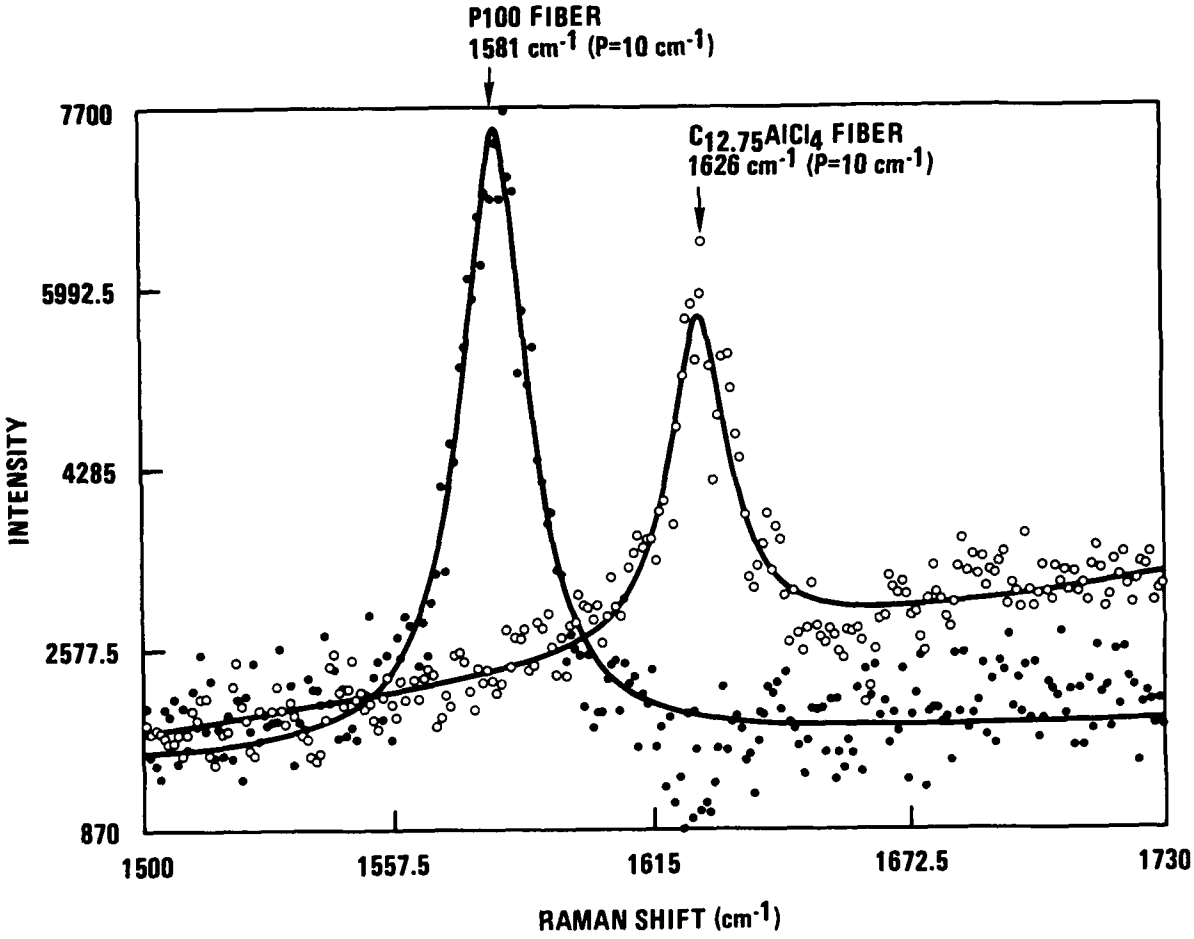

FIGURE 2 Raman spectrum of the stage 1 $AlCl_4$-intercalated sample in comparison with that of the pristine fiber.

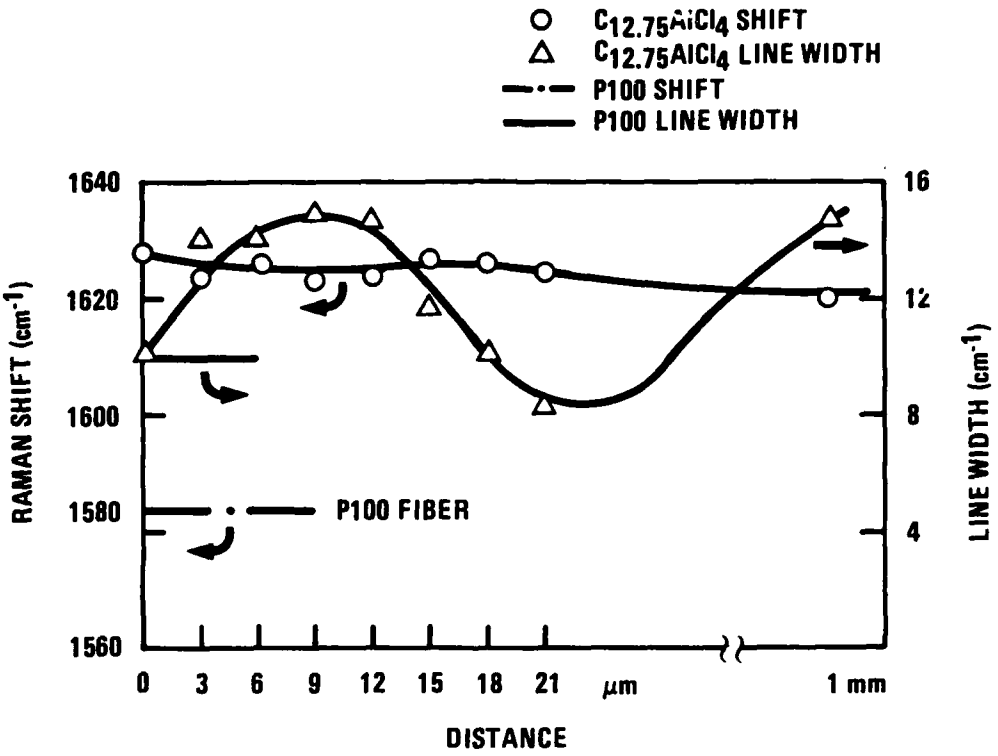

FIGURE 3 The plots of Raman shift and line-width vs. the distance from an arbitrarily determined spot on a single $AlCl_4$-intercalated fiber. The shift is attributed to the E_{2g_2} mode of the stage 1 sample.

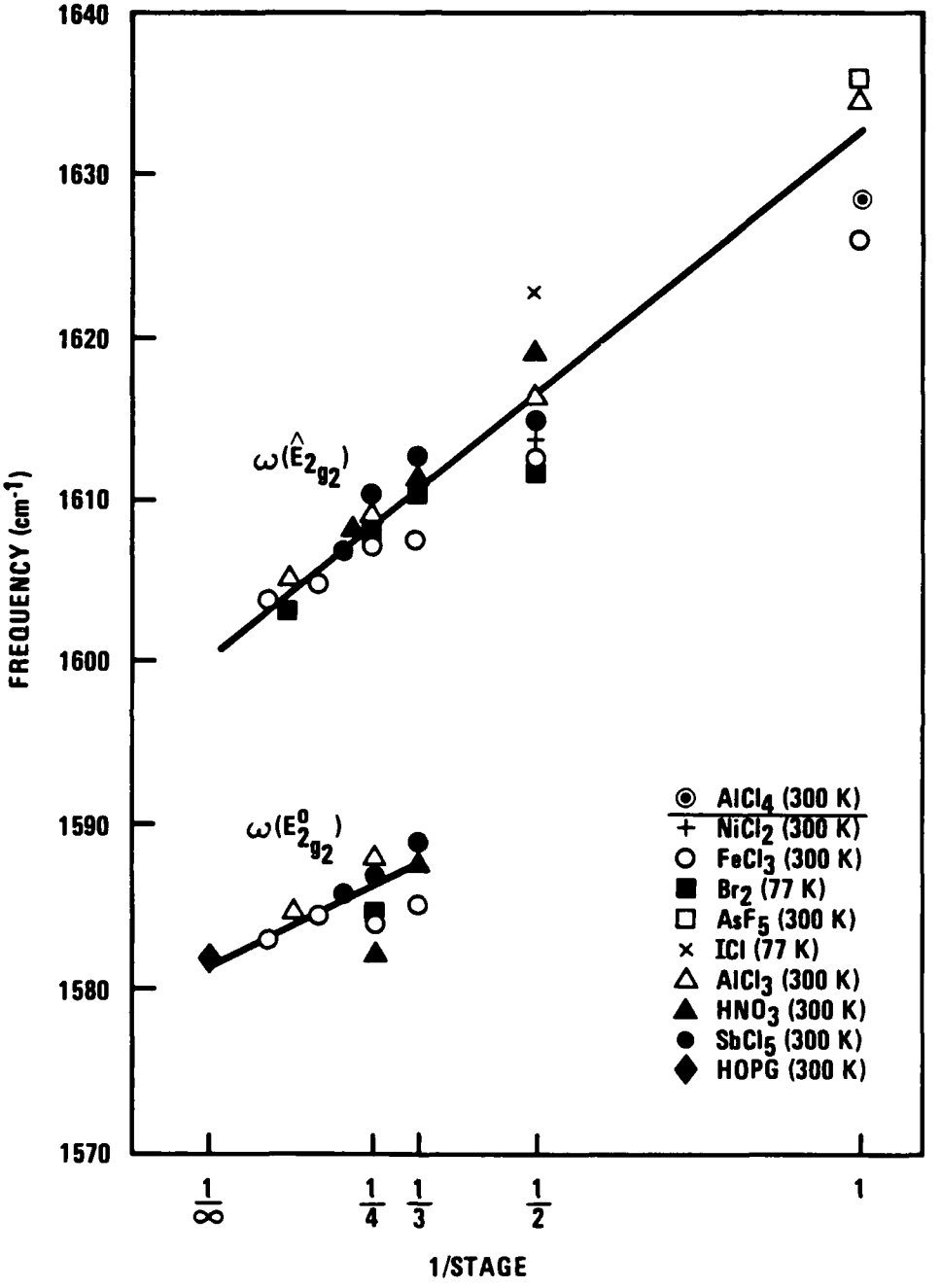

FIGURE 4 The observed Raman shift fitted in the "shifts vs. 1/stage" plot for the acceptor graphite intercalation compounds.

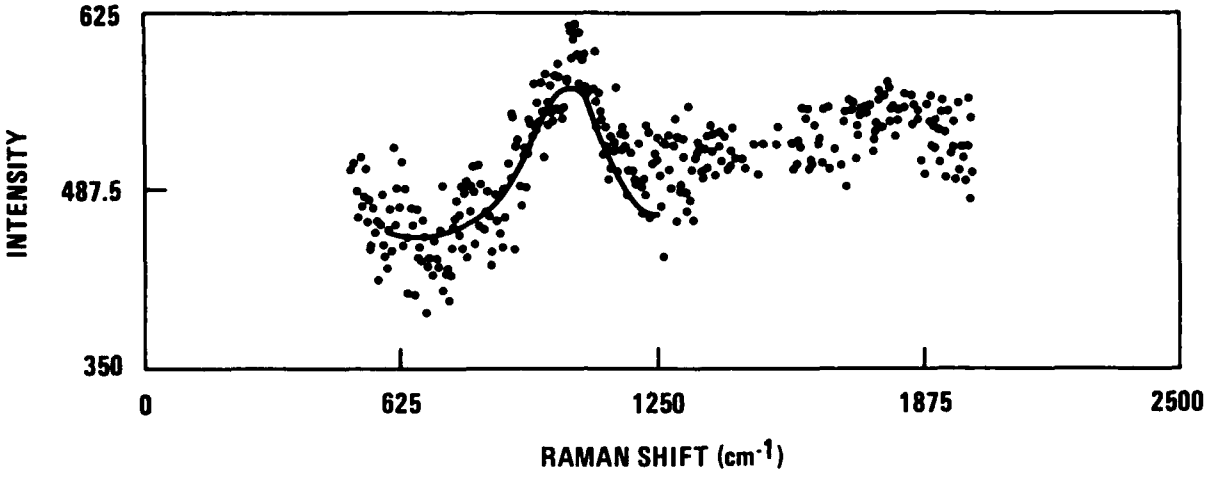

FIGURE 5 Raman shift of γ-Al_2O_3 fiber produced from the $Cl_{12.75}AlCl_4$ sample. A broad ($\Gamma \sim 100cm^{-1}$) resonance at $\sim 1000cm^{-1}$ is indicative of an OH bend seen in γAl_2O_3.

4. MISCELLANEOUS FIBERS

Several tows of intercalated graphite were oxidized at one end, such that one end was white (γ - alumina) and the other end was black (intercalated graphite). The sample was received in a 1/4" glass tubing. Because of the need to transfer some of the fibers into a separate tube for Raman measurements, an attempt was made to open the original ampoule. While this transfer was being carried out in a drybox, the white portions of the bundle broke into pieces, starting from the black-white interface. The white fibers were too porous and brittle to be picked up. A few weeks later, it was found that the white fibers disappeared as white powder formed in the tubing. Therefore, no spectra were taken on this batch.

A C_2YCl_4 sample showed no shift in the Raman frequency from that of the pristine P-100 fibers. This result indicated that the sample had been poorly intercalated. Dr. McQuillan has informed us that YCl_3 wets the graphite tow, but apparently did not intercalate. In the sample he sent us, he had been careful to avoid the wetting problem. We confirm that he had no intercalation.

5. PERSONNEL

This project was under the supervision of Professors M. Dressel and G. Dresselhaus and was conducted by Y. C. Liu.

REFERENCES

1. Fortuin, J.H.M., Thesis, Delft (1955)
2. Fredrickson, L.D., Anal. Chem., 26, 1883 (1954)
3. Cabannes-Oh, C., C.R. Acad. Sci, 244, 2491 (1957)

5. LIST OF WRITTEN PUBLICATIONS

B. W. McQuillan and G.H. Reynolds, "Deintercalation Reactions to Form Ceramic Coatings on Graphite Fibers", Graphite Intercalation Compounds, ed. M.S. Dresselhaus, G. Dresselhaus, and S.A. Solin, Materials Research Society, 1986.

B.W. McQuillan and G.H Reynolds, "Growth of Alumina Fibers from Intercalated Graphite Precursor Fibers", Proceeding of the 3rd International Conference on Ultrastructure Processing of Ceramics, Glasses, and Composites, ed. J.D. Mackenzie and D.R. Ulrich, Academic Press (in press).

H.H. Streckert, F.C. Montgomery, "Surface Modication of Matrix Materials for Oxidation - Resistant Carbon-Carbon Composites" Proceedings of the 3rd International Conference on Ultrastructure Processing of Ceramics, Glasses, and Composites, ed. J.D. Mackenzie and D.R. Ulrich, Academic Press (in press).

B.W. McQuillan and G. Reynolds, "Preparation of Ceramic Oxide Fibers from Intercalated Graphite Fibers", Proceedings of the 18th Biennial Conference on Carbon, Worchester MA, July 1987 (in press).

6. LIST OF PROFESSIONAL PERSONNEL

J.L. Kaae, Project Manager	- GA Technologies Inc.
K.C. Chen	- UCLA
G. Dresselhaus	- MIT
M. Dresselhaus	- MIT
Y.C. Liu	- MIT
J. Mackenzie	- UCLA
B. McQuillan	- GA Technologies Inc.
R. Price	- GA Technologies Inc.
G. Reynolds	- GA Technologies Inc.
H. Streckert	- GA Technologies Inc.
K. Thorne	- UCLA
D. Tilley	- UCSD

END

DATE

FILMED

DTIC

JULY 88